Report Title

Laser Drilling – Drilling with the Power of Light

Continuation of Fundamental Research and Development

Type of Report:	Annual Technical Progress Report
Reporting Period Start Date:	October 2003
Reporting Period End Date:	September 2004
Principal Authors(s):	Brian C. Gahan, P.E. Dr. Samih Batarseh
Date Report was issued:	October 2006
DOE Award Number:	DE-FC26-00NT40917
Submitting Organization:	Gas Technology Institute
Address:	1700 South Mount Prospect Road Des Plaines, Illinois 60018

Disclaimer

Abstract

Gas Technology Institute (GTI) has been the leading investigator in the field of high power laser applications research for well construction and completion applications. Since 1997, GTI (then as Gas Research Institute) has investigated several military and industrial laser systems and their ability to cut and drill into reservoir type rocks. In this report, GTI continues its investigation with a recently acquired 5.34 kW ytterbium-doped multi-clad high power fiber laser (HPFL). The HPFL represents a potentially disruptive technology that, when compared to its competitors, is more cost effective to operate, capable of remote operations, and requires considerably less maintenance and repair.

To determine how this promising laser compares with other lasers used in past experimental work, GTI performed a number of experiments with results directly comparable to previous data. Experiments were designed to investigate the effect of laser input parameters on representative reservoir rock types of sandstone and limestone. The focus of the experiments was on completion and perforation applications, although the results and techniques apply to well construction and other rock cutting applications.

Variables investigated include laser power, beam intensity, external purging of cut materials, sample orientation, beam duration, beam shape, and beam frequency. The investigation also studied the thermal effects on the two sample rock types and their methods of destruction: spallation for sandstone, and thermal dissociation for limestone. Optimal operating conditions were identified for each rock type and condition.

As a result of this experimental work, the HPFL has demonstrated a better capability of cutting and drilling limestone and sandstone when compared with other military and industrial lasers previously tested. Consideration should be given to the HPFL as the leading candidate for near term remote high power laser applications for well construction and completion.

Table of Contents

List(s) of Graphical Materials

Introduction

Rock destruction and removal is a significant issue in the process of oil and gas development. Over the years, billions of cubic feet of rock have been removed, with tremendous capital investment. In 1999, approximately 20,000 wells (oil, gas and dry) were drilled onshore in the United States, averaging about 1829 m (6,000 ft) deep, at a cost of nearly $15 billion[1]. This is equivalent to approximately 37,015 km (23,000 mi), or nearly three times the diameter of the earth (12,756 km, or 7,926 mi).

According to a Gas Research Institute (GRI) study conducted in 1990, 48% of the drilling time of a typical well is spent on making hole, 27% of the time spent changing bits or putting steel tubular casing in place, and 25% of the time spent measuring well and formation characteristics[2]. Major reductions in drilling costs can be obtained by drilling faster and reducing requirements for drill string removal, bit replacement and setting casing.

The 2001 report of the National Energy Policy Development Group, headed by Vice President Dick Cheney titled "Reliable, Affordable, and Environmentally Sound Energy for America's Future" has a primary recommendation for action "to increase domestic production." Under this recommendation is a call for the Departments of Energy and Interior to promote enhanced oil and gas recovery from existing wells through new technology. Characteristics of the laser drilling system make it friendlier to the environment than current state-of-the-art drilling systems and it has the potential to tap known U.S. resources which are currently uneconomical to develop. Drilling is faster so the system is on location for a shorter period of time, thus minimizing interruptions to the natural ecosystems and reducing drilling objections for local residents. It is envisioned that the laser system would have a smaller environmental footprint and the use of hazardous chemicals would be greatly reduced.

Some of the concerns in drilling operations include: rock destruction and removal; drilling time and cost; rig size and transportation; hole shape and deviation; fishing for stuck pipe; and tripping and drilling in hard formations including granite. In well completion operations, perforating with a shaped charge gun causes reduced production by damaging the formation around the perforated tunnel. Depending on the rock type, drilling rates can be significantly reduced using lasers when compared to conventional drilling rates. For example, drilling in hard rocks, such as granite, is extremely difficult or impossible. This research has shown that lasers penetrate hard rock at about the same rate as for soft rocks.

[1] DeGolyer and MacNaughton, 2000

[2] Andersen, et al., 1990.

An Alternative Method: High Power Lasers.

Reducing these costs and eliminating problems would have a significant positive impact on the oil and gas industry. New technologies and tools operate using basic rock destruction mechanisms like thermal spalling, fusion and vaporization, mechanical stresses and chemical reactions[3]. All of these destruction mechanisms can be achieved using lasers. For example, at low laser power, spalling (chipping) can be obtained. Increase in the laser power, with a fixed beam diameter, results in phase changes and reactions in the rock, like dehydration of clays, releasing of gases and inducing thermal stresses. At a certain power, the rock will melt (fuse) and at higher power the rock will vaporize.

Laser technology applied to drilling and completion operations has the potential to reduce drilling time, eliminate the necessity to remove and dispose of drilling cuttings and improve well performance through improved perforation operations.

Although initial GRI laser drilling investigations utilized megawatt-class military lasers, it was soon apparent that an oversized laser could effectively remove a rock mass, however, it did so quite inefficiently due to material phase change and other phenomenon unrelated to cutting and removing rock.

Less powerful industrial lasers were then utilized providing improved SE values when exposed to the same or similar rock types. Under lab conditions, the researchers were successful in proving that the current generation of industrial lasers was capable of removing rock with energy levels comparable to those of existing mechanical rock drilling methods. However, for a laser system to be applied under field conditions, a number of conditions would have to be met, including requisite power delivery to target, reliability, portability, and greater efficiency. Although the overall size or footprint per kilowatt output was improving, industrial class lasers were not necessarily designed to withstand field conditions and would be difficult to economically operate given their low wall plug efficiencies.

Characteristics of Fiber Lasers

Recently, high power fiber lasers have become commercially available and have positioned themselves as a serious alternative to other solid-state and carbon dioxide lasers for industrial material-processing. Over the past two years, fiber lasers have increased in power from several watts to kilowatts, and are fully capable of delivering sufficient rock cutting power via fiber optics.

Of interest to the GTI research team were the nearly 10x higher wall plug efficiency; and greater mobility through a smaller overall size and solid state design. In addition, the beam quality was improved, and projected diode failure was in excess of 50,000 continuous hours, projecting low or no maintenance

[3] Maurer, 1968, 1980

operations (Table 1). Together, these improvements have rapidly advanced fiber lasers as a leading candidate for on-site applications, including hard rock mining, tunneling, pavement cutting and rock drilling.

Table 1. Comparison of laser characteristics for CO_2; lamp-pumped and diode-pumped Nd:YAG; and high power fiber lasers at 4 kW output power.

	CO_2	LP Nd:YAG	DP Nd:YAG	HPFL
E/O Efficiency, %	5-10	2-3	4-6	16-20
Electric Power, kW (no chiller)	~ 50	~ 130	~ 80	20-25
Footprint, m^2 (no chiller)	6	5	3	0.5
Water, m^3/hr	6-8	20-25	~ 15	<2
Maintenance, Khrs	1-2	0.5	2-3	10-15
Pump Replace, Khrs	n/a	0.5-1	2.5	>50

Source: IPG Photonics Corporation

GTI acquired an IPG Photonics 5.34 kW ytterbium-doped multi-clad fiber laser in 2003, at the time the most powerful of its kind available for research in the United States. Power output is rapidly increasing, as more powerful fiber lasers have been manufactured.

For oil and gas industry applications, the fiber laser presents itself as the most likely near-term candidate for successful laser applications in remote locations, capable of delivering a beam to a rock target some 1 to 2 km (3281 to 6562 ft) beneath the Earth's surface. Given the improvement in the fiber laser's wall plug efficiency (16%) over a comparable diode pumped Nd:YAG (6%), an ytterbium fiber laser requires about 62.5% less electrical energy to produce the same output power beam.

For many of the same reasons fiber lasers represent a breakthrough for field applications in oil and gas, it is also being considered for other applications that include cutting or breaking rock and/or similar materials in remote locations, including those in the energy, mining, defense, space, demolition and construction industries.

Results from experiments to date continued to suggest the application of photonic energy may prove to offer a non-explosive alternative for perforating oil and gas wells. By applying this technique downhole through casing and cement, perforations and other directionally controlled completion and stimulation methods could be employed without creating damage to the reservoir. Clearly, with the use of photonic energy, no perforating materials or explosive products are left to contaminate the wellbore and the perforation

tunnel; therefore cleaning the perforated tunnel and the wellbore around the perforation area are not required. In fact, the use of lasers in downhole completions techniques, including perforation, has the potential to stimulate the perforation tunnel while it is constructed.

Laser Parameters

LASER is an acronym for Light Amplification by Stimulated Emission of Radiation. Albert Einstein predicted the possibility of stimulated emission (generation of photons or discrete bundles of energy via transitions between atomic or molecular energy levels) in 1917. Laser use in many applications such as medical, metallurgical, and military, is becoming well understood. The principle of the laser is transforming different kinds of energy (chemical, electrical, etc.) into intense electromagnetic beams of monochromatic and coherent waves. The wavelength of a laser beam (λ) depends on laser's active medium, and ranges from 0.1 micrometers (μm) to 103μm, spanning the ultraviolet, visible, infrared and sub-millimeter ranges of the photonic spectrum[4].

Laser drilling is a developing technology that has been applied to industrial uses such as creating small holes in metal and other materials. This research examines the possibility of expanding the use of lasers to remove rock for oil and gas exploration and production applications, including conventional and horizontal drilling, cutting windows in steel casing and cement, and other completion techniques.

In rock drilling, the type of laser used plays a crucial role in the efficiency and quality of the cut. Laser properties, including discharge type (continuous or pulsed), wavelength, peak power, average power, intensity, repetition rate, and pulse width define the type of laser rock interaction obtained, and thus, affect the amount of energy transfer to the rock. The results of the previous experimental work show that lasers penetrate well through rocks, as they have a low reflectivity of electromagnetic waves, resulting in a good coupling with the laser radiation. Also, the low thermal conductivity of rocks allows for a rapid heating of the rock sample in the vicinity of the beam.

[4]W.T. Silfvast, 1996

Executive Summary

The overall objective of this study is to conduct research to establish the technical feasibility of using laser tools to drill and complete natural gas wells and conduct engineering studies leading to prototype tool development. The proposed tasks for this report include developing an in-situ laser/rock interaction test plan based on Phase I plan and results, including design of pressure vessel and data acquisition using pulsed and continuous wave lasers.

Experiments were performed at Gas Technology Institute in Des Plaines, IL at their High Power Laser Applications Laboratory. The 5.34 kW ytterbium-doped multi-clad fiber laser was used exclusively to perform the experimental work. Tests were conducted on Berea sandstone and Bedford limestone samples. Berea sandstone is a standard quarry rock used in the petroleum industry for laboratory testing. Bedford limestone was procured from a local Illinois quarry, and was selected due to its relatively consistent and uniform characteristics. For both rock types selected, it was important that both were available in large block sizes per the experimental design.

A series of experiments were designed to isolate the effect that specific variables have on the laser/rock interaction as measured by specific energy (SE). SE is simply the amount of energy required to remove a unit volume of rock as measured in kJ/cc. A higher SE value correlates with a less efficient process; therefore a lower SE value is preferred. By using this measurement throughout our experimental work and analyses, comparisons can be easily made as to the relative impact contributed by a specific variable.

Experiments performed, detailed and analyzed in this report include:

- Purge Optimization and Calculating Specific Energy
- Orientation Effect Test
- Determination of Boundary Effect on SE
- Effect of Beam Intensity on SE
- Effect of Beam Duration on SE (Collimated Beam)
- Effect of Laser Power on SE (Collimated Beam)
- Time of Penetration Effect on SE
- Effect of Saturation and Purge Gas Type on SE
- Frequency Effects on SE
- Effect of Beam Duration on SE (Focused Beam)
- Thermal Effects on Limestone
- Thermal Effects on Berea Sandstone
- Effect of Laser Power on SE (Focused Beam)
- Effect of Beam Intensity on SE

Experimental

Proposed Tasks

The work performed by GTI during the 2004 fiscal period was based on the following overall scope of work presented and accepted by DOE (Work performed during this period and presented in this report are in bold):

Task 2.0: Continuation of Fundamental Research and Development
GTI shall continue previous investigations into the feasibility of using high-powered lasers for the purpose of drilling and completing natural gas wells. The objectives of the project are to:

a) Experimentally determine the best laser parameters for creating a hole of a given size, deep into a given lithology under in-situ conditions.
b) Develop a model for the laser/rock interaction process, and
c) Develop the conceptual design of a laser drilling system based on the results of a) and b).
d) Experimentally determine the effect of liquid saturated lithologies on laser beam-rock interactions
e) Ability of lasers to interact with rock in a liquid filled pressure vessel
f) Advantages and disadvantages of pulsed vs. continuous wave CO_2 lasers
g) Specific Energy (SE) dependencies on laser and other process parameters, and
h) Mineralogy changes that occur with exposure to laser energy.

Task 2.1 Experimental Plans

1. **Develop an in-situ laser/rock interaction test plan based on Phase I plan and results, including design of pressure vessel and data acquisition using pulsed and continuous wave lasers**
2. Develop a laser/rock interaction test plan to be performed using a high-power free electron (FE) laser to determine effect of various beam wavelengths on rock samples

Task 2.2 Rock Preparation and Analysis

Acquire and prepare sandstone, shale and limestone target samples for all planned tests, and analyze rock properties pre- and post-test.

Task 2.3 Data Analysis

Collect and analyze diagnostic data, calculate SE and penetration rates, determine lithology-specific relationships and general relationships, and

evaluate effect of pulsed vs. continuous wave lasers, wavelength, and in-situ conditions on the application of laser energy to remove rock.

Task 2.4 Topical Report

Prepare, as part of the Continuation Application, a draft topical report on the technical progress of the project. This report shall follow guidelines set forth in the Federal Assistance Reporting Checklist and accompanying reporting instructions and shall include, but not necessarily be limited to:

1. **The diagnostic data, SE and penetration rate calculations for each lithology tested,**
2. **The conditions that result in spallation, melt, and vaporization mechanisms for rock removal in each lithology, including laser and rock properties**
3. **An analysis of changes in physical and chemical properties to rock samples following laser exposure**
4. **The contributory effects of laser beam wavelength on rock removal**

Task 2.5 Modeled Effects of Energy Transfer From Lasers to Non-Homogeneous Porous Media

Develop a predictive model of the processes that occur during laser/rock interaction based principally on transport equations of mass, momentum and energy conservation.

Task 3.0 Systems Development Issues in Laser Well Construction

GTI shall investigate the significant technical hurdles that are required to allow downhole laser applications in oil and gas wells, including energy delivery downhole, rock cuttings from the wellbore as a material resource for well construction, alternative techniques (i.e., clear water or other transparent coaxial jets) for drilling with a weighted fluid environment.

This study will focus primarily on laser drilling systems development issues. Proposed is a two-phase program that encompasses idea/concept development and demonstration of concept. All phases and tasks proposed will be performed at Gas Technology Institute.

Task 3.1 Downhole Energy Delivery Assessment

Perform a literature review and analysis to determine available commercial options for laser systems and fiber optics, laser optics and lenses, conventional electric transmission applications and energy transfer issues.

Task 3.2 Laser Created Rock Melt Characteristic Study

Investigate the material properties of rock melted by laser energy as a material resource in well construction (i.e., ceramic casing), including

strength properties, mineralogy, structure, thermal properties, porosity and permeability, and influence of additives on melt properties.

Task 3.3 Experimental Plans
Develop an in-situ laser/rock interaction test plan to simulate a variety of downhole drilling environments, including balanced, overbalanced, and underbalanced conditions, in combination with anticipated downhole fluids (i.e., drilling mud, water, brine, hydrocarbons).

Task 3.4 Rock Preparation and Analysis
Acquire and prepare sandstone, shale and limestone target samples for all planned tests, and analyze rock properties pre- and post-test.

Task 3.5 Data Analysis
Collect and analyze diagnostic data, calculate SE and penetration rates, determine lithology-specific relationships and general relationships, and evaluate effect of downhole drilling environments in combination with drilling fluids on these relationships.

Task 3.6 Topical Report
Prepare, as part of the Continuation Application (see Article 2.6, "Continuation Application" contained in Section II -Special Terms and Conditions), a draft topical report on the technical progress of the project. This report shall follow guidelines set forth in the Federal Assistance Reporting Checklist and accompanying reporting instructions, and shall include, but not necessarily be limited to:

- Bibliography and analysis from literature study,
- Laser Created Rock Melt Characteristic Study analysis and results,
- The diagnostic data, SE and penetration rate calculations for each material tested,
- The conditions that result in spallation, melt, and vaporization mechanisms for rock and cement removal in each lithology, including laser and rock properties, and conditions that optimize cutting through a steel liner,
- An analysis of changes in physical and chemical properties to rock, cement and steel samples following laser exposure.

Task 4.0: High Energy Laser Perforation and Completion Techniques
GTI is currently investigating the feasibility of laser perforation and completion techniques with a major service company partner. A proof of concept with planned subsequent investigations are aimed at creating engineering systems for adapting laser energy to puncture steel casing and the cement bonding agent, into the formation deep enough to allow the free flow of hydrocarbons into the wellbore.

GTI proposes to perform investigations into understanding and modeling laser/material interactions involving cladded perforation targets, representing steel casing, cement, and reservoir rock. Although literature exists on the use of lasers for cutting steel in controlled factory environments, limited information addresses laser cutting of steel in the extreme conditions that exist downhole. These investigations will directly complement GTI's existing systems analysis and prototype development with our industry partner.

As with Task 2.0, all tasks proposed will be performed at Gas Technology Institute, however in unforeseen situation where laser or other similar equipment from laser or petroleum industry partners would be required, GTI is confident that access would be made available and supported.

Task 4.1 Experimental Plans
Develop an in-situ laser/rock interaction test plan matrix, including design of pressure vessel and data acquisition using a laser(s) capable of cutting steel, cement and rock samples.

Task 4.2 Rock Preparation and Analysis
Acquire and prepare combinations of sandstone, limestone, cement and steel target samples (individual and cladded) and analyze material properties pre- and post-test.

Task 4.3 Data Analysis
Collect and analyze diagnostic data, calculate SE and penetration rates, determine material-specific relationships and general relationships, and evaluate effect of laser energy to remove combination of materials.

Task 4.4 Topical Report
Prepare, as part of the Continuation Application (see Article 2.6, "Continuation Application" contained in Section II -Special Terms and Conditions), a draft topical report on the technical progress of the project. This report shall follow guidelines set forth in the Federal Assistance Reporting Checklist and accompanying reporting instructions, and shall include, but not necessarily be limited to:

- The diagnostic data, SE and penetration rate calculations for each material tested,
- The conditions that result in spallation, melt, and vaporization mechanisms for rock and cement removal in each lithology, including laser and rock properties, and conditions that optimize cutting through a steel liner
- An analysis of changes in physical and chemical properties to rock, cement and steel samples following laser exposure.

Task 4.5 Modeled Effects of Energy Transfer in a Laser Perforation Shot
Develop a predictive model of the processes that occur during laser/material interaction based principally on transport equations of mass, momentum and energy conservation.

Experimental Methods

Experiments were performed at Gas Technology Institute in Des Plaines, IL at their High Power Laser Applications Laboratory. This lab was developed as a means to investigate alternative methods to conventional rock removal in accessing targeted subsurface accumulations, including energy reserves, minerals, aquifers, and pollutants. The 5.34 kW ytterbium-doped multi-clad fiber laser was used exclusively to perform the experimental work.

Specific Energy Calculations

In order to break rock by mechanically or thermally induced stresses, sufficient power must be applied to the rock such that the induced stresses exceed the rock's strength. Similarly, when fusing rock, sufficient heat must be generated that exceed the melting temperature of the rock. Once these threshold values of power and energy are exceeded, the amount of energy required to break or remove a unit volume of rock remains nearly constant. This energy parameter, which is a measure of the efficiency of the rock destruction technique, is defined as specific energy (SE). The term SE is associated with various definitions and is commonly used by the drilling industry in discussions of the efficiency of mechanical drilling, particularly in measuring effectiveness of new bit designs. SE is defined in this experimental work as the amount of energy required to remove a unit volume of rock and is relationally represented as follows:

$$\text{SE (kJ/ cc)} = \text{Energy input / volume removed} \qquad (1)$$

Parameters Affecting SE Measurements.

There are three basic phenomena evident in the process of radiant energy transfer to solids: reflection, scattering and absorption of radiation. The flow of energy of an incident electromagnetic wave (E_{inc}) is divided into these parts:

$$E_{inc} = E_{refl} + E_{sc} + E_{abs} \qquad (2)$$

Where E_{refl}, E_{sc}, and E_{abs} are reflected, scattered and absorbed fractions of the energy flow of the incident wave, respectively.

If a surface is a planar one, like a mirror, then much of the energy is reflected. Rough surfaces mainly scatter the incident radiation. The reflectivity is determined by the composition of the solid, while the scattering of radiation is determined by wavelength, λ. It is the absorbed energy that gives rise to the

rock heating and destruction. Reflection and scattering represent energy losses that occur apart from the absorbed energy. Minimizing fractions of reflected and scattered energy losses will, consequently, maximize the energy available for transfer to a rock for destruction.

There are factors that affect the amount of absorbed energy transferred to the rock samples, known as secondary effects, and include the creation of melted materials, beam absorbing exsolved gases in the lased hole and induced fractures in the surrounding rock. When applying high power lasers on rocks, the laser can spall, melt, or vaporize the rock as the energy transferred to the rock raises its temperature locally. Mineral melt begins to occur when the rate of heat dissipation by the rock is exceeded by the rate of energy absorbed by the rock. As time increases, energy accumulates in the form of heat, raising the local temperature of the minerals to their melting points, forming a glassy melt.

The amount of melt is a function of the mineralogy of the rock and the intergranular space of the rock matrix. The closer the grains are to one another, the more heat will be transferred, resulting in more melt in the rocks. However, for tightly packed grains, the heat conductivity could reach higher values dissipating the heat at a faster rate, reducing the amount of melted material. Also, some minerals decompose and produce gas. As a result, the melt and gases require part of the laser energy for their creation, so a smaller percentage of the total laser energy is transmitted to rock.

Fractures that form in the samples also have an impact on SE. It may be that fractures extending out from the laser created hole are beneficial to the removal process. However, it is our conclusion that the fractures seen in the tests are an artifact of the sample size and do not represent what will occur in the subsurface under in situ conditions.

For the purposes of this study, fractures represent losses of energy, which result in higher SE values. Fractures are classified as macro- and micro- fractures. The behavior of fractures is different from one rock type to another. This difference depends on intrinsic factors such as mineralogy, thermal properties of the rocks, volume of void space, dimension of the sample and the amount of stress applied. Mineralogy also affects fracture formation. Clays contain water and by subjecting the clays to higher temperatures, water will escape in the form of vapor. This increases the volume and pressure in the pore and can cause fractures. Sandstones and shales have high thermal conductivities and contain clays. Limestones, on the other hand, have low thermal conductivity and have low amounts of clay and quartz. Therefore, fractures are expected in sandstones and shales, but not in limestones.

Rocks, having a high thermal conductivity, transfer heat more efficiently and the temperature is more uniform within the rock. Therefore, for this type of rock, cooling occurs gradually along the core sample. For example, fractures in

sandstones developed regularly, not randomly. High temperatures resulting from the energy of the laser beam causes quartz grains to expand. At 600 ^{o}C (1112 ^{o}F) quartz grains expand by 1.75% of the original size. In the case of full grain contact (low void space), grains have less space to expand and fractures develop[5].

The dimensions of the sample can affect the behavior of the fractures. It has been observed from the previous tests[6] that the 2.54-cm (1.0 in.) diameter cores are highly fractured around the hole, while the 5.08-cm (2.0 in.) diameter cores are less fractured. Finally, stress applied to the core minimizes the macro fractures, while the micro fractures will still remain.

Rocks Used in this Investigation

Characterization of the Samples

Tests were conducted on sandstone and limestone samples. Berea sandstone is a standard quarry rock used in the petroleum industry for laboratory testing. Other notable Berea sandstone characteristics include: relative homogeneous physical characteristics including high silica content; common use in laboratory studies of rock; and extensive body of experimental data and literature.

Bedford limestone was procured from a local Illinois quarry, and was selected due to its relatively consistent and uniform characteristics.

For both rock types selected, it was important that both were available in large block sizes due to experimental design. Although actual sandstone and limestone reservoir core samples were available, sample size and consistent physical characteristics were more limited than quarry samples.

General Rock Properties

Microscopic properties, such as mineralogy, clay content, and microfractures, were determined using a scanning electron microscope with the energy dispersive system (SEM-EDS), x-ray diffraction (XRD), and thin sections. Melting temperatures of these rocks were measured using differential thermal analysis (DTA).

The Pressure Decay Profile Permeameter (PDPK) was used to characterize the rocks before and after lasing. The PDPK measures point permeability at ambient conditions, Klinkenberg slip factor and the non-Darcy flow coefficient (Forchheimer). The PDPK is reliable down to a permeability of 0.001 md and experience has shown it to be repeatable and accurate. This non-destructive, unsteady-state test can measure permeability on irregular shapes, therefore, it an excellent tool to analyze permeability before and after beam exposure.

[5] W.H. Somerton, 1992.

[6] R.M. Graves and D.G. O'Brien, 1998

Thermal Effects and Boundary Conditions

Previous GRI studies have shown that the rock samples will crack due to thermal stress created by a high power laser beam. What was not understood is how the formation of the cracks affects the SE. An analysis of the data indicated that cracking should be treated as an energy absorbing boundary affect and should be avoided. For this reason, beam exposure was made on larger bulk samples of rock. The larger sample mass acted as a more capable thermal dump, significantly reducing fracturing due to thermal and boundary stresses. This application method was used whenever possible. When the beam was exposed to dimensional core samples, efforts were taken to reduce thermal and boundary stress fractures. Figure 1 illustrates the relative comparability of calculating SE values using block and core samples, where no visible fracturing takes place.

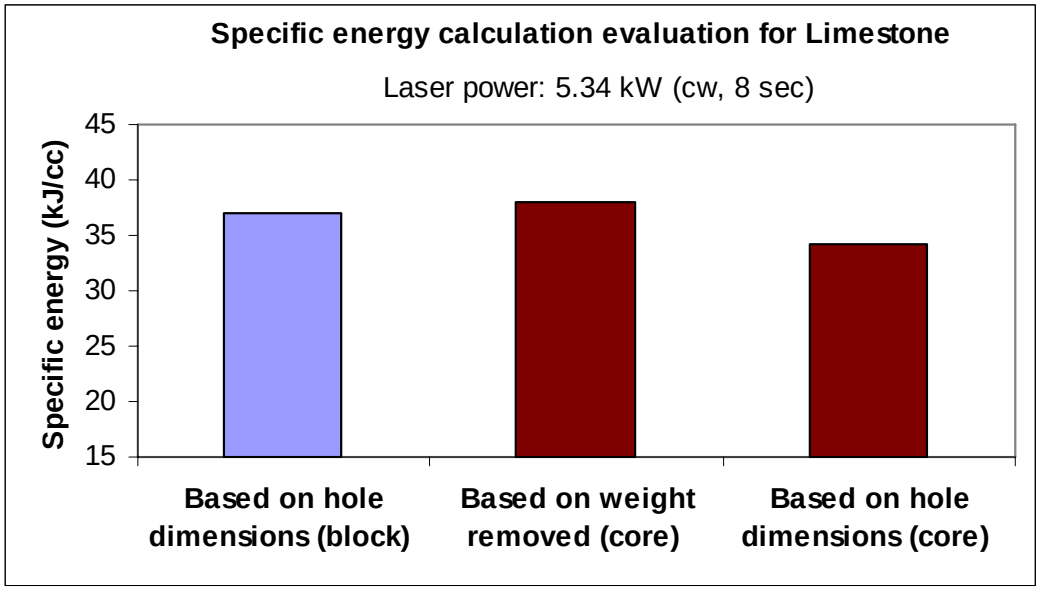

Figure 1. Comparison of specific energy calculation methods.

Results and Discussion

Purge Optimization and Calculating Specific Energy

Previous experiments have shown debris created from laser cutting must be moved as quickly as possible from the beam's path to reduce energy losses. Any material that blocks the path of the beam to its target will absorb a portion of that energy, thus redirecting it away from the cutting process. As there are a number of variables and methods of purging this material as it is cut, experiments were performed to determine an optimized process. Although incompressible fluids may be considered in a downhole system, only pressurized gasses were tested in this set of experiments.

Purge Optimization

Two gas purging systems were evaluated: an air amplifier and gas nozzle. The principle of the air amplifier is to provide a flow of purge gas on the target, while directing the laser beam through the open center of the amplifier on to the target (Figure 2). The air amplifier can operate in both vacuum and purging modes, and each was evaluated to determine any difference on specific energy while lasing. Different gas purging nozzles were also evaluated based on size, shape, angle, and fluid pressure.

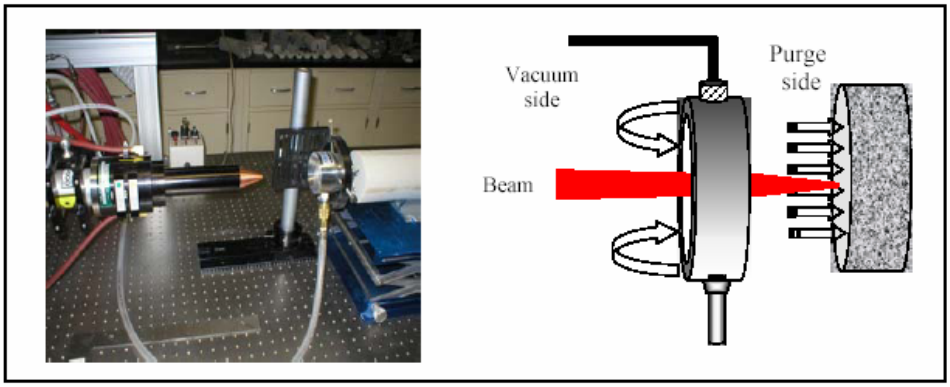

Figure 2. Schematic of purge system and experimental set up for purge optimization

An example of the purging calibration experiment is presented in Figure 3. The calibration was performed by adjusting the distance between the purging system and the target, as well as by adjusting the angle of the purging nozzles. The beam was exposed to the target for 4.0 s to determine deepest penetration with minimal mineral melt.

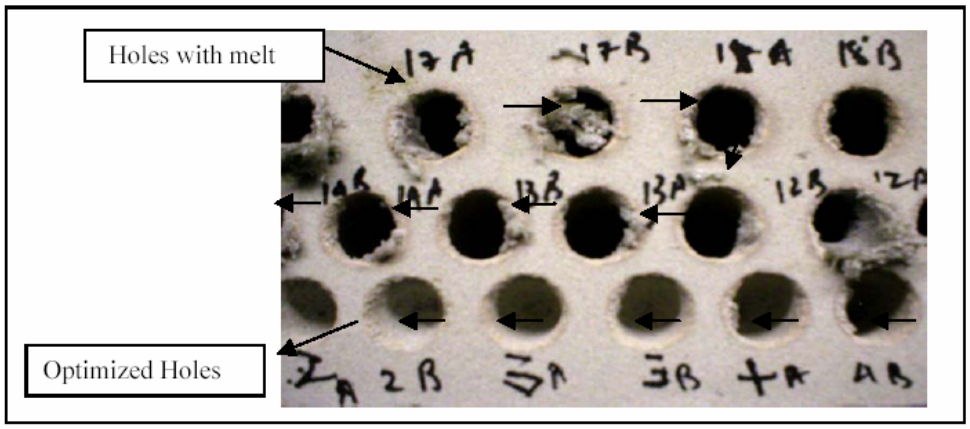

Figure 3. Figure showing holes created by changing purge type and parameters

The selection of the best gas nozzle was based on experimental observation and specific energy calculations. The selected gas nozzle was made from 6.35 mm (0.25 in) stainless steel tubing with 517 kPa (75 psig) line pressure (house-supplied air) and co-axial purging.

It was observed that in the case of limestone, the air amplifier and nozzles have the same effect on specific energy, however the nozzles provide for a better purging mechanism on sandstone. Sandstone consists of a high percentage of silica, which will melt when beam exposure allows sufficient thermal accumulation to raise the temperature of the silica grains beyond the melting point. When allowed to occur, a ceramic-like sheath material is produced. The co-axial high velocity-purging nozzle is better at quickly removing silica cuttings from the beam path, reducing thermal accumulation and subsequent phase change.

Calculating Specific Energy

Specific energy is defined as amount of energy required to remove a unit volume of material (Equation 3).

$$\text{Specific energy} = (\text{energy input})/(\text{volume removed}) = (\text{laser power} * \text{beam duration}) / (\text{volume removed}) \quad (3)$$

Volume removed can be calculated by,

- Weight Differential Method: difference between weight of sample taken before and after lasing multiplied by bulk density of sample

  Under ideal conditions, if the purging is efficient, the laser should create a hole identical to the shape of the beam. The volume of material removed the relationship to SE can be seen in Equation 4:

$$SE = \frac{Energy\ input}{Volume\ removed} = \frac{P}{dV/dt}$$

$$= \frac{\left[\frac{kW}{cm^2}\right].Time}{cm} = \frac{kW}{cm^3/\sec} = \frac{kJ}{cm^3} + C.....(4)$$

$$\rho = \frac{m}{v}\ g/cc$$

- Geometric Method - measuring diameter and depth of penetration of hole and applying correct geometric equation: cylindrical for collimated beam and conical for focused beam (Figure 4).

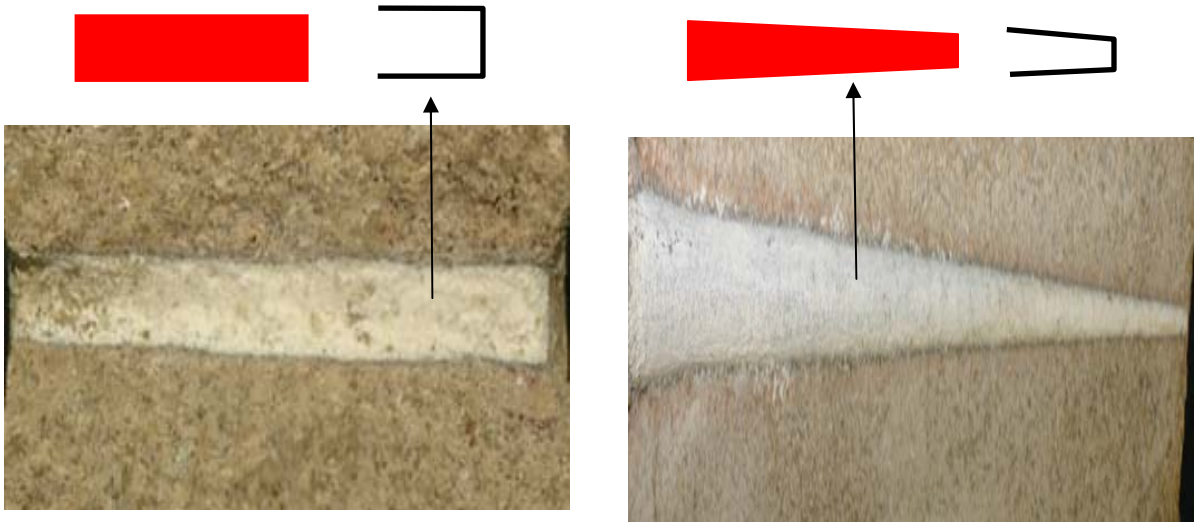

Figure 4. Effect of shape of the beam on resulting hole with various purge mechanisms

As mentioned above, debris removal using an efficient purging method is of more concern in creating a deep hole in sandstone than in limestone. Because of this, it was easier to visually gauge the effect of various purging parameters on sandstone. Using the methods above, SE values were calculated for each beam interaction.

Ten core samples of sandstone measuring 5.08 cm (2.0 in) diameter x 5.08 cm height (2.0 in) were weighed before lasing. Each sample was lased for 8 s at 5.34 kW power (CW beam) in presence of optimized purge system (gas nozzle). The spot size was fixed at 8.9 mm (0.35 in).

Samples were then weighed after lasing. Bulk density of each sample was calculated by measuring their dimensions and weight. Volume removed was then estimated by multiplying bulk density and weight removed by lasing.

The second SE method based on hole dimensions was determined by measuring the hole diameter and depth to calculate volume of rock removed. By optimizing the purging conditions, the SE values for both weight differential and geometric methods were comparable. This indicates that the purging was

efficient and a clean hole was created with no melt. The average SE results obtained from both methods are shown in Figure 5.

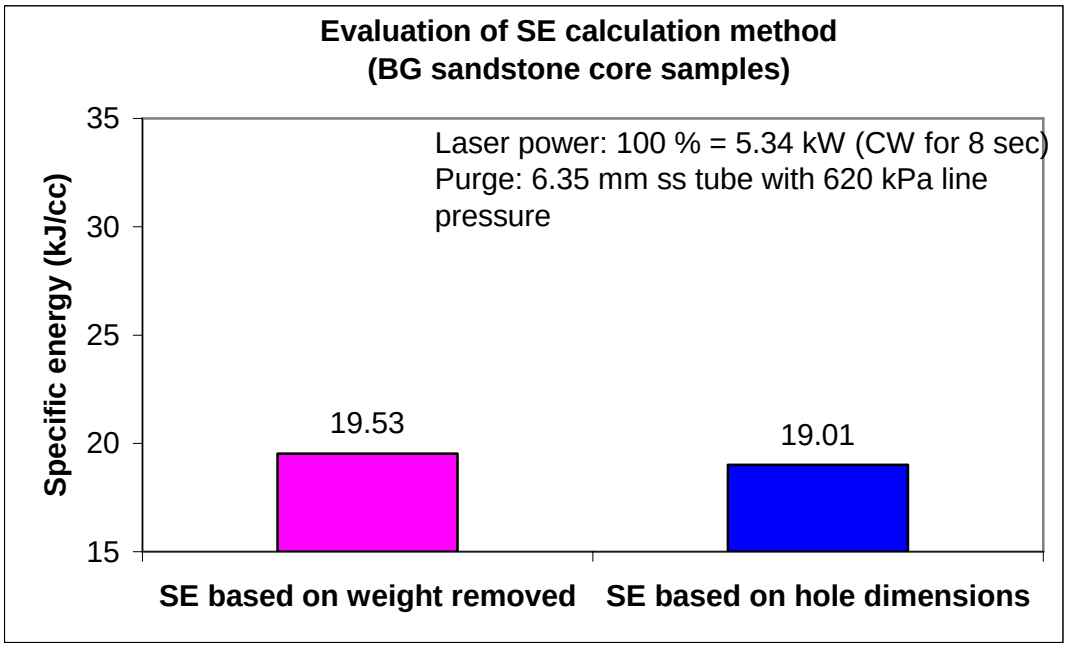

Figure 5. Comparison of specific energy calculated by weight removal and hole dimension

Result and Analysis: Purging is an important element in removing rock with high power lasers as a clear path for the beam is maintained for energy delivery to the rock. Dust, debris and cuttings will absorb beam energy resulting in less energy delivery to the target (Figure 6), and can be measured in a relative sense through observed SE calculations.

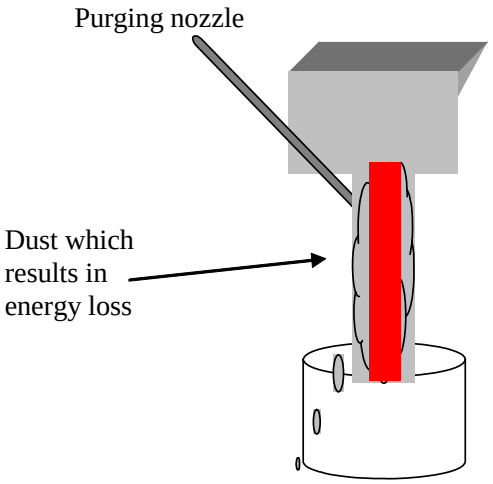

Figure 6. Schematic of purging mechanism

The purging method was improved by adjusting the distance between the purging nozzle to the surface of the rock sample, the angle of the purge and the flow pressure (Figures 7a and 7b).

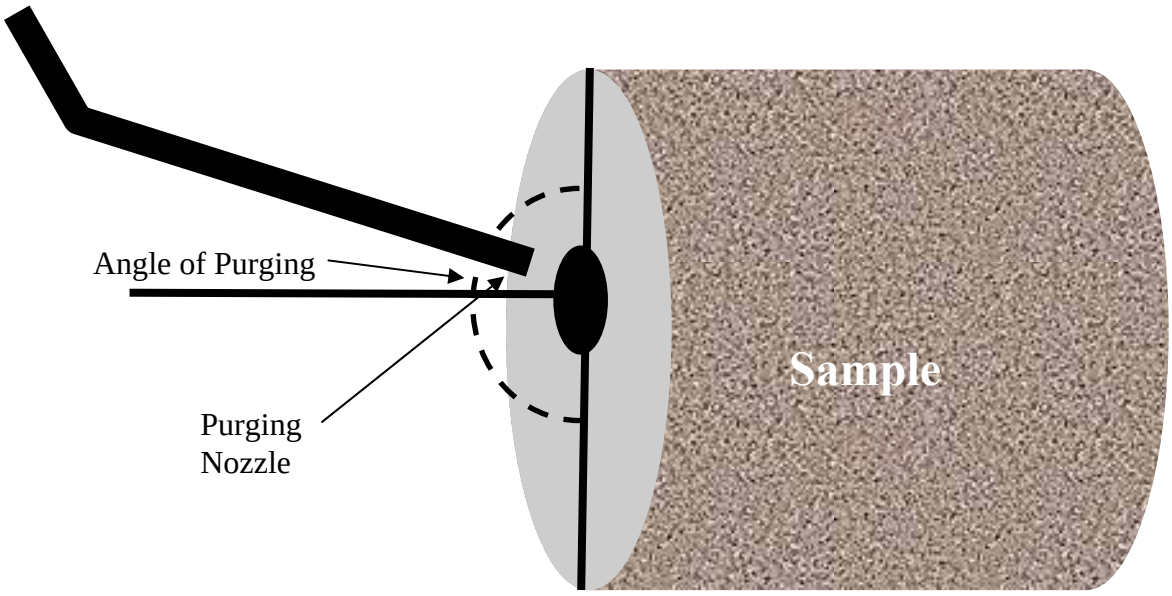

Figure 7a. Relative positions of sample and purging nozzle.

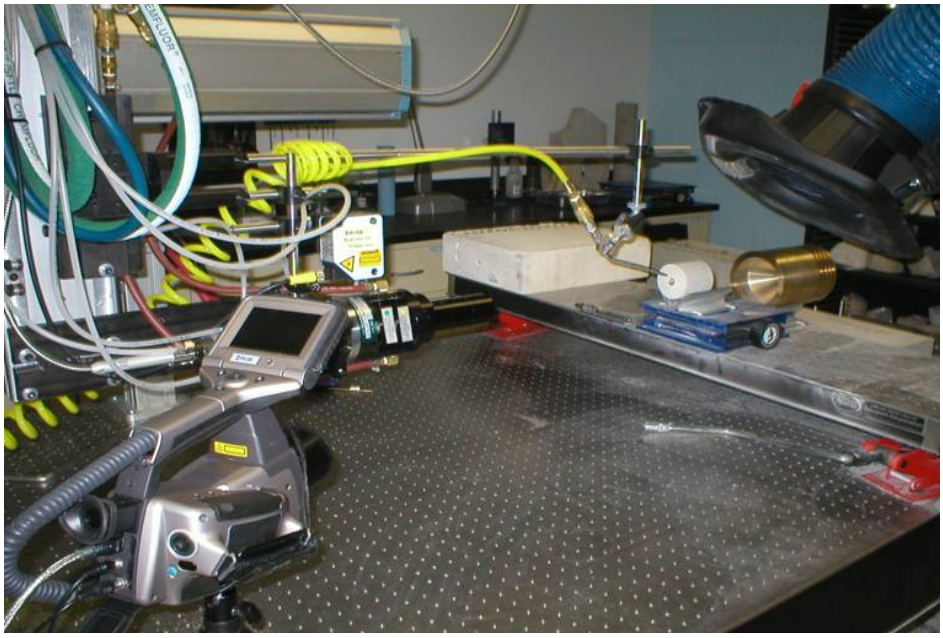

Figure 7b. Experimental set up showing purge gas delivery system

The optimized angle for a horizontal beam application was found to be 35^{o} from the horizontal. The optimized nozzle distance from the target was 2.54 cm (1.0 in) with pressurized gas at 517 kPa (75 psig) flowing through 6.35 mm (0.25 in) stainless steel tubing. This combination of nozzle angle and distance from the target at the given pressure was most efficient in removing the dust and debris while the laser actively removed material. Figure 8, a video capture from the experiment, shows the purging set up while lasing.

Figure 8. Purging mechanism while lasing.

Once the nozzle purging method was optimized, the same process was repeated using the air amplifier. Again, the weight differential and geometric methods were used to calculate the specific energy. Sandstone and limestone samples (10 each) were exposed to a 5.34 kW CW beam for 8.0 s with a beam diameter of 8.9mm (0.35 in). There was a noted difference between these methods as evidenced by the data presented in Figures 9 and 10.

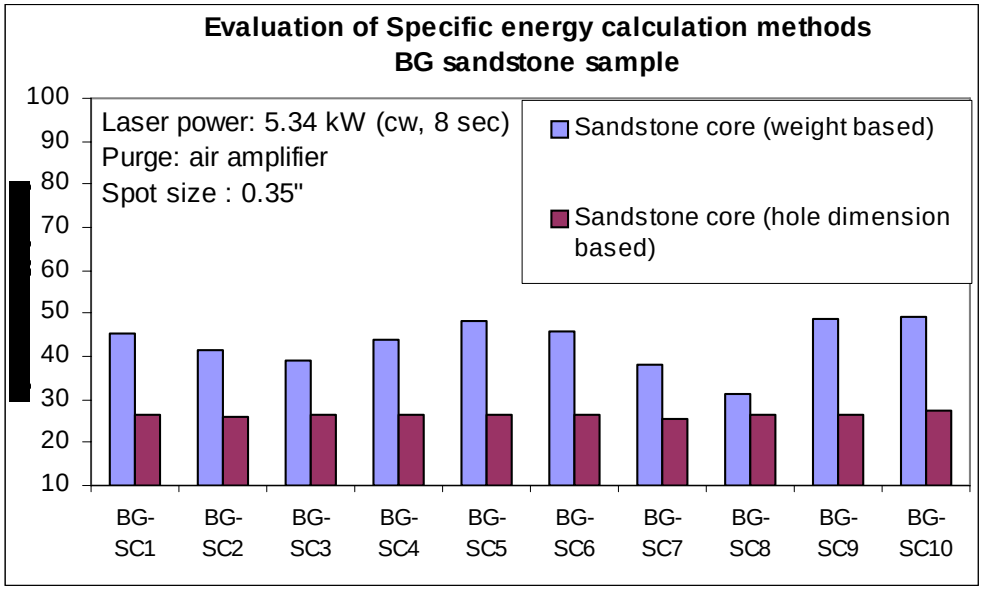

Figure 9. Comparison of specific energy calculation methods for sandstone samples

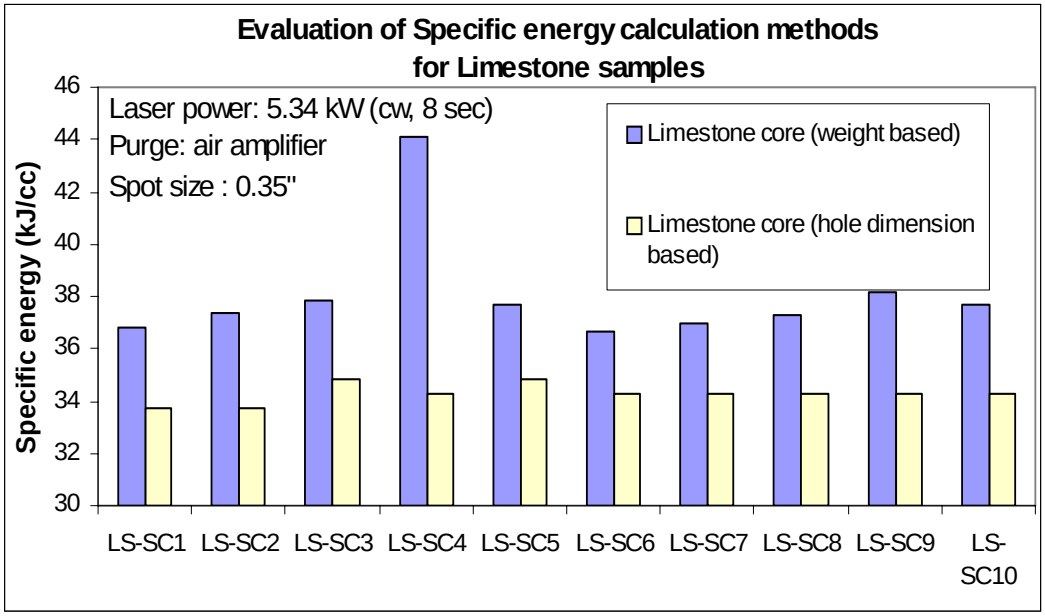

Figure 10. Comparison of specific energy calculation methods for limestone samples

Comparison of the air amplifier purging method with the nozzle purging method is presented in Figure 11. It is clear to see that nozzles are more efficient than the amplifier in removing debris from the hole. The average observed SE for the air amplifier purging method was nearly twice that of the nozzle purging method.

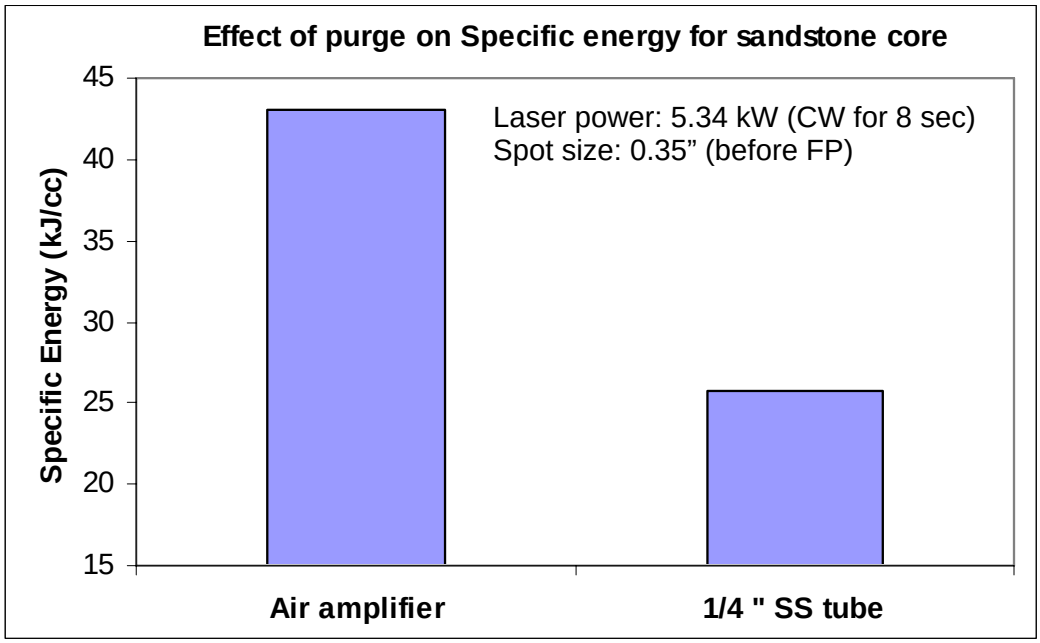

Figure 11. Effect of purge methods on specific energy for sandstone.

Orientation Effect Test

Objective: To determine the effect of depositional orientation (face and side) on SE for both limestone and sandstone samples.

Procedure: A test was conducted to determine if a change in depositional orientation (face and side) of the rock would affect SE when exposed to the beam. An identical exposure was targeted on all faces of 10.0 cm (3.94 in) sandstone cube and 5.0 cm (1.97 in) limestone cube with 5.34 kW continuous wave (CW) beam for 8.0 s. An optimized nozzle purge system was used with compressed air at 620.5 kPa (90 psig) line pressure. Distance between purge and sample was about 2.54 cm (1.0 in). Lenses with 1000 mm (39.37 in) focal length were used to focus 2.54 cm (1.0 in) collimated beam. Spot size (penetrating laser beam diameter) on the rock face was at 8.9 mm (0.35 in). Figure 12 shows the holes created on different faces of the sandstone block. Figures 13 and 14 chart the observed SE for each face of sandstone and limestone samples.

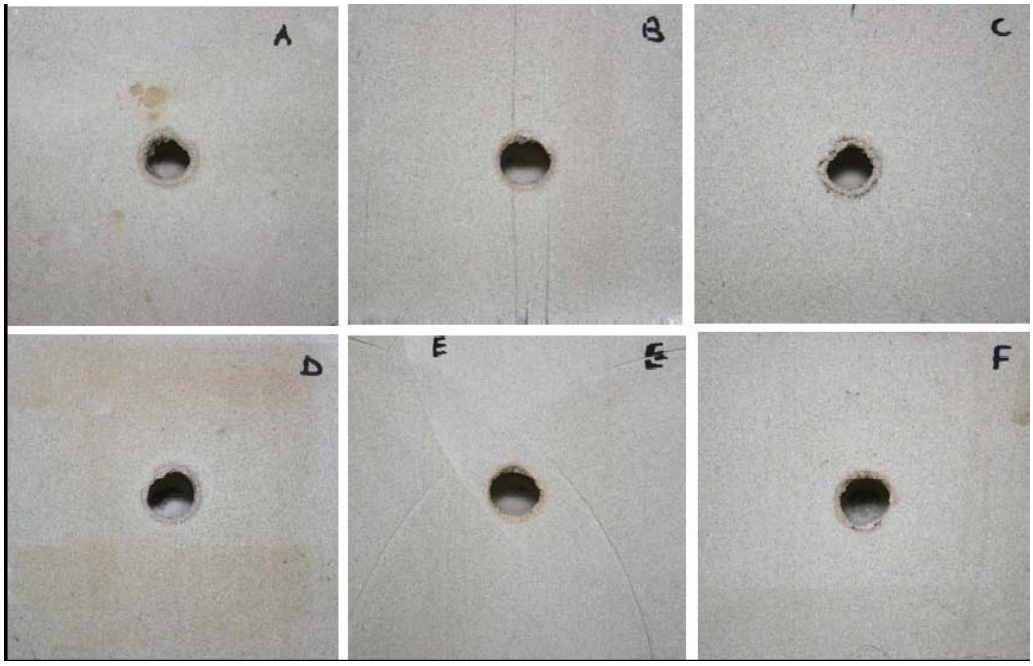

Figure 12. Six faces of sandstone block using identical laser parameters.

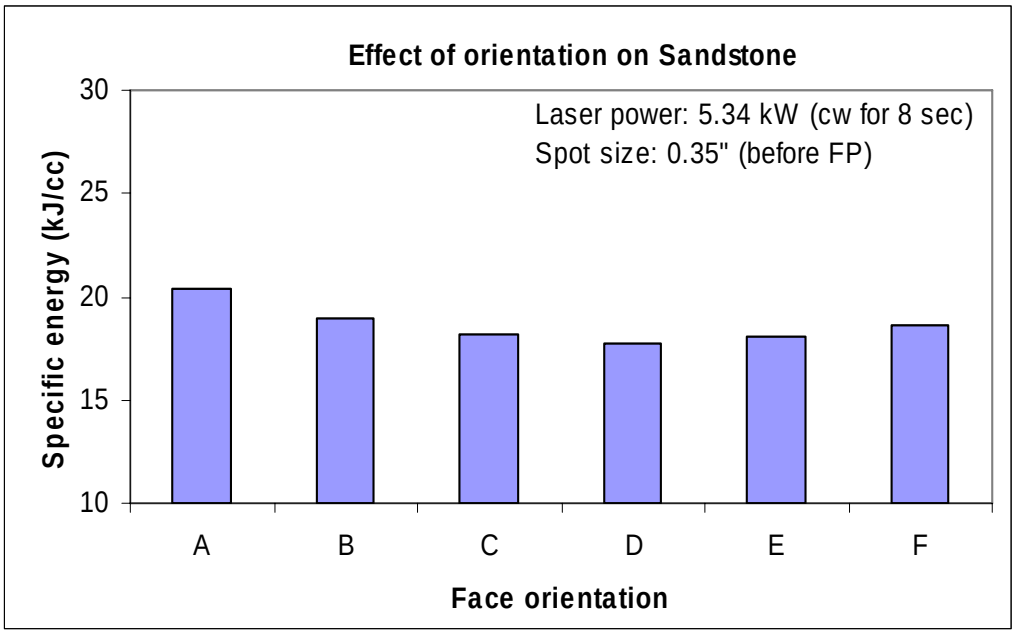

Figure 13. Effect of orientation on specific energy for sandstone.

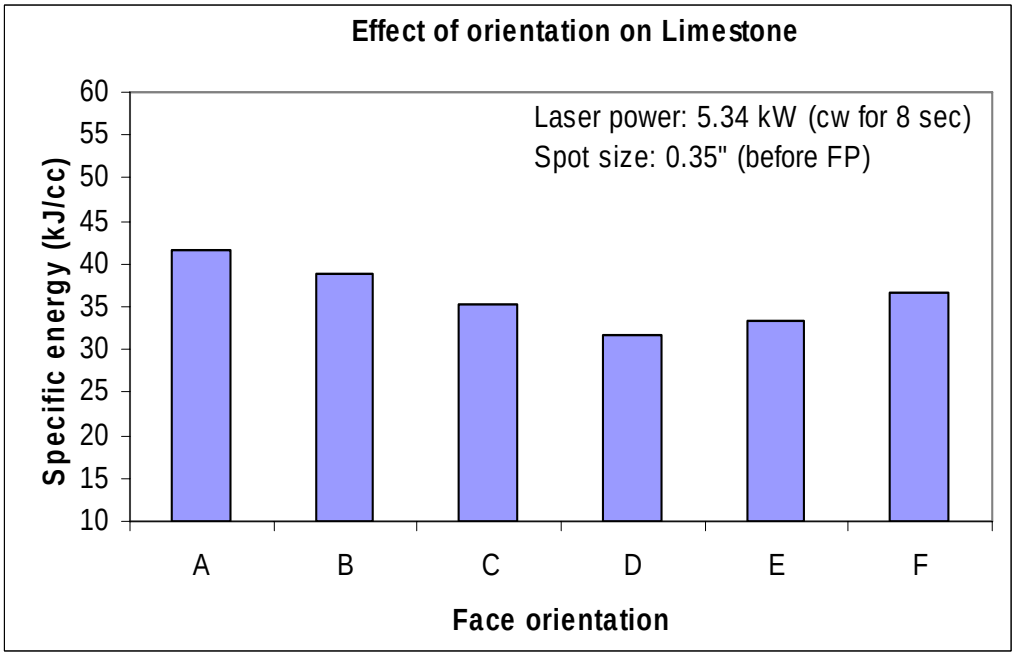

Figure 14. Effect of orientation on specific energy for limestone.

As shown in the graph, depositional orientation is not a significant variable in the observed SE values. Although there are minor differences in SE from face to face, the impact of orientation is insignificant. This suggests that data is comparable regardless of its orientation to the beam, and perhaps rock strength associated with orientation may not be an issue in the design of a downhole tool.

Determination of Boundary Effect on SE

Objective: To determine the effect of sample size on specific energy.

Procedure: A set of experiment was conducted to determine the effect of sample size on specific energy.

Sandstone/Limestone cores of diameter 1.91 cm, 2.54 cm, 5.08 cm, 6.985 cm, 7.62 cm, 10.16 cm (0.75 in, 1.0 in, 2.0 in, 2.75 in, 3.0 in, 4.0 in) and 5.08 cm (2.0 in) length were used for this experiment. Each experiment was repeated 3 times to determine repeatability. Each core was lased for 4.0 s with a 5.34 kW focused beam. An optimized nozzle purge system was used with compressed air at 620.5 kPa (90 psig) line pressure. Distance between purge and sample was about 2.54 cm (1.0 in). Lens with 1000 mm (39.37 in) focal length was used to focus 2.54 cm (1.0 in) collimated beam. Spot size (penetrating laser beam diameter) was kept 8.9 mm (0.35 in). Weight differential method (explained in methods of calculating SE) was used to calculate specific energy.

Values of specific energy for sandstone and limestone samples are shown as a function of core diameter (Figures 15 and 16). The 10.16 cm (4.0 in) core diameter shows no boundary effect as shown in graph. A comparison for specific energy values for sandstone and limestone is also given below in Figure 17.

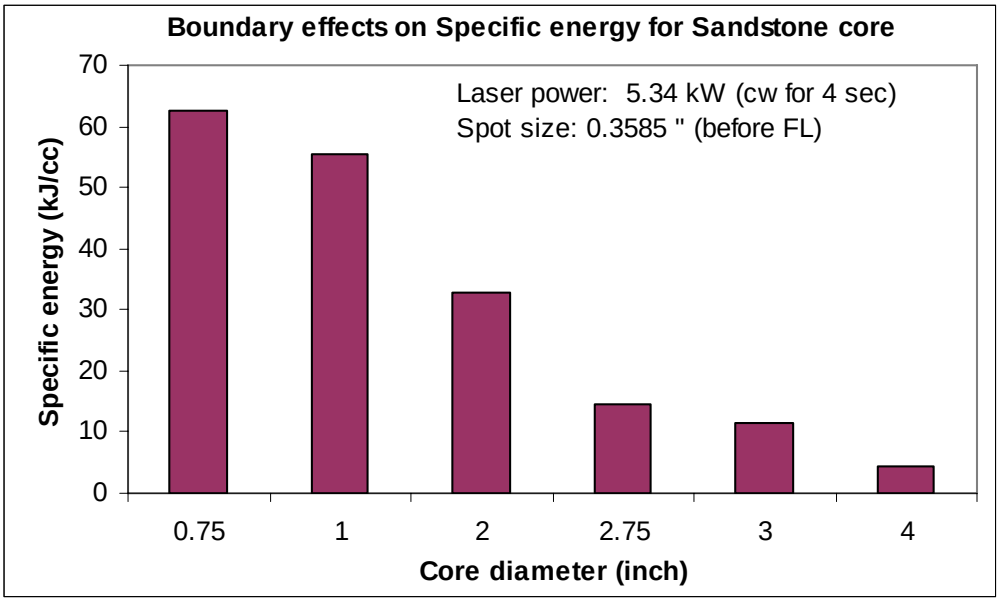

Figure 15. Effect measuring of sample on specific energy for Berea sandstone

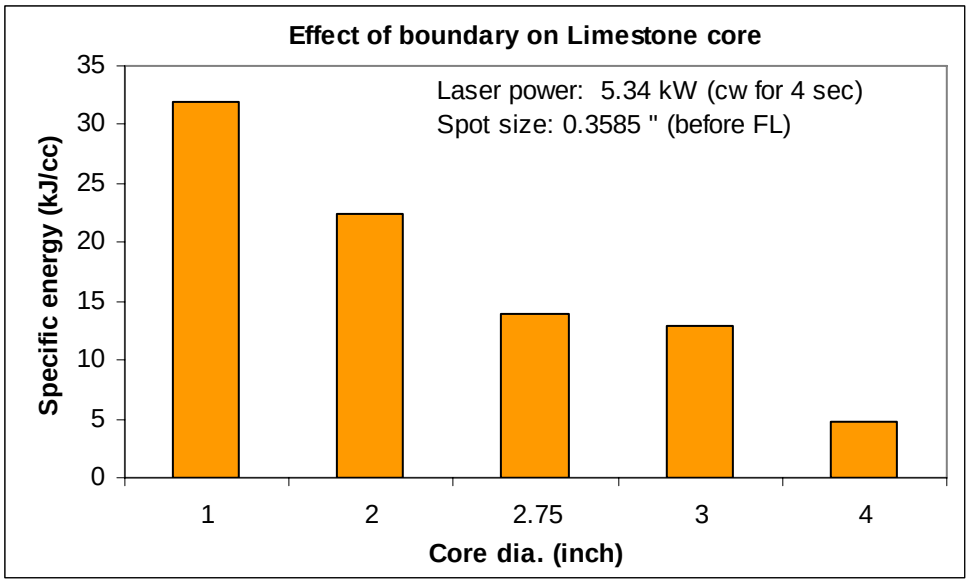

Figure 16. Effect measuring of sample on specific energy for limestone

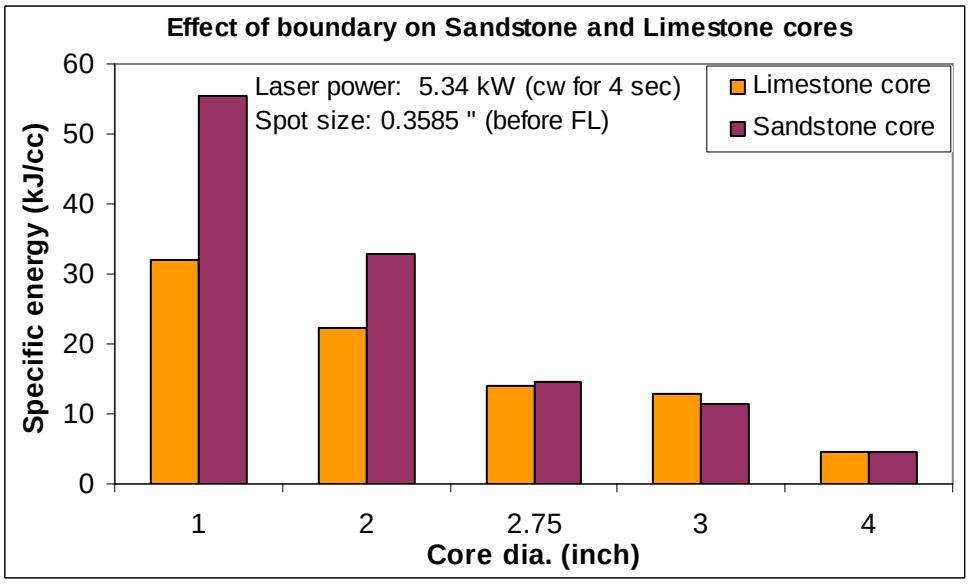

Figure 17. SE Comparison for sandstone and limestone for various sample sizes

Result and Analysis: This test was performed to assist in the dimensional design of a high pressure perforation cell with minimal boundary or secondary effects. The beam spot size was constant at 8.9 mm (0.35 in). It was determined that 10.16 cm (4.0 in) diameter rock sample would be sufficient in minimizing boundary and secondary effects using a 8.9 mm (0.35 in) beam spot size. There were no further tests to confirm the relationship of beam spot diameter and core

diameter. Visual observation of the lased core samples determined that no fractures or cracks developed in the 10.16 cm (4.0 in) rock sample, which correlates with the low observed SE value.

Effect of Beam Intensity on SE

Objective: To determine the effect of beam intensity by lasing the sample with focused and diverged beam of same spot size

Procedure: The shape of the laser beam, and therefore the shape of the resultant hole in rock can be changed by using different types of lenses. A conical shape hole (Figure 18, right) can be created with a focused beam, where the beam diameter increases or decreases along the length of the beam. The sample can be placed either before or after beam's focal point while using a convex lens. Changing the distance between the target sample and lens or altering the focal length changes the dimensions of this cone.

A cylindrical hole was obtained by using a collimated beam (Figure 18, left), where the beam diameter remains relatively constant at any distance from the optics. Controlling the shapes of the hole is significant in terms of fluid flow from the reservoir to the well.

Figure 18. Different hole geometry produced by shaping laser beam with different lenses

The same spot size can be achieved for both converging and diverging beams equidistant on either side of the focal point. To study the difference between energy required to remove same material for both cases, sandstone block measuring 30.48 cm x 15.24 cm x 15.24 cm (12.0 in x 6.0 in x 6.0 in) was exposed to a 5.34 kW (CW) beam for 4.0 s with a converging beam providing a 8.9 mm (0.35 in) beam diameter at the rock face.

The block was lased again with same parameters; however a diverging beam provided an 8.9 mm (0.35 in) beam diameter at the rock face. An optimized nozzle purge system was used with compressed air at 620.5 kPa (90 psig) line pressure. Distance between sample and purge nozzle was fixed at about 2.54 cm (1.0 in). Each experiment was repeated 5 times.

Specific energy achieved with sample placed before and after focal point was calculated for each case. Average values are presented in graph shown below. Less SE was observed to create the same size hole on converging side of focal point as the intensity of the beam continues to increase and less material is removed per unit length as it nears the focal point (Figure 19).

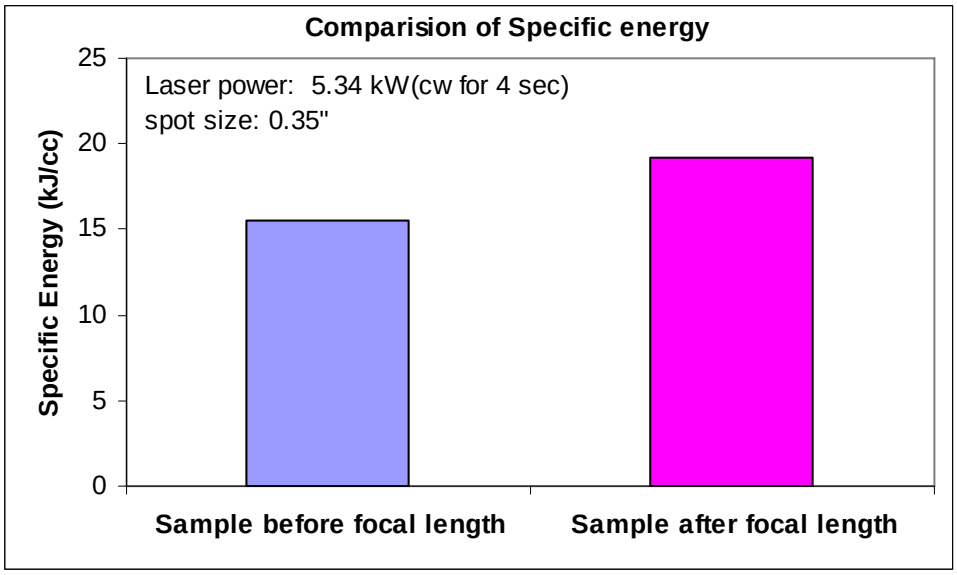

Figure 19. Comparison of SE at different beam density for sandstone

Result and Analysis: Previous tests were conducted using different high power lasers, including MIRACL, COIL, Nd:YAG, CO, diode and CO_2 lasers with focused lenses. The samples were placed before the focal point and sometimes after the focal point (Figure 20). For consistency and accuracy, this test was conducted to learn more about the differences in observed SE values taken before and after the focal point.

The difference between placing the sample before or after the focal point is the beam intensity, or irradiance. The intensity is defined as the beam power applied over an area, (Equation 5)

$$Intensity = \frac{Power}{Area} \quad \text{.....(5)}$$

If the samples are placed before the focal point, keeping the power constant, the area will decrease as the hole deepens toward the focal point. Therefore, the beam intensity will increase up to the focal point. If the sample is placed after the focal point, then the area will correspondingly decrease resulting in a decrease in the intensity with power constant. The result in Figure 19 shows that the SE was less when placed the sample before since volume of material

removed decreases as the intensity increases toward the focal point. The opposite effect occurs when the sample is placed after the focal point, however, as intensity decreases, a minimum intensity will be reached where the rock is no longer cut.

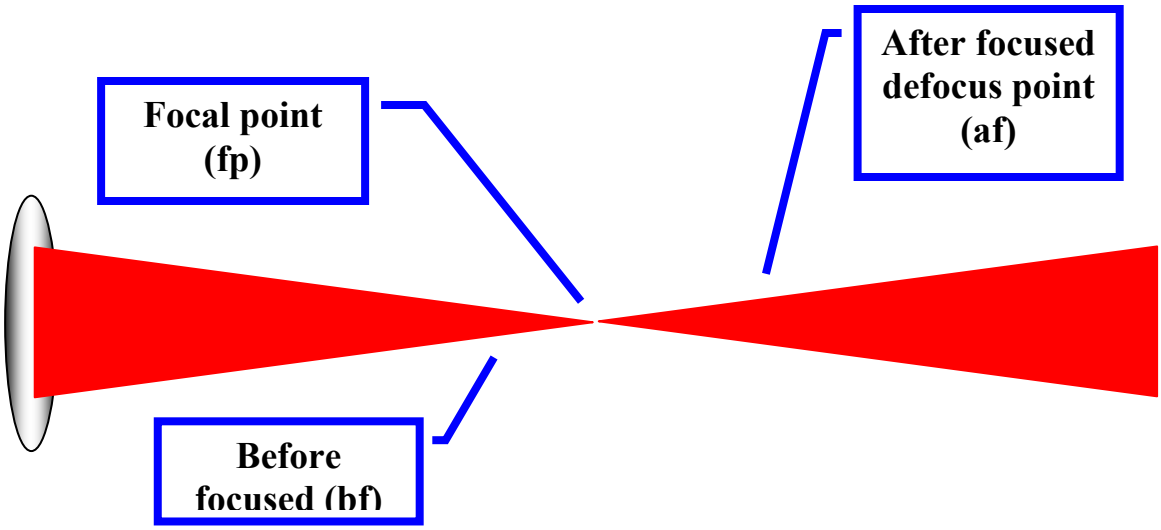

Figure 20. Schematic of laser beam producing same spot size before and after focal point

Position of the samples should be taken into consideration when comparing SE values derived from different laser types. For example, a sample is placed after the focal point with an Nd:YAG laser (Figure 21) and before the focal point while using a COIL (Figure 22).

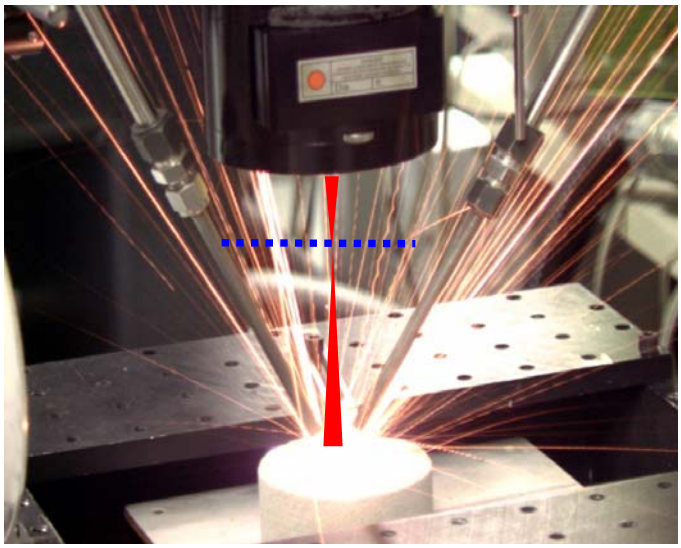

Figure 21. Sample placed after focal point

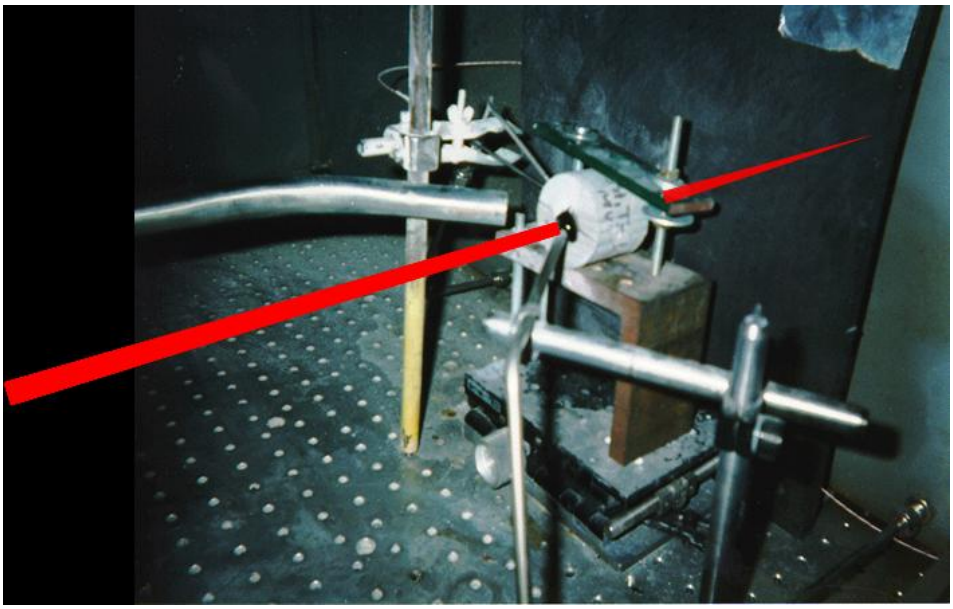

Figure 22. Sample placed before focal point

To understand how effective fiber lasers are in drilling and cutting rock, comparisons were made to results obtained from other lasers used in laser/rock interaction experiments. Figure 23 presents minimum SE values for Berea sandstone and limestone obtained using the fiber laser, as compared to those recorded using other high power lasers.[7,8,9]

The experimental conditions for these reported SE values were not identical, and the methods employed were not consistent. However, each value represents a best attempt at determining optimal conditions of rock removal, thus providing a minimal SE value for the laser/rock combination presented.

To date, the SE values obtained for both sandstone and limestone with the fiber laser were the lowest achieved from reported laser/rock interaction data. Also, there was little difference in the best fiber laser SE values between sandstone and limestone; however there were distinctly higher SE values for limestone as compared to sandstone with the other laser types. Another comparison of SE values was made for each of the same lasers and is presented in Figure 24. In this case, comparisons were made between the average observed SE values obtained using the fiber laser with average SE values recorded using the COIL, CO_2, and Nd:YAG lasers.[10,11]

[7] W.P. Walters, & J.A. Zukas, 1998.

[8] C.B. Reed, *et al*, 2002.

[9] B.C. Gahan, *et al*, 2004

[10] W.P. Walters, & J.A. Zukas, 1998.

[11] C.B. Reed, *et al*, 2002.

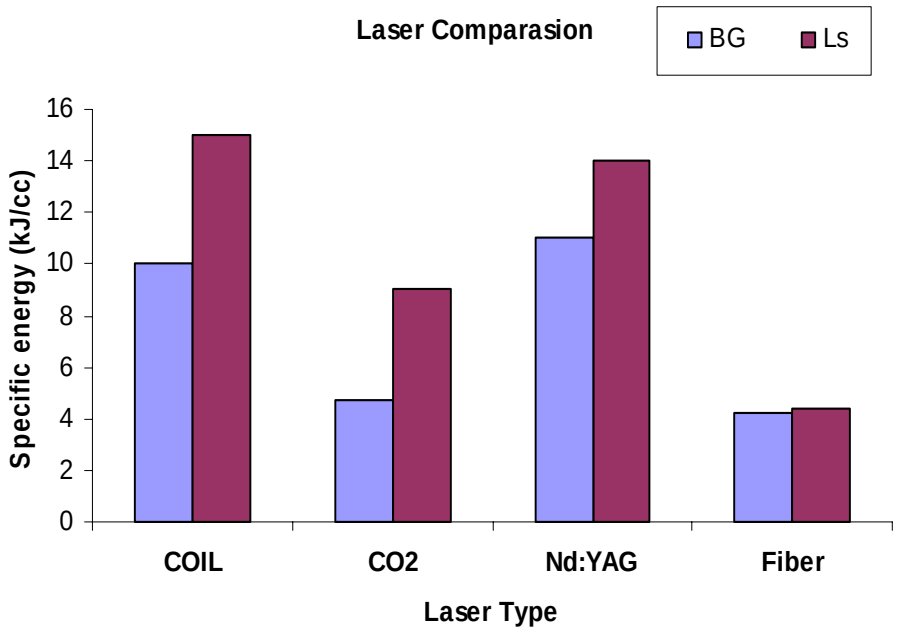

Figure 23. Lowest SE values observed from laser/rock interaction experiments using COIL, CO_2, Nd:YAG and ytterbium fiber lasers on Berea sandstone (BG) and limestone (Ls) at lowest SE conditions.

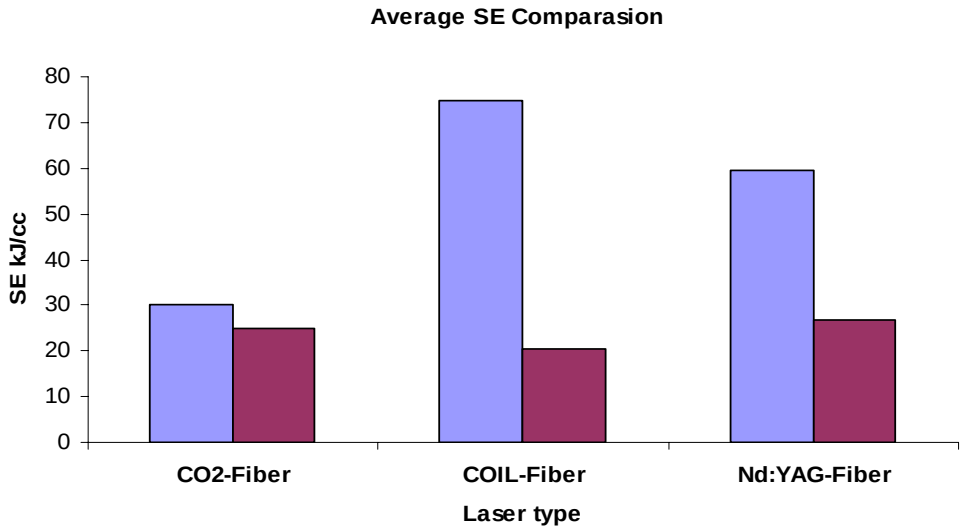

Figure 24. Average specific energy observed from laser/rock interaction experiments comparing results from ytterbium fiber lasers with COIL, CO_2, Nd:YAG on Berea sandstone at identical conditions.

The fiber laser data was collected by repeating the experiments previously performed on Berea sandstone with other laser types under the same conditions (Table 2). The average SE values for all laser types were much higher than the

Table 2. Test parameters per laser type used to experimentally determine comparative fiber laser data and average SE values for Berea sandstone samples.

Test Parameters	COIL	CO_2	Nd:YAG
Average Power, kW	1.40 - 5.34	3.5 - 5.0	0.77 - 1.20
Rep Rate, pulse/sec	CW	CW	100 - 400
Beam Diameter, cm	1.61	0.71	0.15
Exposure Time, sec	8.0	3.0 - 6.9	0.5 - 1.5
Core Diameter, cm	5.08	5.08	2.54
Core Length, cm	5.0 - 10.6	5.00	2.54

best values observed in Figure 23, since SE values at non-optimal conditions were included in the average, and hole diameters were the same as their respective beam diameters. Given these conditions, the fiber laser performed slightly better than the CO_2 laser, and significantly better than the COIL and Nd:YAG lasers.

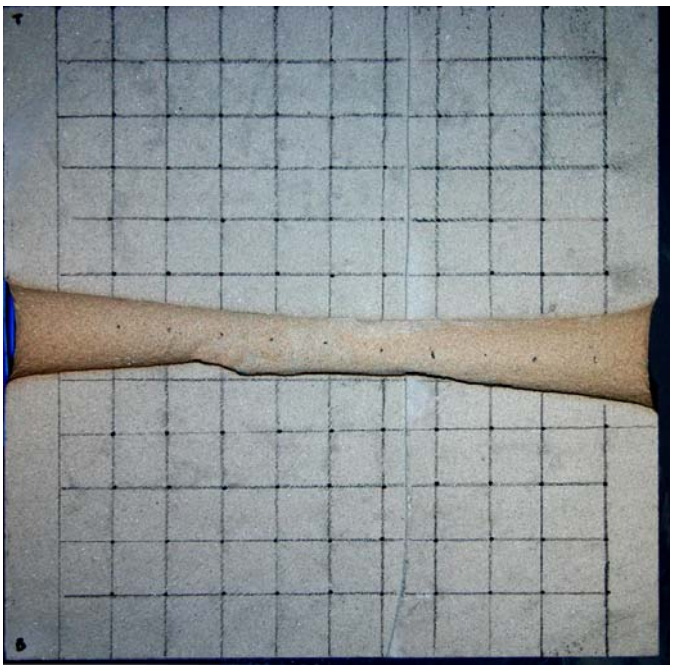

Figure 25. Post-laser cross-section through a cube of Berea sandstone (30.48 cm per side) formed by spallation with 3.2 kW fiber laser beam for 360 s. Tunnel diameter ranges between 2.8 and 5.1 cm.

Recently, a perforation-like tunnel was created under lab conditions in a cubic block of Berea sandstone measuring 30.48 cm (12.0 in) per side using GTI's 5.34 kW ytterbium fiber laser (Figure 25). A borehole fully penetrated the block at an average diameter of 3 cm (1.18 in). A power level of 3.2 kW was

applied to the block for approximately 6.03 minutes, and an SE was calculated at 5.5 kJ/cc[12]. This is the deepest and most energy efficient high power laser application in Berea sandstone reported to date.

Effect of Laser Power on SE (Focused Beam)

Objective: To determine the effect of laser power on limestone and sandstone rock samples using the optimized beam conditions with beam diameter 8.9 mm (0.35 in).

Procedure: For this series of experiments, laser power was applied to limestone and sandstone samples at intervals between 0.5 to 5.0 kW while keeping application time constant (4.0 sec and 8.0 sec). Limestone and sandstone blocks measuring 50.8 cm x 12.7 cm x 12.7 cm (20.0 in x 5.0 in x 5.0 in) were used in this study. One of the 50.8 cm x 12.7 cm (20.0 in x 5.0 in) surfaces was divided into 2.54 cm x 2.54 cm (1.0 in x 1.0 in) grids as shown in the Figure 26. Each grid was lased at power levels from 0.5 to 5 kW in 0.5 kW increment. The beam duration of each hole was kept constant at 4.0 s and 8.0 s for two sets of

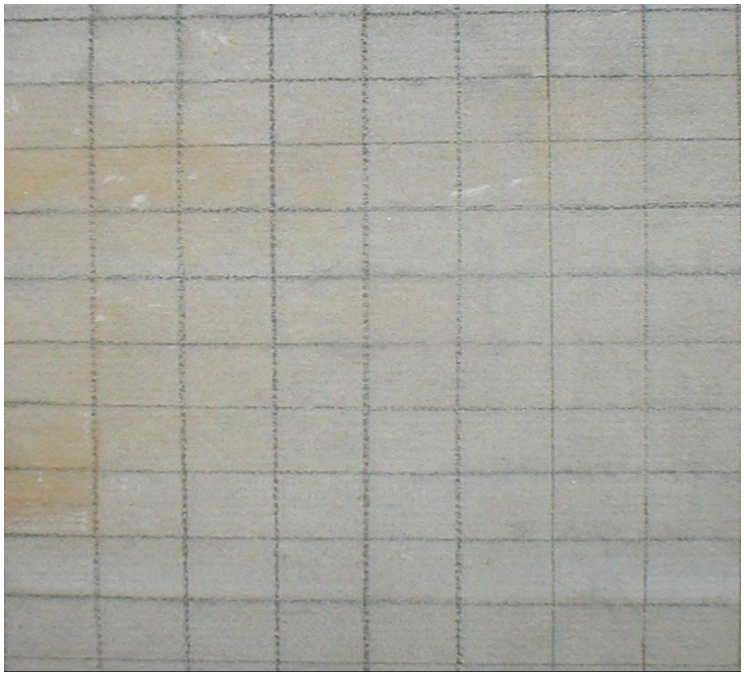

Figure 26. Test block showing grids

experiments. The beam was CW with 8.9 mm (0.35 in) spot size. An optimized nozzle purge system was used with compressed air at 620.5 kPa (90 psig) line pressure. Distance between purge nozzle and sample was about 2.54 cm (1.0 in). Lens with 1000 mm (39.37 in) focal length was used to focus a 2.54 cm (1.0 in) collimated beam. Specific energy values were calculated and are presented in Figure 26.

[12] B.C. Gahan, *et al*, 2004.

Result and Analysis: When a high power laser beam strikes the surface of a rock, energy will be reflected, scattered and absorbed. The absorbed energy is that which is transferred to the sample, and is responsible for breaking and cutting rock. Depending on the sample composition and properties, absorbed energy will be consumed by various mechanisms, including dehydration, vaporization, grain expansion, melting, pore expansion, decomposition, and other factors (Equation 6). Each mechanism occurs within a specific temperature range.

$$E_{Absorb} = E_{Dehy} + E_{Vap} + E_{GrainExp} + E_{Melt} + E_{PoreExp} + E_{Decomp} + E_{Other} \qquad (6)$$

Given this, there are energy absorption/thermal accumulation issues that may affect the laser's cutting efficiency. For example, as high power lasers transfer energy to silica-based rocks, quartz mineral grains begin melting around 1900°C (3452 °F). This phase change in the mineral results in a reduction in rock cutting capability as the melted material absorbs and reflects beam energy.

An initial test firing of the laser system was made by exposing a Berea sample to a 2.54 cm (1.0 in) diameter beam at 3.0 kW for 62.0 s. A hole with dimensions of 7.62 cm (3.0 in) deep and 2.54 cm (1.0 in) diameter at opening was created through spallation of the grains with no evidence of grain melt (Figure 27).

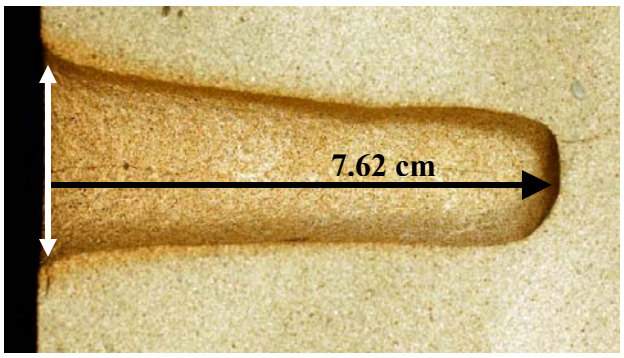

Figure 27. Post-laser cross-section of a hole in Berea sandstone formed by spallation with 3 kW for 62 s. Dimensions are 7.62 cm (3.0 in) deep and 2.54 cm (1.0 in) diameter at opening.

To further analyze this result and learn more about the spallation mechanism, a test was designed to investigate more about spallation and the sample went through a series of analyses that include mineralogy, infrared and thermal analyses.

Spallation Test in Berea Sandstone:

To investigate the conditions by which the Berea sandstone quartz grains begin to melt with the fiber laser, and thus the limit for efficient spallation conditions, a block of Berea sandstone was exposed to several beams where the laser power was increased from 0.5 kW to 5.0 kW at 0.5 kW increments.

Visual analysis is presented in Figure 28, with images of laser interaction on sandstone at increasing power increments of 0.5 kW. Visual observations between 0.5 kW and 5.0 kW range from scorched surface to production of melt.

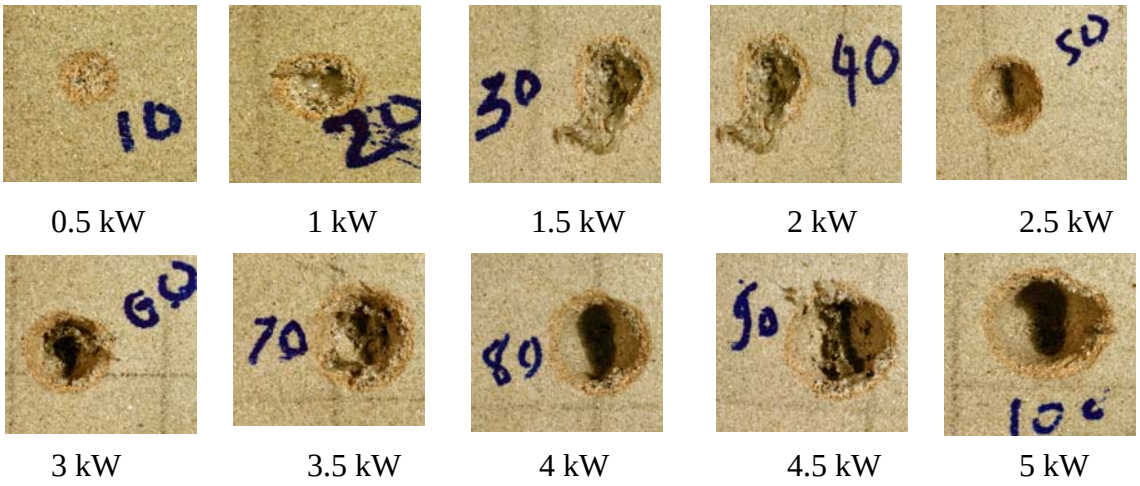

Figure 28. Sandstone sample lased by HPFL at different power level, the top left shows lowest power percentage

This was accomplished while holding all other variables constant, including beam duration and spot size at 4.0 s and 8.9 mm (0.35 in), respectively. As a result, beam intensity on the target ranged from 1607 to 8037 kW/sq. cm.

A single hole was created in the block for each exposure, and the results are presented in Figure 29. Given the conditions of the tests, a power level of about 3.0 kW provided a clean hole (no melted quartz grains) at a minimum SE value of 25 KJ/cc. Exposures at power levels less than 3.0 kW produced less rock volume removed and no evidence of mineral melt. However, exposures at power levels greater than 3.0 kW produced holes greater than 5.0 cm (1.97 in) deep with accompanying mineral melt.

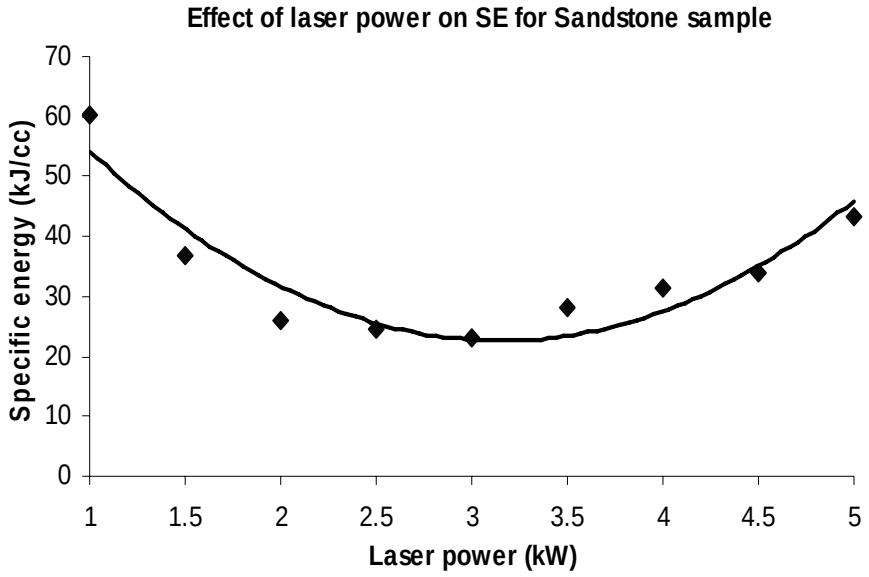

Figure 29. Laser power vs. SE for fiber laser exposed to Berea sandstone at constant beam duration and spot size.

A 3-D image of a hole lased in Berea sandstone at 3.0 kW, 4.0 s beam duration, and 8.9 mm (0.35 in) is presented in Figure 30a and Figure 30b.

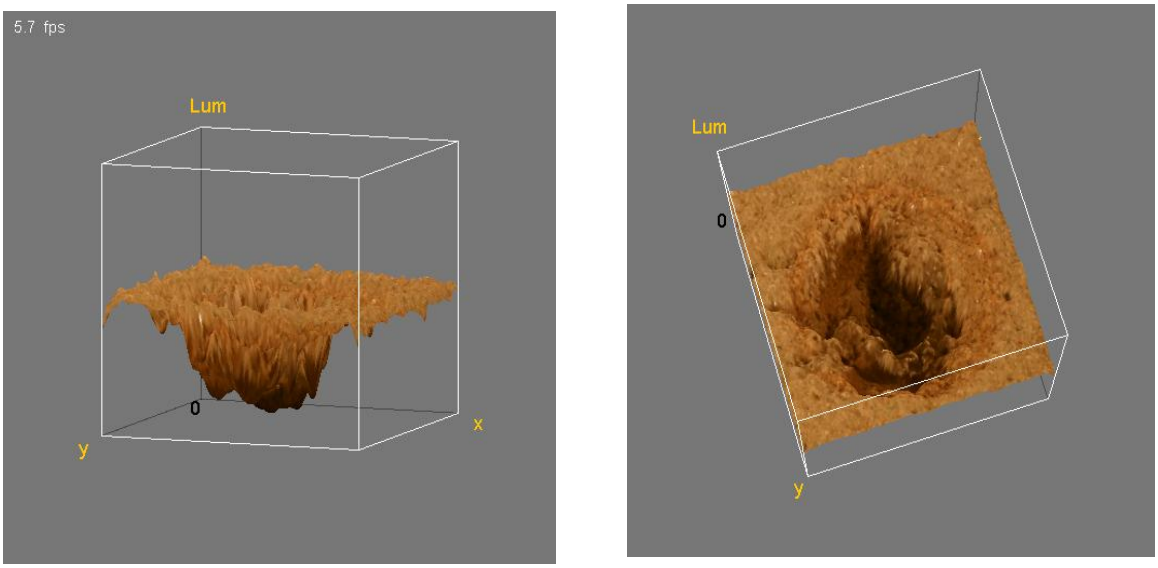

Figures 30a and 30b. Lased hole of Berea sandstone by HPFL at 3.0 kW.

Thermal Effects on Berea Sandstone

Thin section, thermographic and thermogravimetric methods were used to evaluate and analyze the resulting data.

Thin Section Analysis

This analysis (Figure 31) provides the physical properties and composition of the Berea sandstone sample. Mineral composition consists mainly of quartz (95%) with other constituents, including feldspars (5%) and traces of black organic material and fragments. The type of cementation that binds the grains together is silica (SiO_2).

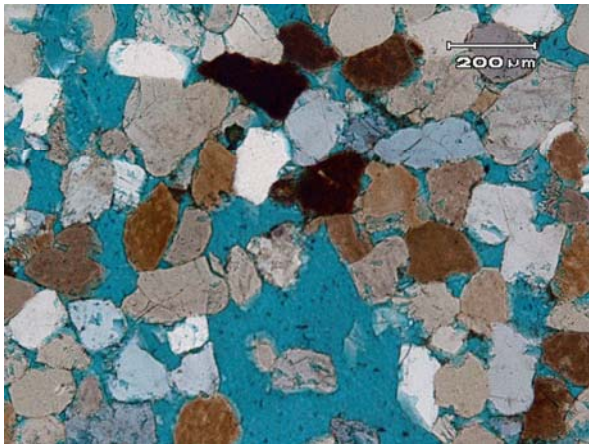

Figure 31. Thin section of sandstone sample showing mineralogy, cementation and grains.

Thermographical Analysis

Figure 32 illustrates the thermal behavior of rock when exposed to the beam as a function of time. The average temperature of the rock during lasing was about 1200 °C (2192 °F).

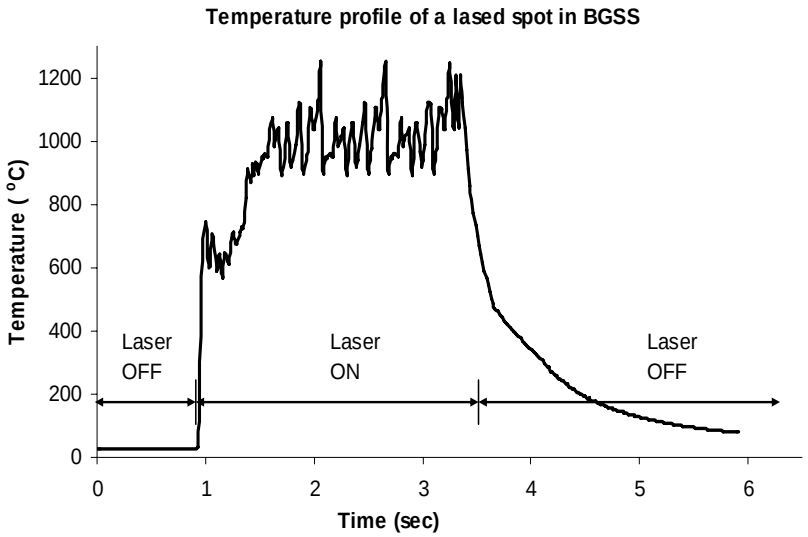

Figure 32. Temperature vs. time profile of fiber laser beam on Berea sandstone with 3.0 kW power beam and 8.9 mm (0.35 in) beam diameter.

As seen in Figure 32, there is a sharp rise in the temperature of the rock as the rate of absorbed energy from the beam greatly exceeds the rocks ability to dissipate heat away from the exposed area. The temperature range of the rock induced by a 3.0 kW beam with 8.9 mm (0.35 in) diameter was sufficient to break the cementation material and cause dehydration, decomposition, vaporization and grain expansion that resulted in the spallation of the rock grains. An external purge gas quickly removed spalled grains out of the hole and away from the beam.

Figure 33 shows an image of the Berea sandstone block captured with an infrared camera while exposed to this 3.0 kW beam. Temperature profiles across lines L1 and L2 are presented below the image. Thermal stress, produced by high temperature gradient and differential thermal expansion of minerals, breaks the bonds between the grains. Thermal accumulation in the sample is not sufficient to induce melting of quartz grains (>1900 °C [3452 °F]).

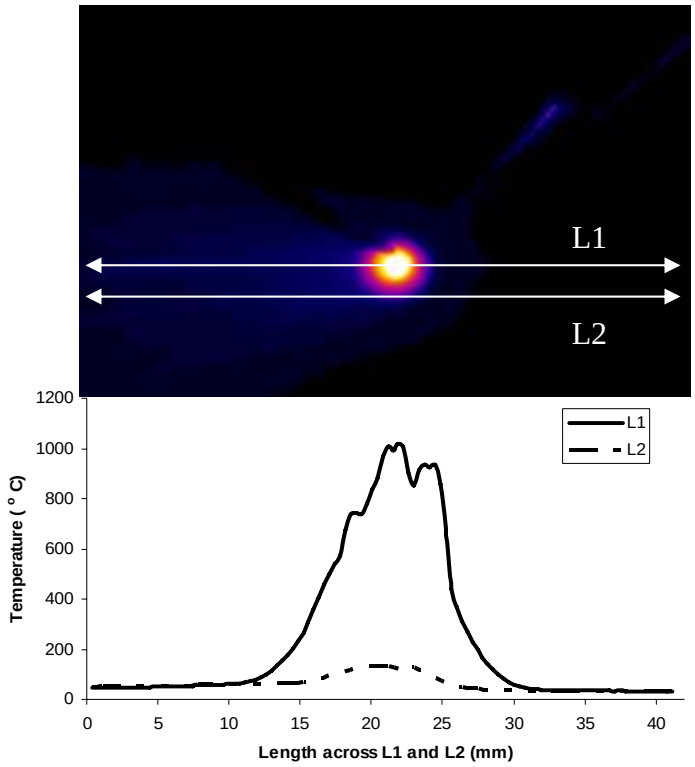

Figure 33. Infrared video capture during laser exposure on Berea sandstone with temperature profile across the laser contact point (line L1) and immediately below the laser contact point (line L2).

Since the temperature of the exposed rock sample remains below the melt temperature of the quartz grains, the primary rock removal method is spallation. The spallation temperatures in sandstone have been documented as ranging between 400 – 800 ^{o}C (752 – 1472 °F)[13]. Should local temperatures rise and

[13] W.H. Somerton, 1992.

phase changes occur in the rock minerals, such as melting and vaporization, absorbed energy is redirected away from the rock cutting process.

There are physical and chemical changes occurring throughout this temperature range associated with the process of spallation. A primary physical change associated with spallation of the rock results from the thermal expansion of the grains. A sudden temperature increase in sandstone, results in the expansion of quartz and plagioclase grains.

The degree of expansion in each mineral is different. Table 3 presents the thermal expansion of the principal Berea sandstone minerals in one direction, as a percent

Table 3: Single-axis Thermal Expansion of Sandstone Minerals at Different Temperatures as a Percent of Original Size[14].

Mineral	100 ^{o}C	200 ^{o}C	400 ^{o}C	600 ^{o}C
Quartz	0.14	0.3	0.73	1.75
Plagioclase	0.09	0.14	0.22	0.83

of original size, at temperatures between 100 °C (212 °F) and 600 °C (1112 °F). As closely packed grains in the matrix expand with a rapid rise in temperature, they develop stress fractures and cracks within the grains, as well as break the cementation of adjacent grains. As a result, the affected grains will begin to break free from one another. A purge gas assists in removing the loose grains away from the hole and the beam path.

The effects of differential thermal expansion can be seen by comparing the physical characteristics between pre- and post-lased grains. Figure 34 shows a magnified view (32X) of loose grains from Berea sandstone, carefully prepared and extracted from the rock sample before lasing. The grains observed in this sample are well sorted, and the shapes of the grains are characterized as round and sub-round.

Figure 35 shows the same magnified view of sandstone grains collected following their spallation and ejection from the rock sample during lasing. Note the angular broken grains and poor sorting due to stresses imposed by thermal expansion and cooling.

[14] W.H. Somerton, 1992.

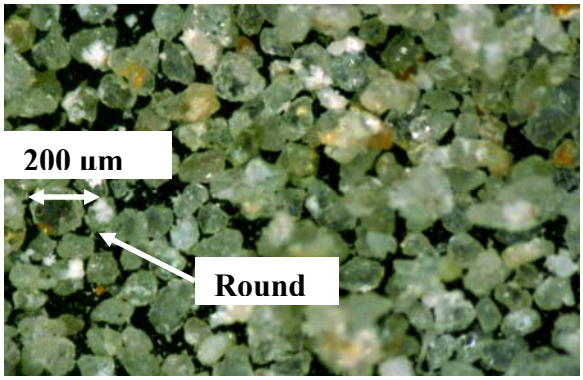

Figure 34. Berea sandstone grains (pre-lase) at 32X.

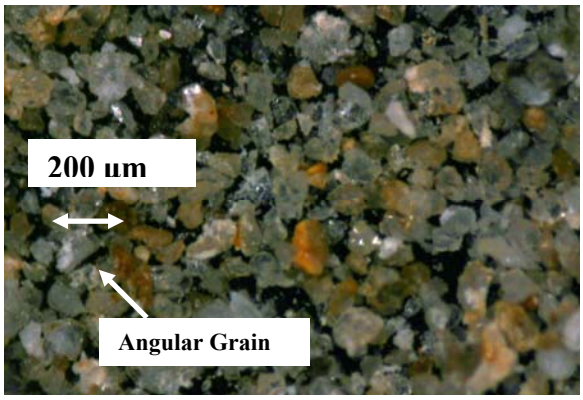

Figure 35. Berea sandstone grains (post-lase) at 32X.

Chemical changes to the rock matrix occur as black organic material and other fragments present in the sandstone matrix dissociate, dehydrate, decompose and/or vaporize at temperatures lower than that required to melt quartz. The Berea sandstone sample was composed of less than 5% of this material by volume. As this material was altered or removed during lasing, adjacent mineral grains were allowed to break free from the matrix.

Thermogravimetric Analysis:

The chemical changes that occur in rock over a temperature range can be observed using thermogravimetric analysis (TGA). A fragment of the Berea sandstone sample with a mass of about 31 mg (0.0011 oz) was heated from 50°C (122 °F) to 1200 °C (2192 °F) at the rate of 3.33 °C/s (6.53 °F/s) to measure weight loss at elevated temperatures. Results confirmed the weight loss due to organics present in the matrix. Nearly 2.0 percent weight loss was observed as a function of temperature, and occurred as predicted between 400 and 800 ^{o}C (752 and 1472 °F).

Figure 36 shows the spallation temperatures at which the bonds between the grains weaken and break. It illustrates the thermal effects of exposure from a 3.0 kW beam at 8.9 mm (0.35 in) diameter on Berea sandstone as temperatures increase from room temperature to 1200 °C (2192 °F). Of note is the response

in the 400 to 800 °C (752 to1472 °F) range, where much of the rock's physical and chemical changes occur, confirming the spallation temperature zone as presented in the literature.[15]

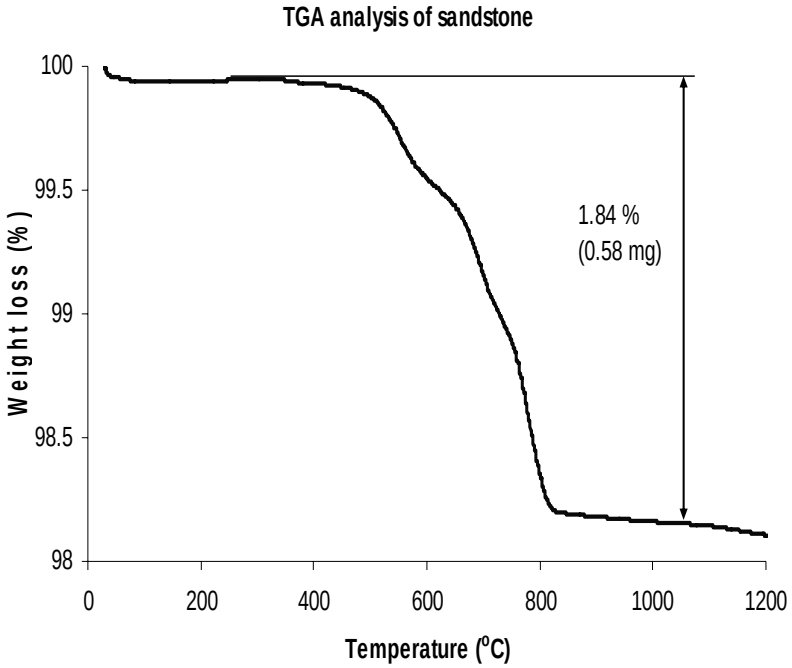

Figure 36. Weight loss as a function of temperature for Berea sandstone using TGA.

Thermal Effects on Limestone

The removal mechanism of laser rock interaction with carbonates, including limestone, is different from sandstone due to mineralogy and chemical composition. Thermal dissociation, or calcination, takes place when the beam is exposed to limestone, producing lime (CaO) and carbon dioxide gas (CO_2), (Equation 7). No melting was observed in limestone.

$$CaCO_3 \rightarrow CaO + CO_2\uparrow \qquad (7)$$

The dissociation takes place at less than 1200 °C (2192 °F), as can be seen from results of a DTA analysis (Figure 38).

For applications to limestone, a higher beam power is required than sandstone using the same beam dimensions and duration. HPFL power of at least 3.5 kW was required for an 8.9 mm (0.35 in) beam at 4.0 s to remove material through thermal dissociation. Although there was no significant material loss at lower power levels, enough mass loss was measured to allow the calculation of SE values (Figure 37). In order to drill into limestone at lower power levels, beam

[15] Maurer, W.C., 1968, 1981.

diameter was reduced accordingly to achieve a minimally required beam intensity.

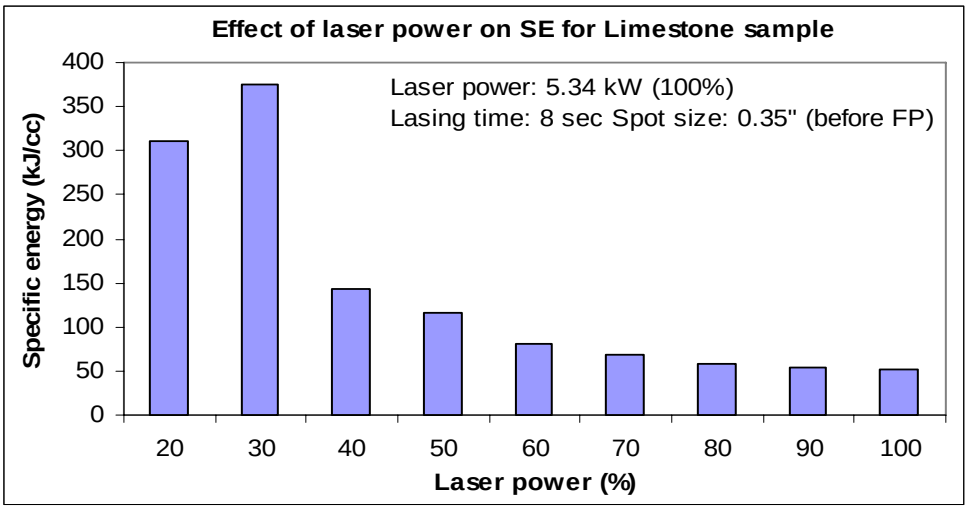

Figure 37. HPFL optimization test for limestone showing SE value as the power increments of 10%, beam duration of 8 s, and beam diameter of 8.9 mm (0.35 in).

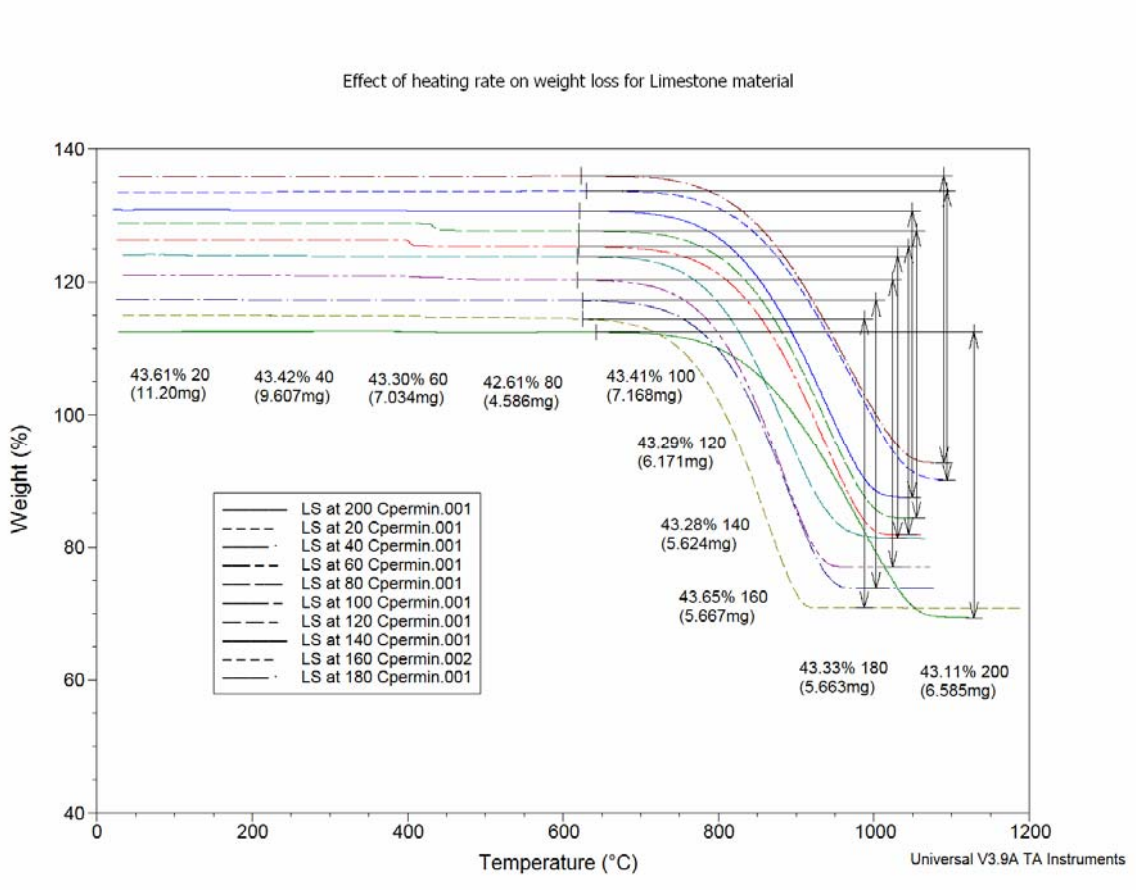

Figure 38. DTA analysis of limestone showing weight change as a function of temperature.

Effect of Beam Duration on SE (Focused Beam)
Objective: To determine the effect of laser power on limestone and sandstone rock samples using the optimized beam conditions with beam diameter 8.9 mm (0.35 in).

Procedure: The purpose of this test was to study the effect of beam duration varying time from 1 s to 20 s on limestone and sandstone samples. Limestone and sandstone blocks measuring 50.8 cm x 12.7 cm x 12.7 cm (20.0 in x 5.0 in x 5.0 in) were used in this study. One of the 50.8 cm x 12.7 cm (20.0 in x 5.0 in) surfaces was divided into 2.54 cm (1.0 in) square grids. Each grid was lased at 5.34 kW laser power. The beam duration of each hole was increased incrementally by 1.0 s from 1.0 s to 20.0 s. The beam was CW at 8.9 mm (0.35 in) diameter and 5.34 kW power.

An optimized nozzle purge system was used with compressed air at 620.5 kPa (90 psig) line pressure. Distance between purge nozzle and sample was about 2.54 cm (1.0 in). Lens with 1000 mm (39.37 in) focal length was used to focus a 2.54 cm (1.0 in) collimated beam. Specific energy values were calculated and presented in the figures below.

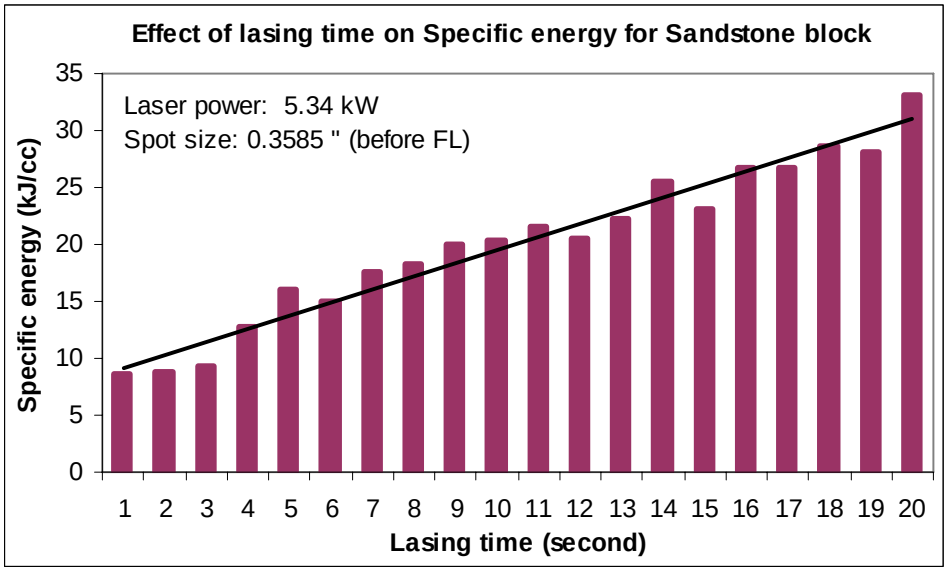

Figure 39. Beam duration vs. SE for Berea SS, from 1.0 s to 20.0 s at 1.0 s increments.

Result and Analysis: The first test was conducted on a block of Berea sandstone and limestone. One block for each rock type was used so that the rock properties will be constant. Laser power remained constant for each application at full power (5.0 kW), while varying beam duration. Beam durations were increased from 1.0 s to 20.0 s at increments of 1.0 s. Figure 39 shows the application results on sandstone.

There was a trend between beam duration and SE. This indicates that beam penetration is proportional to beam duration. Although, beam time on the rock

increases interaction with the rock, more plasma formation and exsolved gases exit through the beam with a reduction in energy efficiency. As the hole deepens, external purging is less effective from a fixed nozzle position.

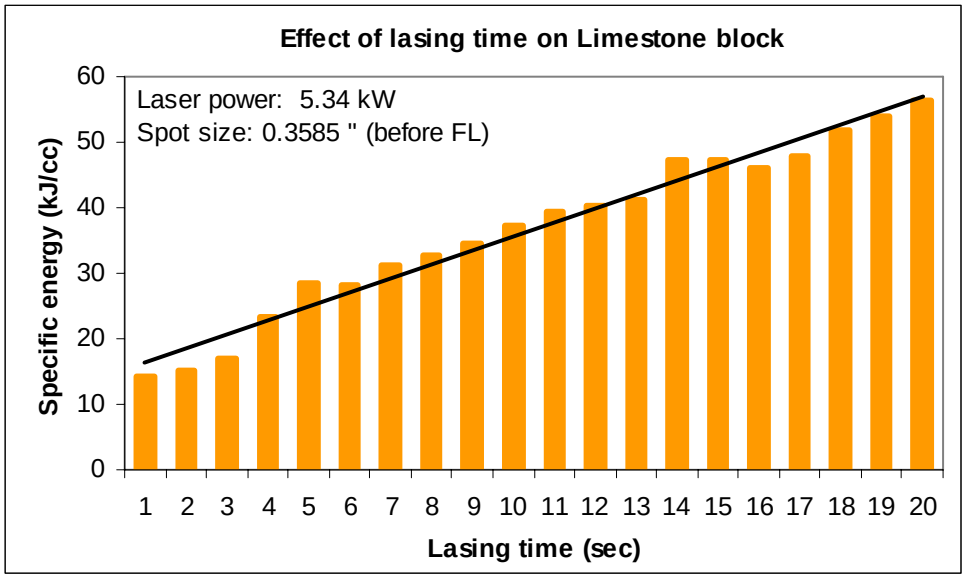

Figure 40. Beam duration vs. SE for limestone, from 1.0 s to 20.0 s at 1.0 s increments.

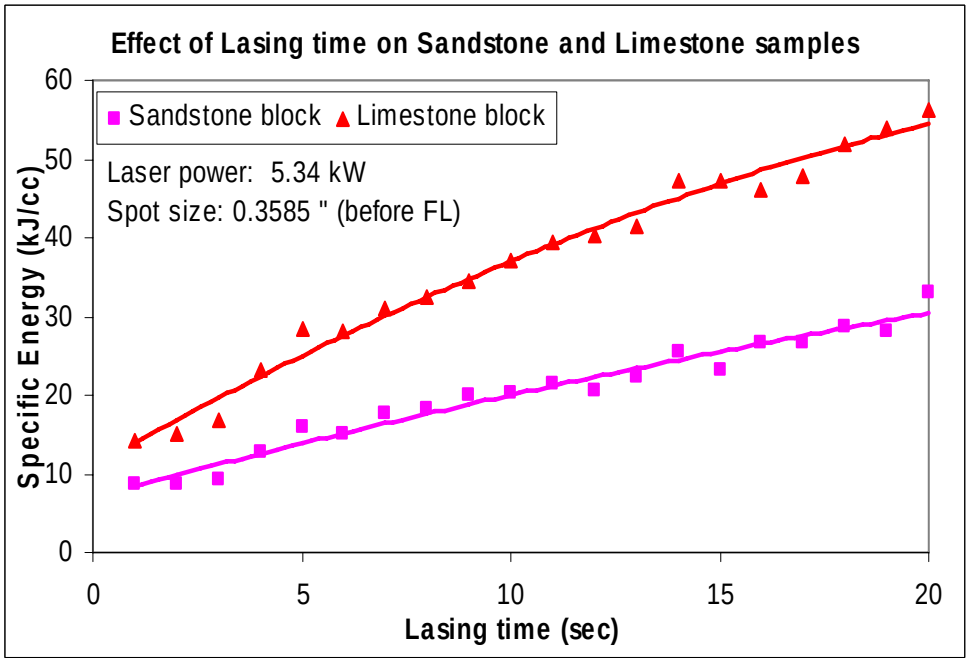

Figure 41. Beam duration vs. SE for LS and Berea SS, from 1.0 s to 20.0 s at 1.0 s increments.

Another test was conducted on limestone (Figure 40). The data present a relationship between SE and beam duration, where an increased continuous application time results in a higher observed SE. Comparing beam duration results from both samples in Figure 41, both samples show a similar trend of

decreasing rock removal efficiency as greater continuous beam application results in a higher SE.

Frequency Effects on SE

Objective: To study the effect of beam repetition rate on depth of penetration and SE for limestone and sandstone using a focused beam.

Procedure: A block of limestone measuring 50.8 cm x 12.7 cm x 12.7 cm (20.0 in x 5.0 in x 5.0 in) was prepared. One of the 50.8 cm x 12.7 cm (20.0 in x 5.0 in) surfaces was divided into 2.54 cm (1.0 in) square grids as shown in the Figure 42. A Berea sandstone block measuring 30.48 cm x 40.64 cm x 10.16 cm (12.0 in x 16.0 in x 4.0 in) was also prepared. One of the 30.48 cm x 40.64 cm (12.0 in x 16.0 in) surfaces was divided into 2.54 cm (1.0 in) square grids. Each grid was exposed to a 5.34 kW beam for 8 s with frequency varying from 1 to 999 Hz (Figure 42).

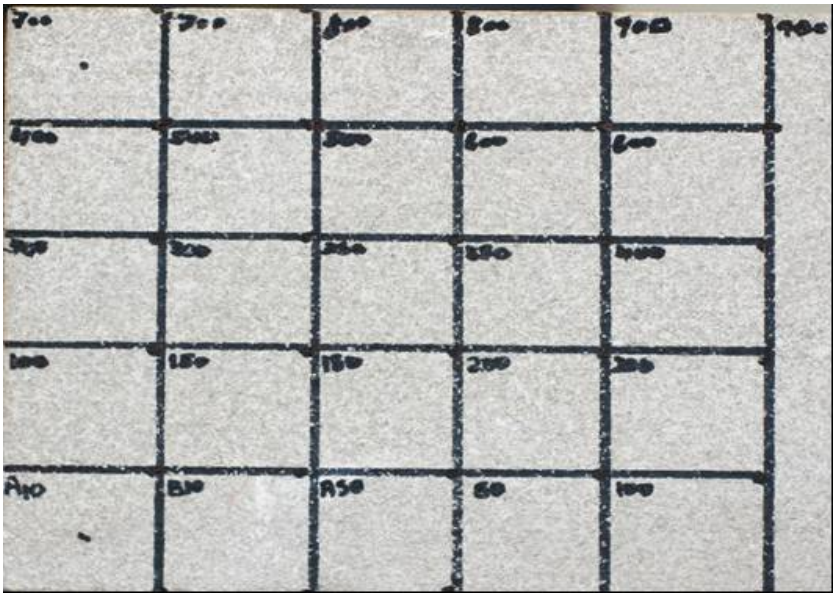

Figure 42. Surface of limestone block with experiment grid.

This experiment set up is presented in Figure 43. An optimized nozzle purge system was used with compressed air at 620.5 kPa (90 psig) line pressure. Distance between purge nozzle and sample was about 2.54 cm (1.0 in). Lens with 1000 mm (39.37 in) focal length was used to focus 2.54 cm (1.0 in) collimated beam. Spot size (penetrating laser beam diameter) was kept 8.9 mm (0.35 in). A PLC pulsar (Omron CPM2C) was used to control the repetition rate of laser

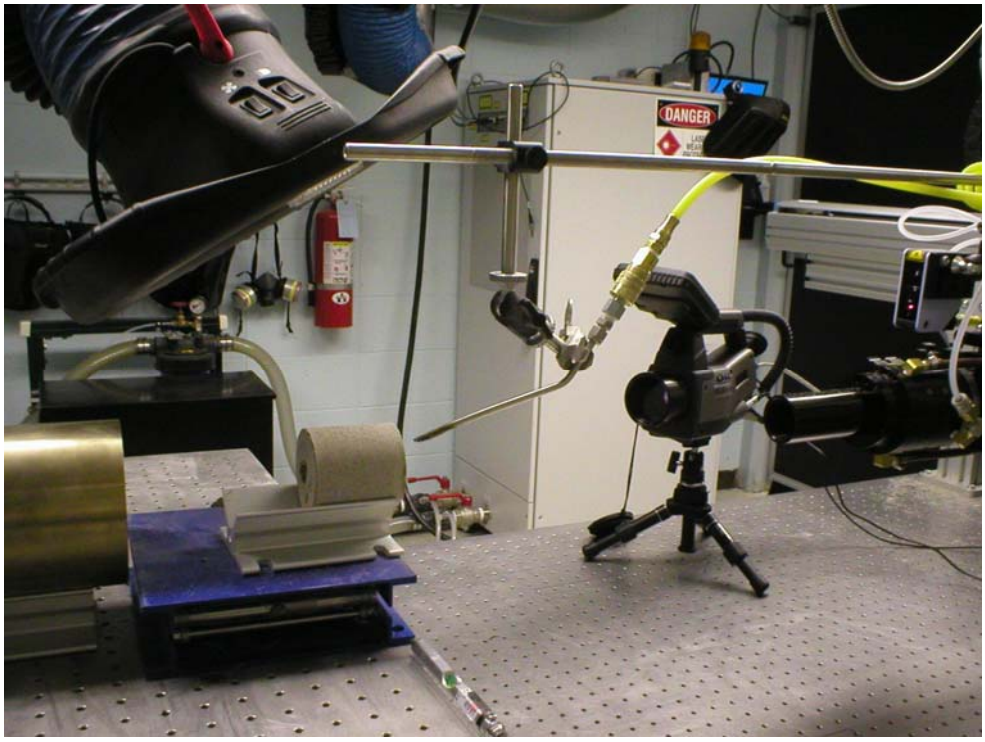

Figure 43. Experimental set up for frequency test

exposure. The PLC pulsar can alter the beam frequency from 0.1 Hz to 999.9 Hz, as well as beam duration for each frequency cycle. All experiments were performed at a 50 % and 99 % duty cycle.

Result and Analysis: Two sets of experiments were conducted to evaluate the effect of frequency on the SE. The first set was performed by changing the frequency from 1 to 10 pulses per second at an increment of 1 pulse per second for both sandstone and limestone samples. The second set was performed by changing the frequency from 10 to 999 Hz at a frequency of 10 pulses per second.

Visual observations of the sample failed to identify any significant change in terms of melt or damage. Some melt was formed on exposures at the edge of the rock sample which can be attributed to a boundary effect. (Figure 44)

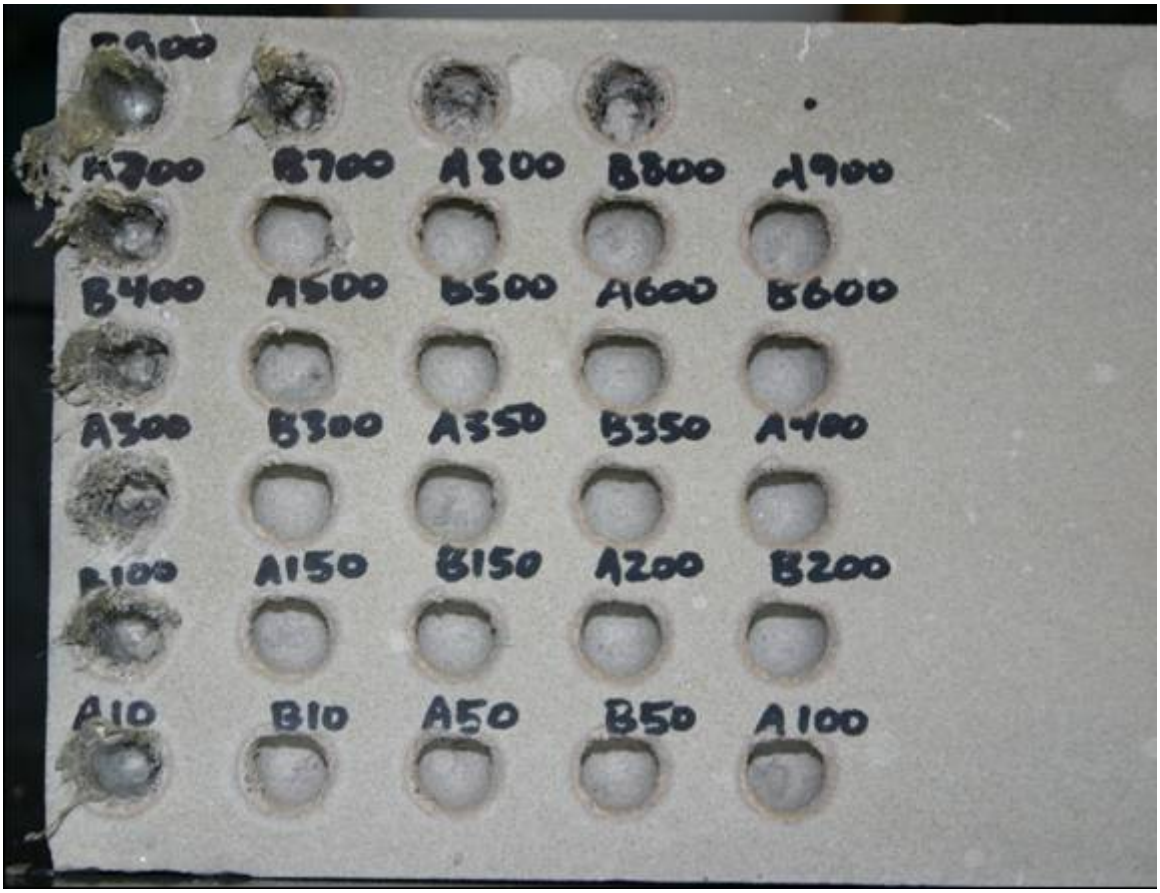

Figure 44. Berea sandstone results from changing frequency from 10 to 999 Hz.

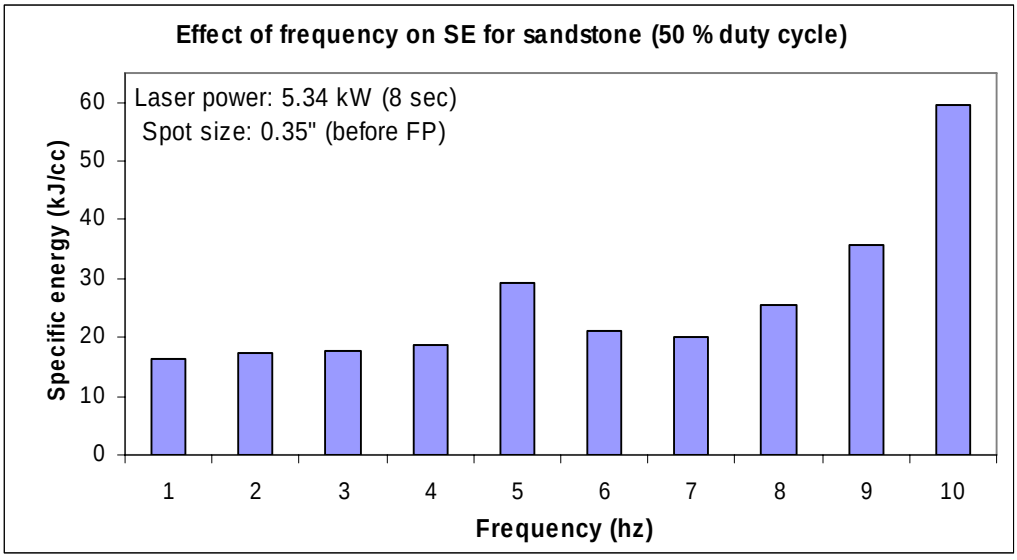

Figure 45. Pulsation from 1 to 10 Hz for sandstone at 50% duty cycle.

The results of lasing sandstone from 1 to 10 Hz are presented in Figure 45. There was a not significant change from 1 to 8 Hz, however observed SE increased noticeably at 9 Hz, with a more significant increase at 10 Hz.

The result indicates that frequency less than 9 Hz results in lower relative SE values since pulsing the beam allows intermittent interaction with the rock sample. The continuous purge allowed energy absorbing dust and gas plumes to be cleared of the beam path. When increasing the frequency from 10 to 999 Hz, the beam behaves similarly to a continuous wave beam (Figure 46).

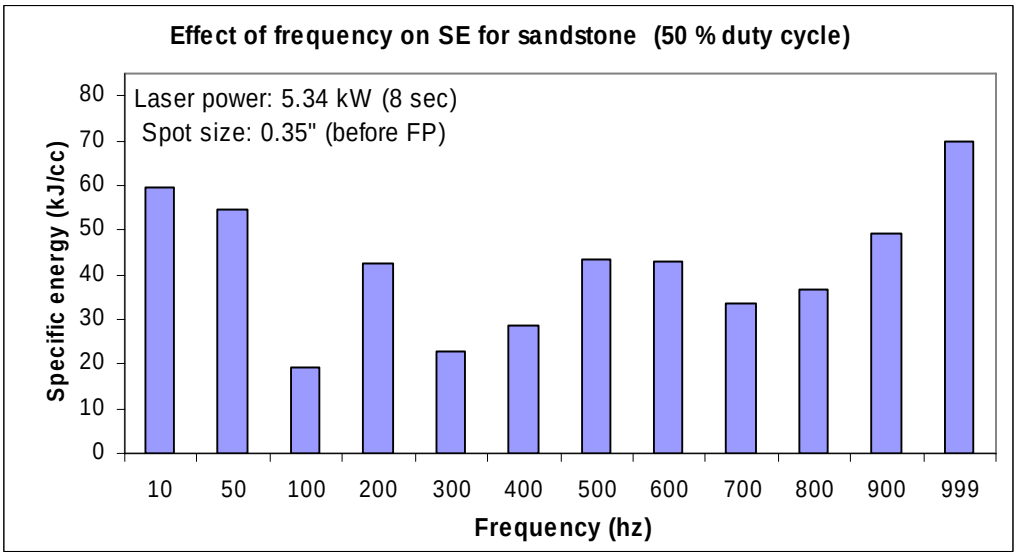

Figure 46. Pulsation from 10 to 999 Hz for sandstone at 50% duty cycle.

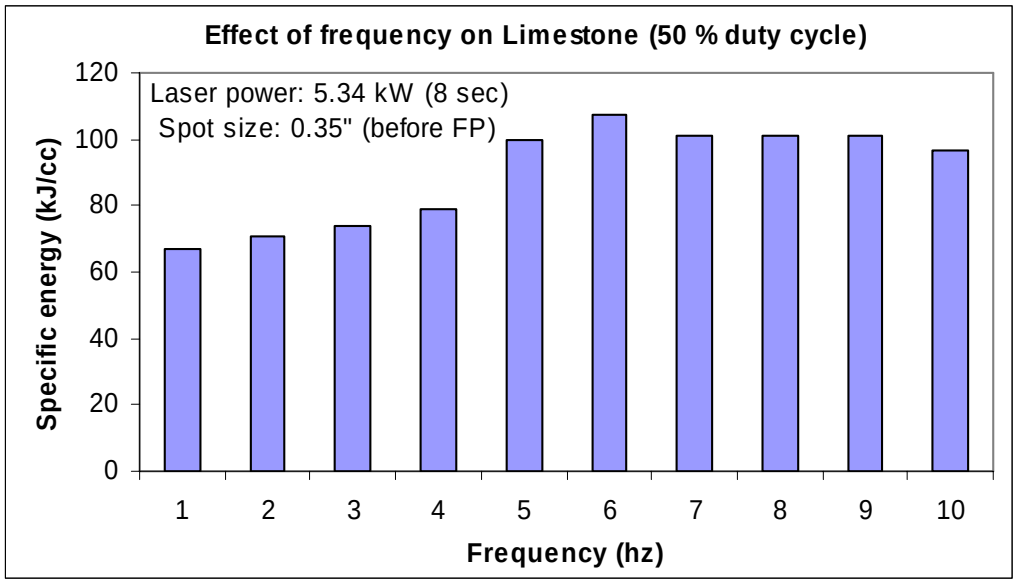

Figure 47. Pulsation from 1 to 10 Hz for limestone at 50% duty cycle.

A repeated test on limestone exhibited the same trend as seen in sandstone. An increase in beam frequency generally resulted in an increase in observed SE, and the beam behaved more as a continuous wave (Figure 47). Limestone requires greater beam intensity to initiate thermal disassociation, and therefore a greater relative observed SE than in sandstone.

Effect of Saturation and Purge Gas Type on SE

Objective: To study the effects of beam interaction on SE with limestone and sandstone saturated in brine, oil and water in the presence of different non-reactive purge gases.

Procedure: The laser-rock-fluid interaction test was conducted on Berea sandstone and limestone. Sandstone and limestone cores measuring 5.08 cm (2.0 in) diameter x 5.08 cm (2.0 in) height were placed in vacuum environment for about 6 hrs and then saturated separately with water, brine or oil for at least 24 hours.

The composition of the brine was a mixture of 25,000 ppm potassium chloride (KCl) and 25,000 ppm sodium chloride (NaCl) in 1,000 ml of water. The density of the brine was 1.039 gm/cm^3. The oil used in testing had a density of 0.841 gm/cm^3.

Each sample was placed in Plexiglas chamber specifically designed to contain debris and harmful vapor as shown in Figure 48. Each saturated sample was lased for 8 s with 5.34 kW (CW) laser power. Lens with 1000 mm (39.37 in) focal length was used to focus 2.54 cm (1.0 in) collimated beam. Spot size was kept constant at 8.9 mm (0.35 in) before focal point. Air, argon, nitrogen and helium were used independently on sandstone and limestone samples saturated with water, brine and oil to see the effect of purge gas on specific energy. The purging gas provided a simulated reservoir condition (an oxygen-free environment) while removing rock debris and vapor from the beam path.

An optimized nozzle purge system was used with compressed air at 620.5 kPa (90 psig) line pressure. Distance between purge nozzle and sample was about 2.54 cm (1.0 in). Specific energy was calculated based on weight differential and geometric methods. Results are presented in graph below for both sandstone and limestone.

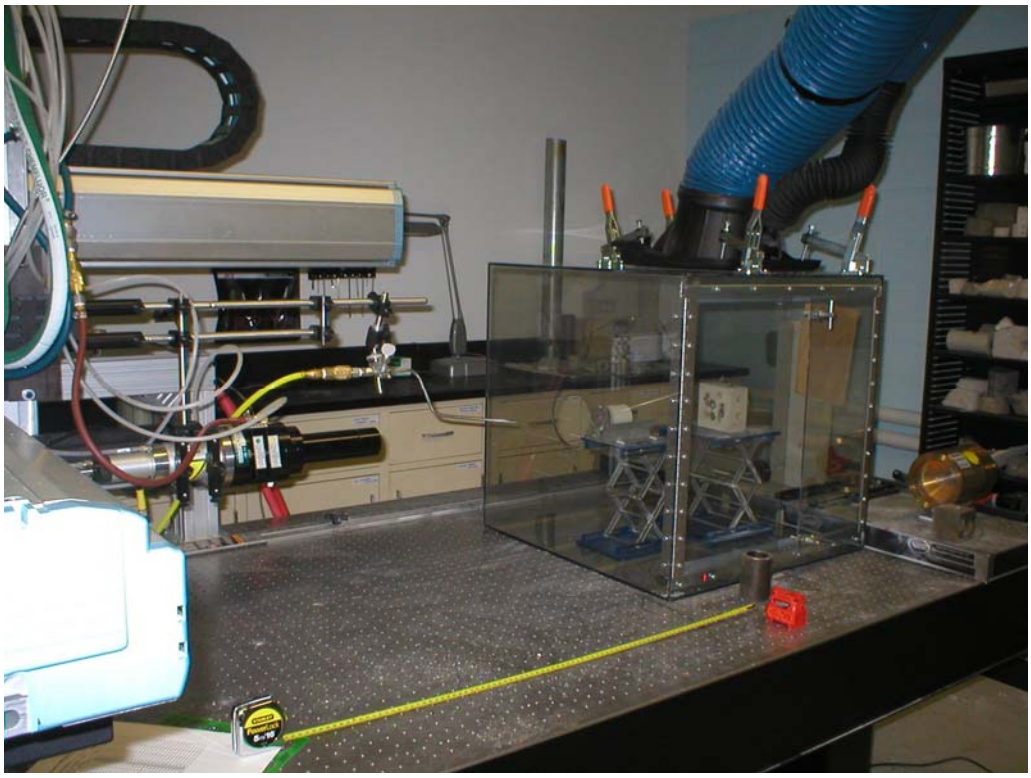

Figure 48. Experimental set up showing Plexiglas chamber to contain hazardous fumes

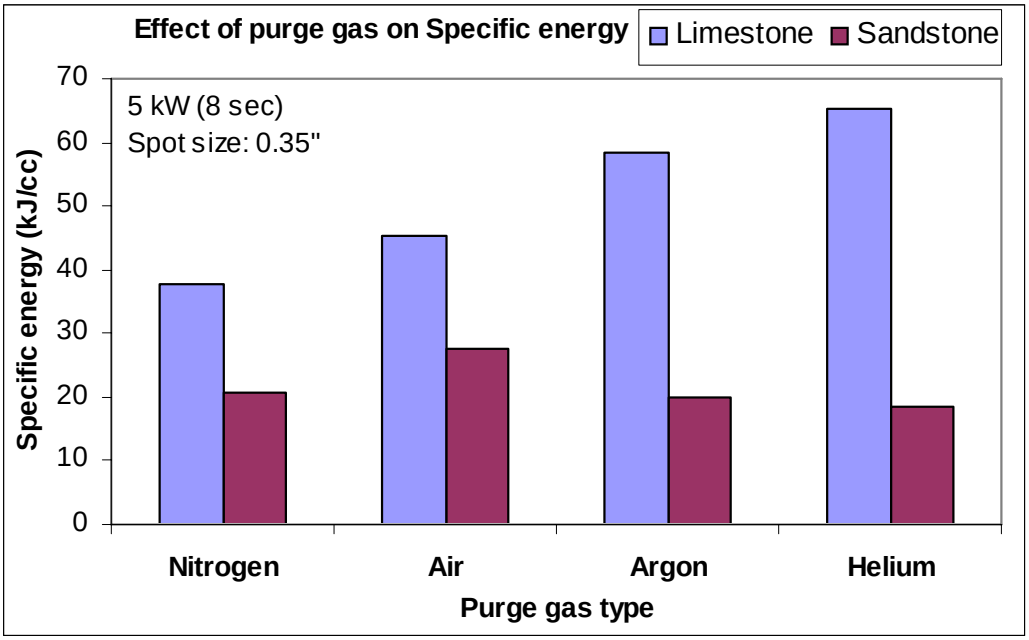

Figure 49. Effect of purge gas type on SE for limestone and sandstone

Results and Analysis:

Purge Gas Type: This test was performed to determine if a change in the gas atmosphere near the hole during lasing affected SE. Four types of gas were used; nitrogen, compressed air, argon and helium. The purge gas was used to simulate reservoir conditions (oxygen-free environment) while removing debris and gases from the beam path.

For both sandstone and limestone, nitrogen provided the lowest observed SE values. The results are favorable given that operation of the tool in a pressurized hydrocarbon environment downhole will require a non-reactive gas, and nitrogen is commonly used in this environment.

Purge Gas Type with Saturated Samples: Saturated samples in general resulted in higher observed values of SE than unsaturated samples (Figure 50). More energy was required to initiate a phase change from liquid to vapor. Additionally, this vapor served to partially block and absorb energy from the beam, therefore, less energy can be delivered to the rock sample. Also of note, as liquid in the pore volume changes to gas, the fluid expansion assists in the spallation process. This process provides a lowering effect on observed SE.

More complex oil saturated samples consumed the highest SE values of the fluids tested. More research is required to determine how gas composition effects SE while lasing saturated samples. The figure below can be used as guide or correlation when using gasses on saturated samples.

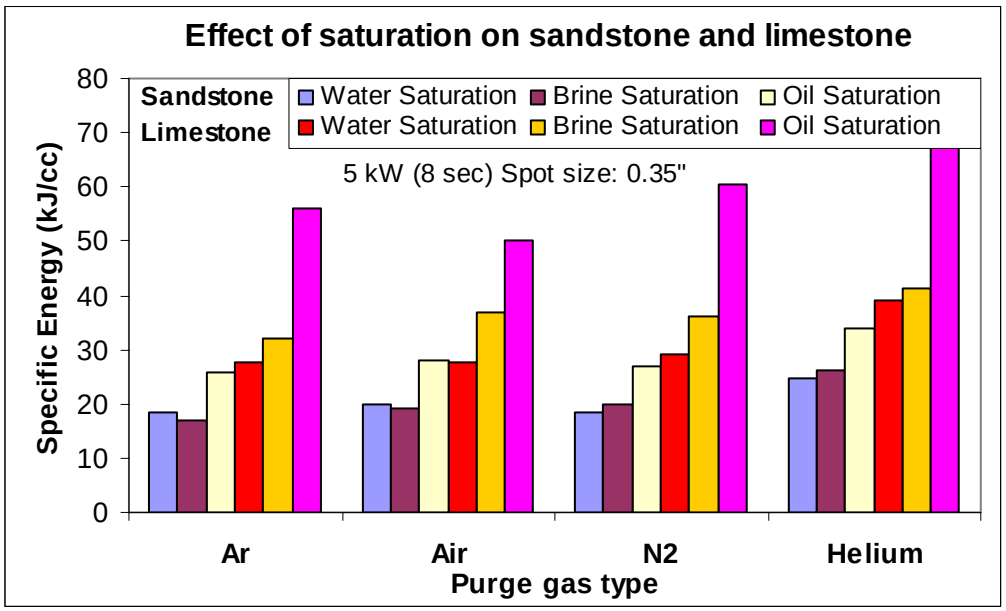

Figure 50. Effect of saturation media on SE for sandstone and limestone

Time of Penetration Effect on SE

Objective: To find the time of beam penetration of steel, cement and multi-layered target of steel, cement and rock (limestone or sandstone) as material thickness ranged from 0.635 cm (0.25 in) to 2.54 cm (1.0 in).

Steel Target Tests

Procedure: Steel plates of 0.635 cm (0.25 in), 0.889 cm (0.35 in), 1.016 m (0.4 in), 1.27 cm (0.5 in), 1.524 cm (0.6 in), 1.905 cm (0.75 in), and 2.54 cm (1.0 in) were cut from a 5.08 cm (2.0 in) diameter steel rod. Each steel plate was exposed to a 5.34 kW focused beam (CW) for such time required to penetrate the sample. An optimized nozzle purge system was used with compressed air at 620.5 kPa (90 psig) line pressure. Distance between purge nozzle and sample was about 2.54 cm (1.0 in). Lens with 1000 mm (39.37 in) focal length was used to focus 2.54 cm (1.0 in) collimated beam. Spot size (penetrating laser beam diameter) was kept 8.9 mm (0.35 in). The experiments were repeated with a nitrogen purge gas to determine the effect on time of penetration.

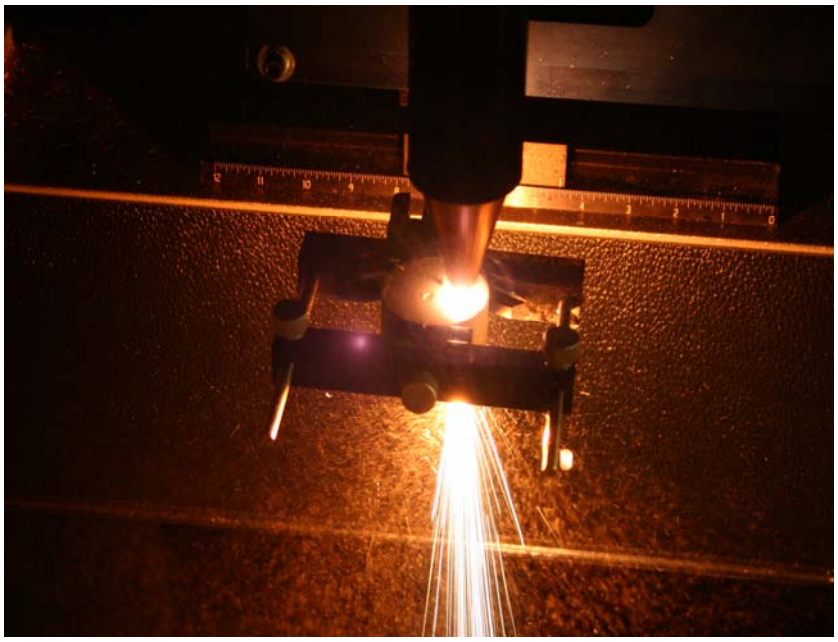

Figure 51. Penetration test of steel sample from a fixed beam position.

Two methods were evaluated for steel cutting. The first method exposed the sample directly to one beam from a fixed position (Figure 51). Sample pictures were taken before and after lasing as shown in Figures 52 and 53, respectively.

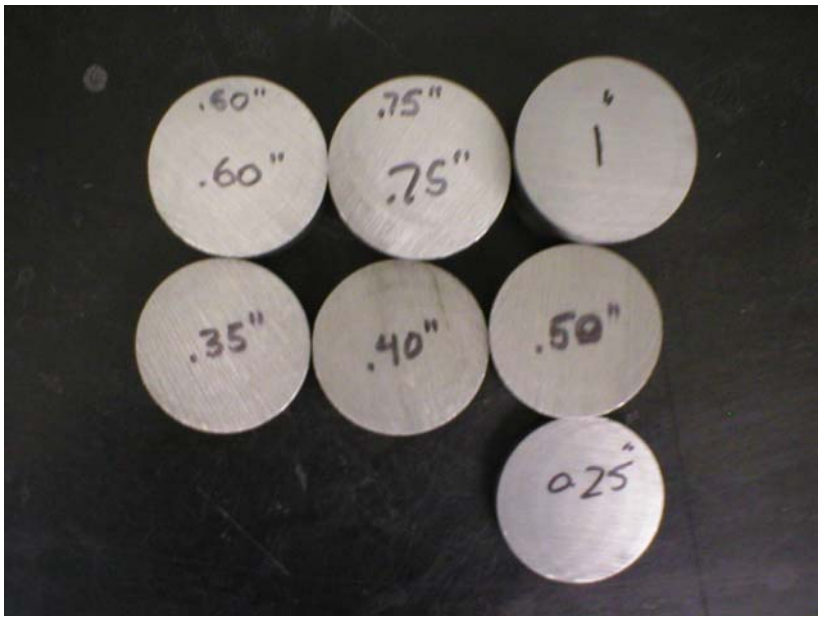

Figure 52. Steel samples before lasing

Figure 53. Steel samples after lasing

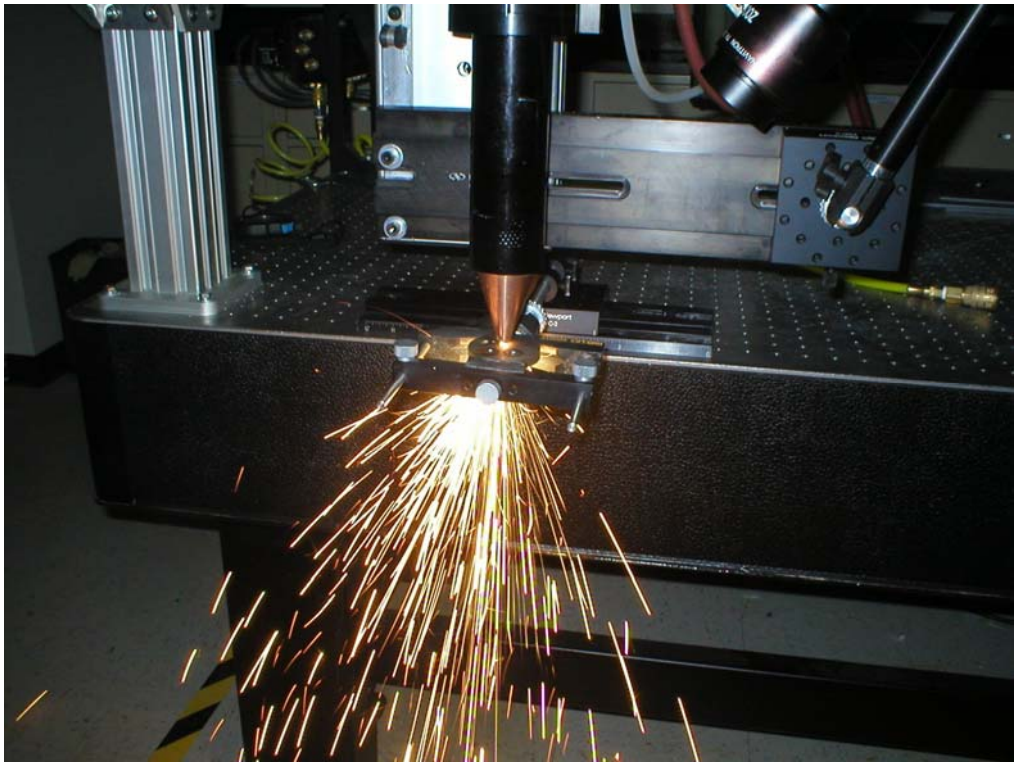

Figure 54. Penetration test of steel sample with beam rotating in circular motion.

A second method penetrated the sample by cutting a hole while moving the beam in a circular motion as shown in figure 54. The less complex method of a fixed beam position, however, best represents a likely initial downhole method and is used for the remaining experiments.

The results of using compressed air and nitrogen as purge gases for different thickness samples of the steel is shown in Figure 55. The resulting time required for beam penetration through steel increases as steel thickness increases. As can be seen in the graph, a slightly longer time is required per sample thickness using nitrogen as a purging medium. The slight presence of oxygen in the compressed air enhances the rate at which penetration can be achieved. Although beneficial from this perspective, downhole conditions of hydrocarbons at pressure exclude any options that include the presence of oxygen.

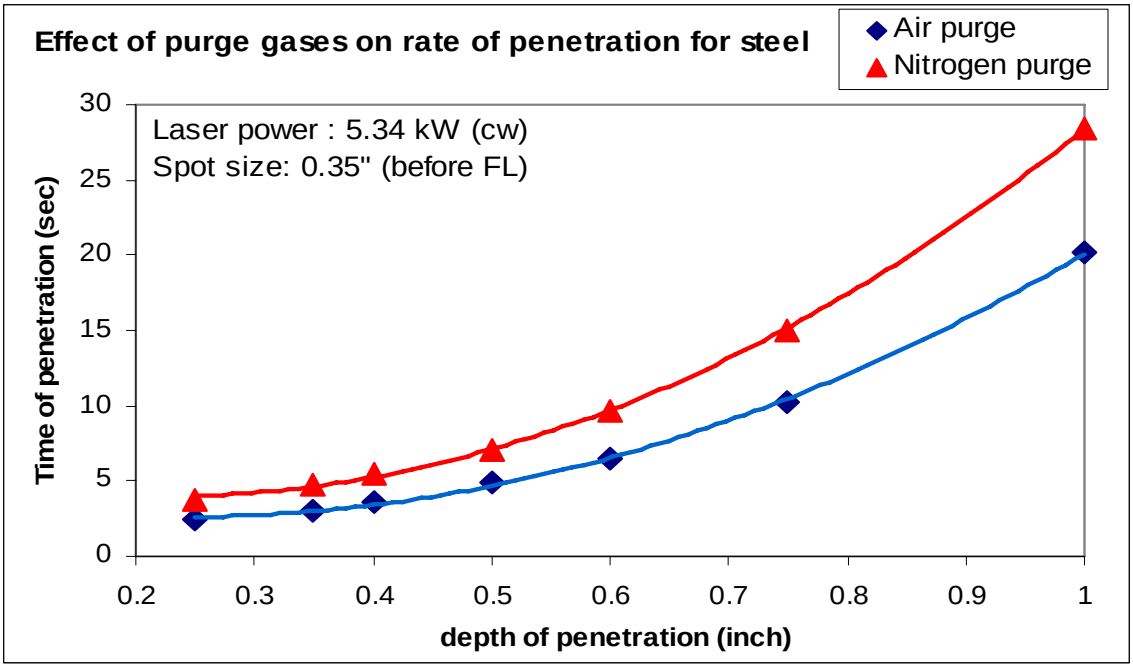

Figure 55. Time vs. depth of penetration on steel using air and nitrogen purge

Cement Target Tests

Three different representative types of cement were used for this study: Class A, Class G and YS 250. Cement plate sample targets measuring 5.08 cm (2.0 in) diameter were made in a 5.08 cm (2.0 in) ID Teflon tube with the following thicknesses: 0.635 cm (0.25 in), 0.889 cm (0.35 in), 1.016 m (0.4 in), 1.27 cm (0.5 in), 1.524 cm (0.6 in), 1.905 cm (0.75 in), and 2.54 cm (1.0 in). The target samples cured for 24 hours prior to beam exposure at 5.34 kW power (CW).

An optimized nozzle purge system was used with compressed air at 620.5 kPa (90 psig) line pressure. Distance between purge nozzle and sample was about 2.54 cm (1.0 in). Lens with 1000 mm (39.37 in) focal length was used to focus 2.54 cm (1.0 in) collimated beam. Spot size (penetrating laser beam diameter) was kept 8.9 mm (0.35 in). Time of penetration increased correspondingly with an increase in cement layer thickness (Figure 56).

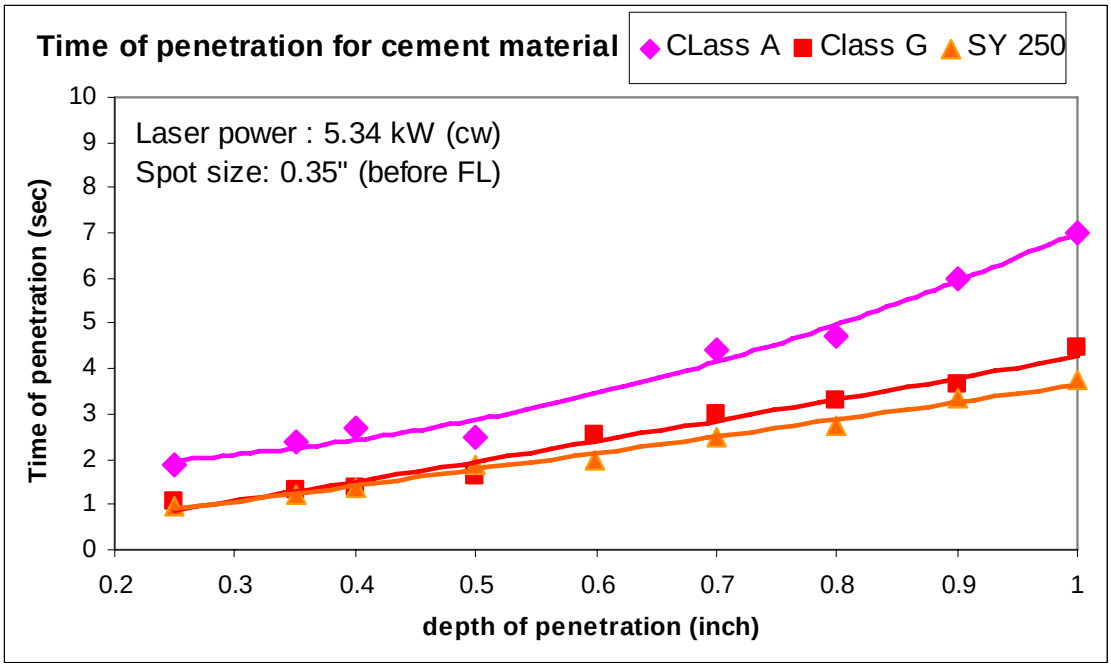

Figure 56. Time vs. depth of penetration for various cement types

Composite Target Tests

Composite core samples were constructed of various cement layer thicknesses 0.635 cm (0.25 in), 0.889 cm (0.35 in), 1.016 m (0.4 in), 1.27 cm (0.5 in), 1.524 cm (0.6 in), 1.905 cm (0.75 in), and 2.54 cm (1.0 in). These cement layers were sandwiched between 0.635 cm (0.25 in) steel plate and 5.08 cm (1.0 in) core of limestone or sandstone. The composite core diameter of all samples was 5.08 cm (1.0 in).

Each composite sample was lased at 5.34 kW power (CW) until the focused beam penetrated the axial core height. An optimized nozzle purge system was used with compressed air at 620.5 kPa (90 psig) line pressure. Distance between purge nozzle and sample was about 2.54 cm (1.0 in). Lens with 1000 mm (39.37 in) focal length was used to focus 2.54 cm (1.0 in) collimated beam. Spot size (penetrating laser beam diameter) was 8.9 mm (0.35 in) at steel surface. Time of penetration was also measured for 5.08 cm (2.0 in) thick cores of limestone and sandstone. A comparison was made between composite sample tests and calculated sum of beam exposure to individual materials (cement, steel and Ls/SS) as shown in Figure 59 and Figure 60.

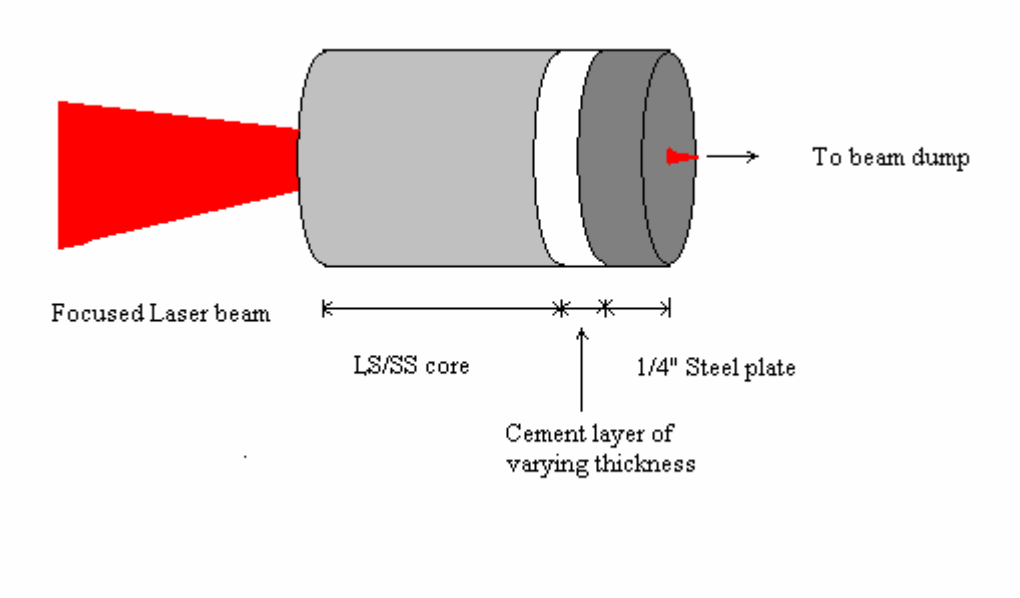

Figure 57. Drawing of penetration concept for composite samples

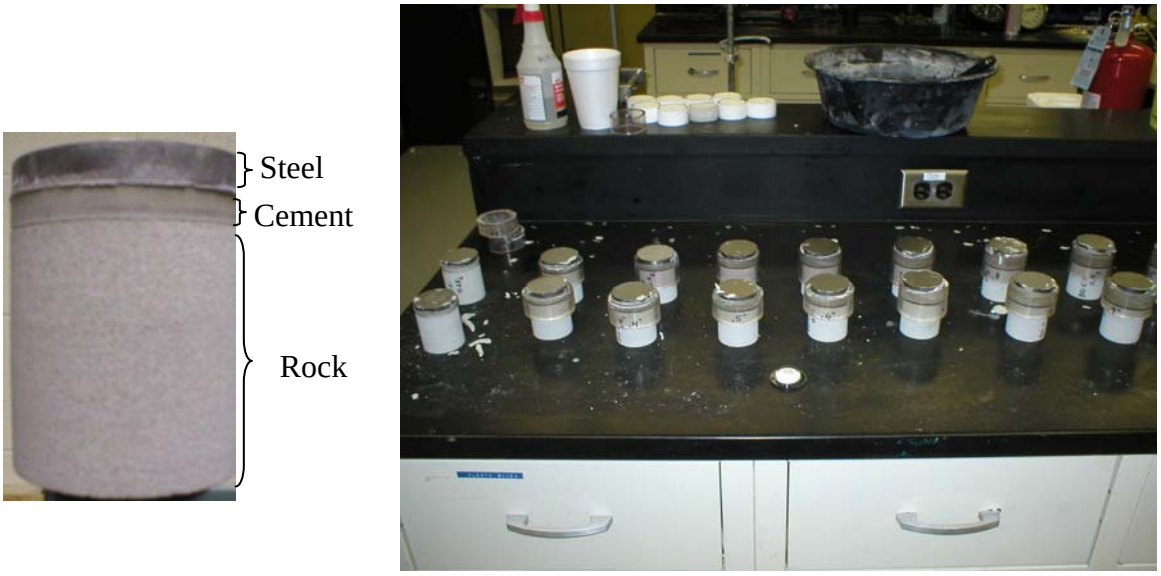

Figure 58. Preparation of the composite samples (steel, cement and rock).

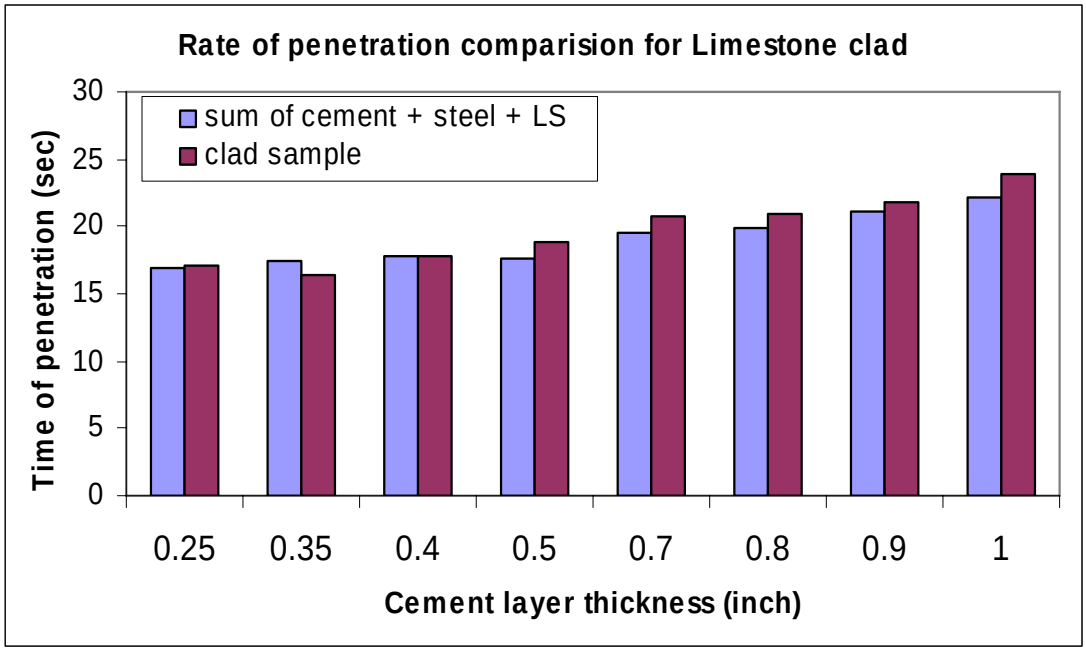

Figure 59. Penetration time for limestone composite sample and combined sum.

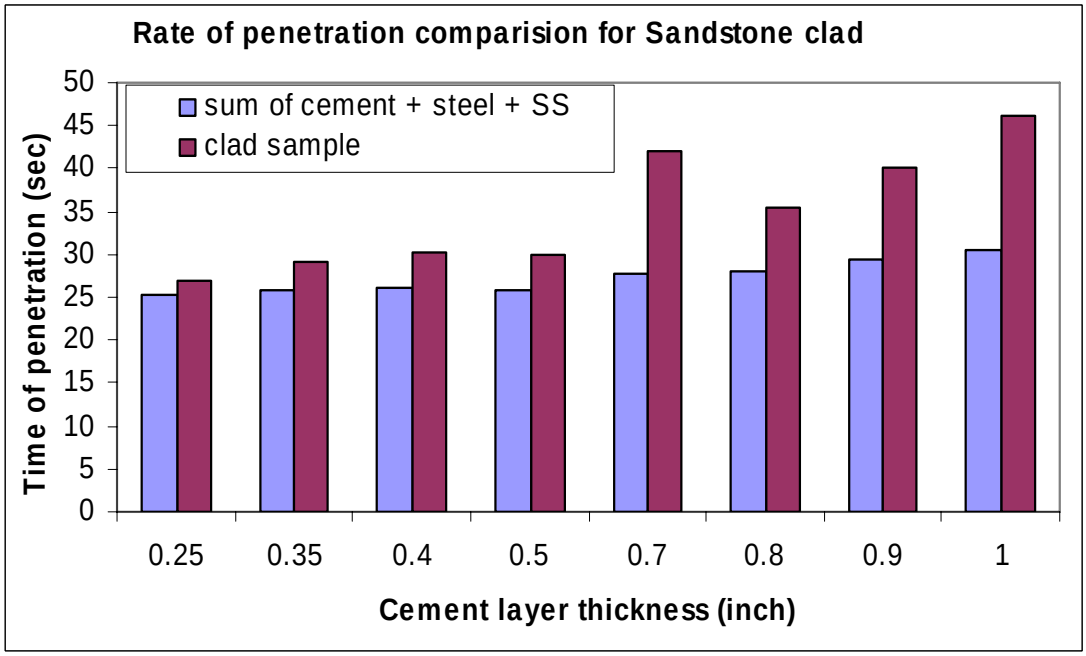

Figure 60. Penetration time for sandstone composite sample and combined sum.

Effect of Laser Power on SE (Collimated Beam)

Objective: To determine the effect of a collimated beam with a beam diameter of 8.9 mm (0.35 in) on limestone and sandstone.

Procedure: Laser power was applied to limestone and sandstone samples by varying power from 0.5 to 5.0 kW at constant time intervals of 4.0 s and 8.0 s. Limestone and sandstone blocks measuring 50.8 cm (20.0 in) x 15.24 cm (6.0 in) x 15.24 cm (6.0 in) were used in this study. One of the 50.8 cm (20.0 in) x 15.24 cm (6.0 in) surfaces was divided into 2.54 cm (1.0 in) square grids. Each grid was lased at different power level from 0.5 to 5.0 kW in 0.5 kW increments. A collimator lens assembly was used to deliver a 8.9 mm (0.35 in) diameter collimated beam at CW. Samples were placed in waste area (highest intensity for given collimation) of beam. An optimized nozzle purge system was used with compressed air at 620.5 kPa (90 psig) line pressure. The distance between the purge nozzle and sample was 2.54 cm (1.0 in). Specific energy values were calculated and presented in figures below.

Results and Analysis: For the limestone samples, the collimated beam did not create any noticeable material loss up to 2.0 kW power level for both 4.0 s and 8.0 s beam duration at a beam diameter of 8.9 mm (0.35 in). For sandstone, material was removed with beam power levels higher than 1.0 kW for both 4.0 s and 8.0 s duration with diameter of 8.9 mm (0.35 in). Figure 61 compares observed SE values for collimated beams at 4.0 and 8.0 s for limestone.

When comparing the effect of focused beam vs. collimated on limestone (Figure 62), SE values were generally higher with a collimated beam delivery as intensity of the beam remained the same at any cross section of the beam, while the focused beam intensity increased as it traveled into the sample. With increasing power levels, SE values of both focused and collimated beams tend toward convergence as the intensity of the beams approach that required to initiate an efficient thermal dissociation process in the carbonate.

When comparing 8.0 s and 4.0 s beam duration for sandstone using a collimated beam (Figure 63), a higher SE value is observed for the longer beam duration as local energy accumulations in the sample raise the quartz temperature to its melting point.

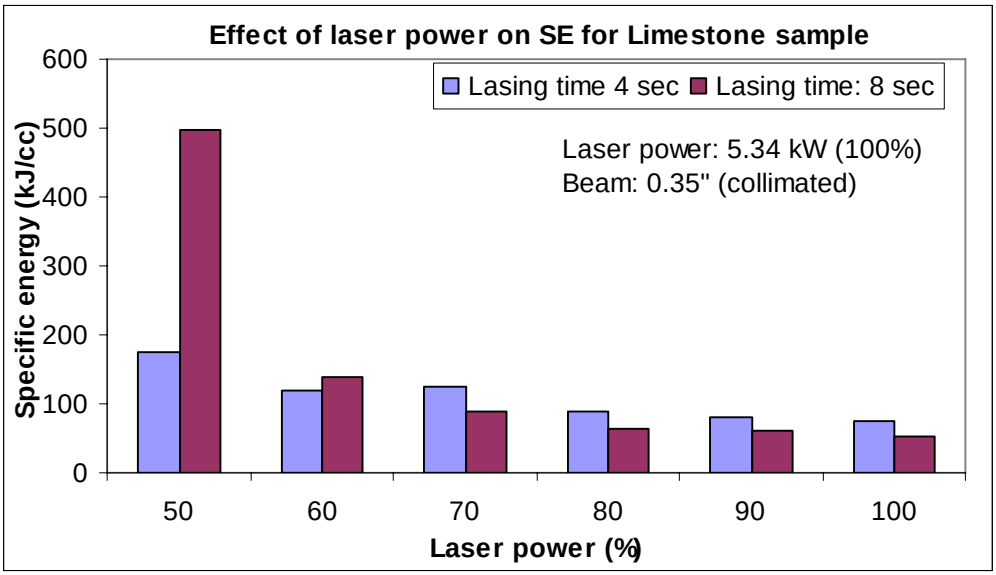

Figure 61. Comparison of 4 s and 8 s collimated beam application on limestone, increasing power from 50 to 100% at increments of 10%

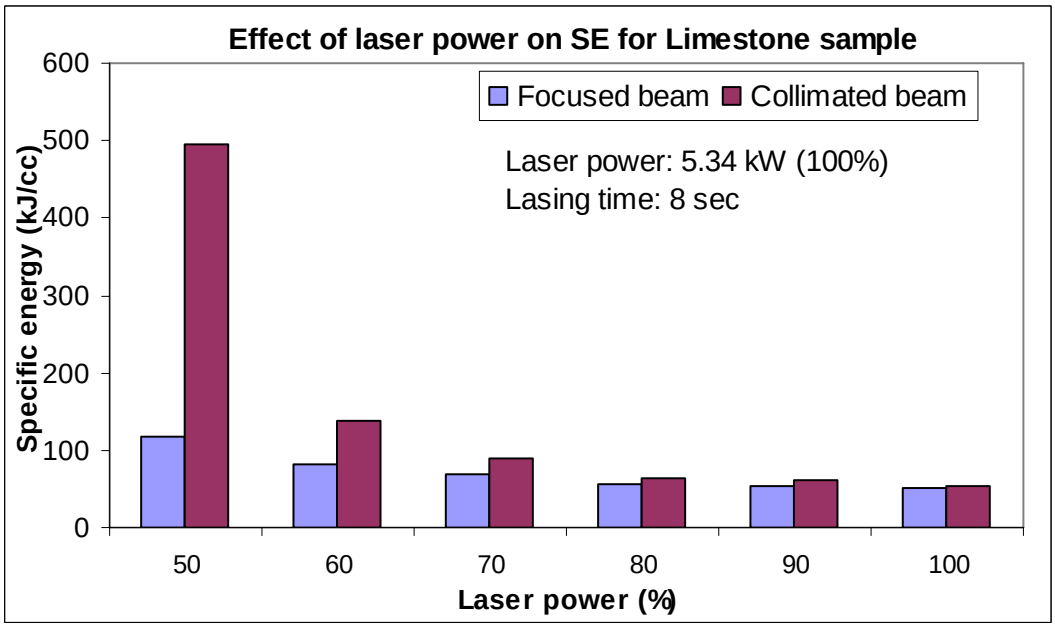

Figure 62. Comparison of collimated and focused beam for 8 s for limestone, increasing power from 50 to 100% at increments of 10%

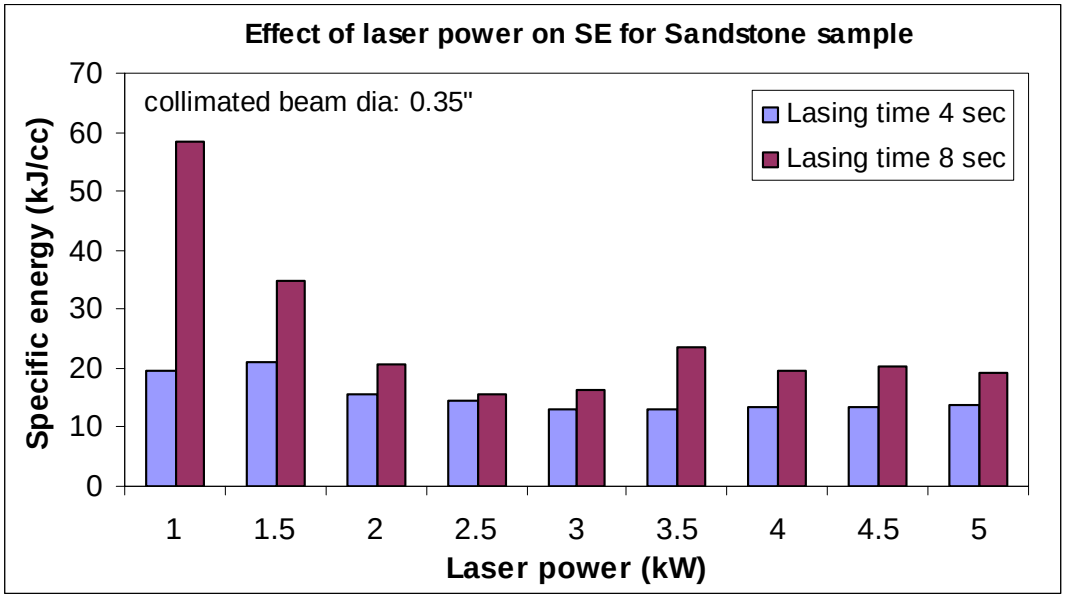

Figure 63. Comparison of 4 s and 8 s collimated beam application on sandstone, increasing power from 1.0 to 5.0 kW at increments of 0.5 kW.

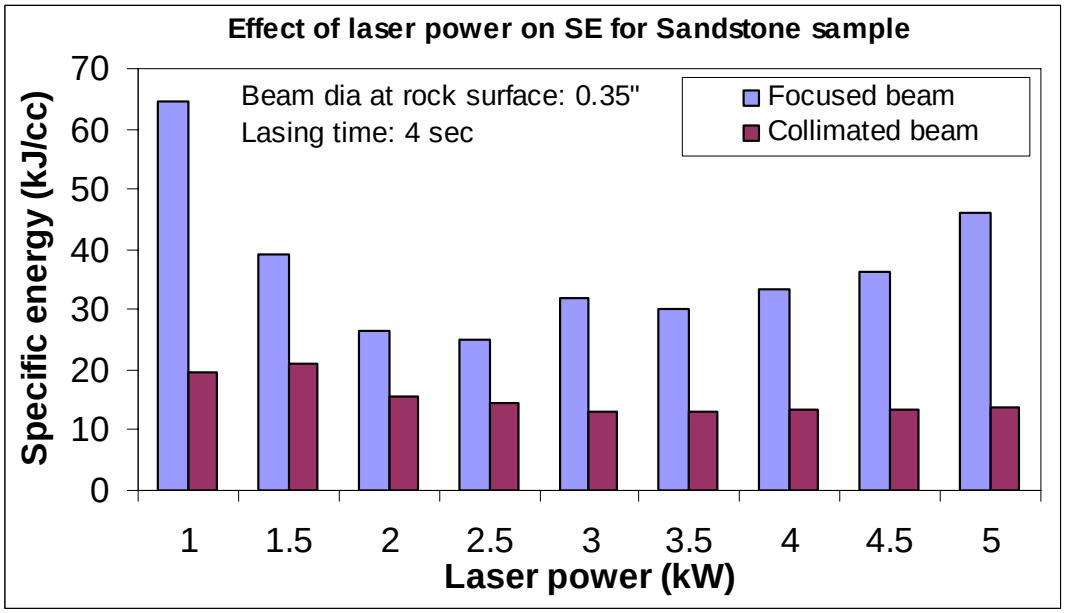

Figure 64. Comparison of collimated and focused beam for 4.0 s on sandstone, increasing power from 1.0 to 5.0 kW at increments of 0.5kW.

Collimated and focused beam applications on sandstone are presented in Figure 64. The observed SE values for focused beam applications are significantly higher than those of the collimated beam. For this rock type, quartz can reach its melting point more easily with a focused beam shape as compared to the even intensity distribution of the collimated beam.

The collimated beam shape can be seen in Figure 65, where the beam shows a flat surface, indicating uniform distribution of the beam's energy.

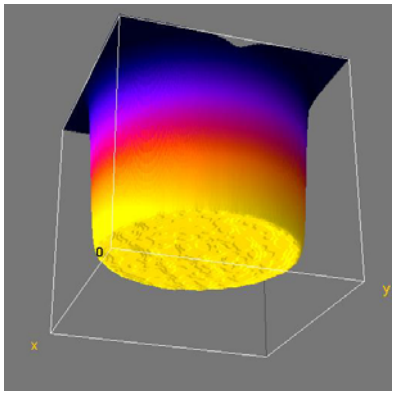

Figure 65. Collimated laser beam showing uniform energy distribution of HPFL.

Effect of Beam Duration on SE (Collimated Beam)

Objective: To determine the effect of beam duration of a collimated beam at 8.9 mm (0.35 in) diameter on limestone and sandstone.

Procedure: In this test, beam duration varies from 1.0 s to 20.0 s on limestone and sandstone samples. Limestone and sandstone blocks measuring 50.8 cm (20.0 in) x 15.24 cm (6.0 in) x 15.24 cm (6.0 in) were used in this study. One of the 50.8 cm (20.0 in) x 15.24 cm (6.0 in) surfaces was divided into 2.54 cm (1.0 in) square grids. Each grid was lased at 5.34 kW laser power. The beam duration of each hole was increased incrementally by 2.0 s starting from 2.0 s up to 20.0 s. Collimator lens assembly as presented in Figure 66 was used to deliver 8.9 mm (0.35 in) collimated beam.

An optimized nozzle purge system was used with compressed air at 620.5 kPa (90 psig) line pressure. Distance between purge nozzle and sample was about 2.54 cm (1.0 in). Lens with 1000 mm (39.37 in) focal length was used to focus 2.54 cm (1.0 in) collimated beam. The same set of experiments was repeated for sandstone at a 3 kW power level. Specific energy values were calculated and presented.

Result and Analysis: One difference between a focused and collimated beam is the shape of the beam. The focused beam presents a conical shape while the collimated beam is of a cylindrical shape whose dimensions and waste are theoretically constant. Figure 67 presents the results of applying a 8.9 mm (0.35 in) collimated beam at two powers, at 3.0 and 5.0 kW, on Berea sandstone. The trend shows that the 3.0 kW beam achieves a consistently lower SE value.

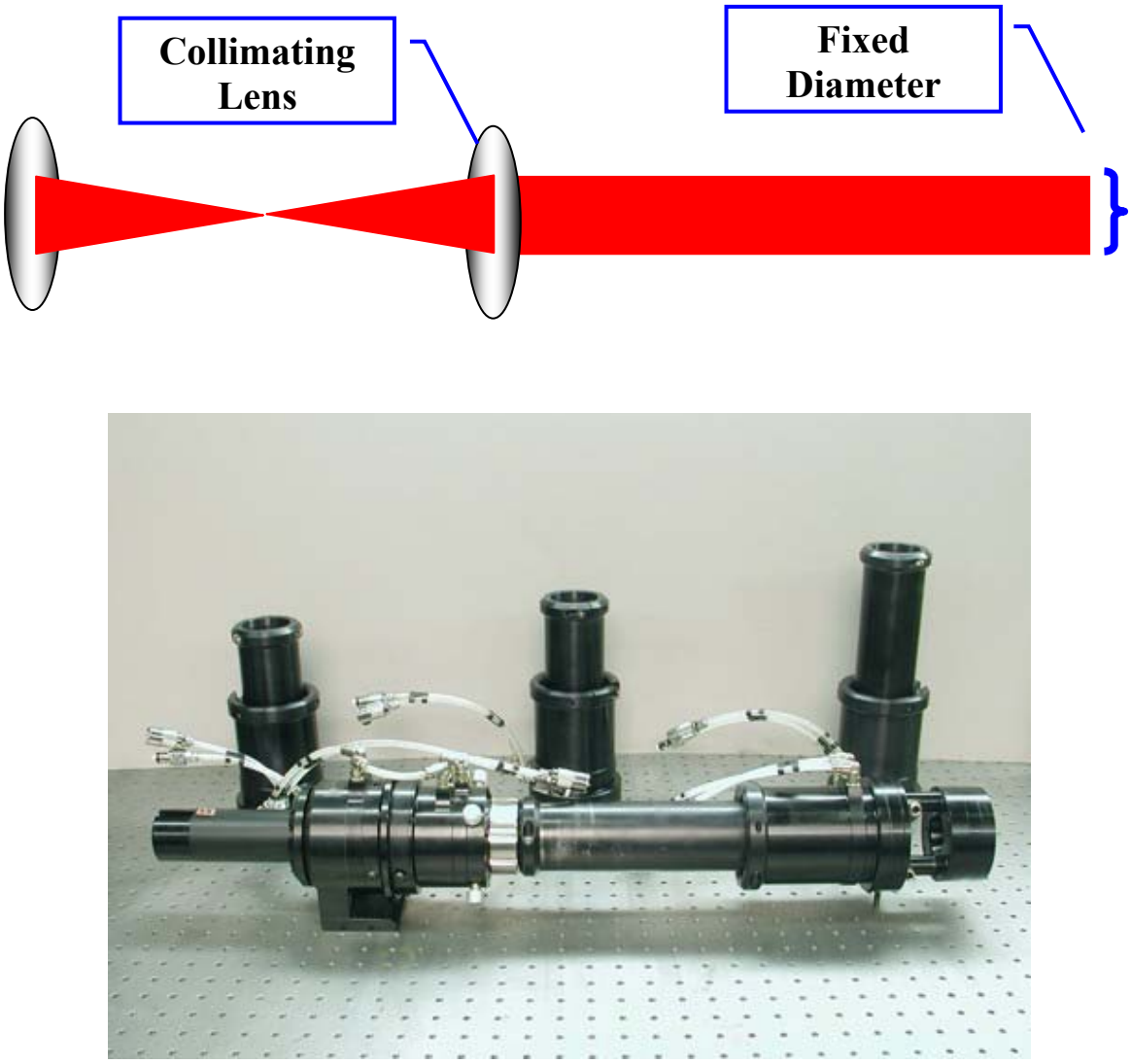

Figure 66. Collimator for HPFL provides beam from 6.35 mm (0.25 in) to 2.54 cm (1.0 in) diameter

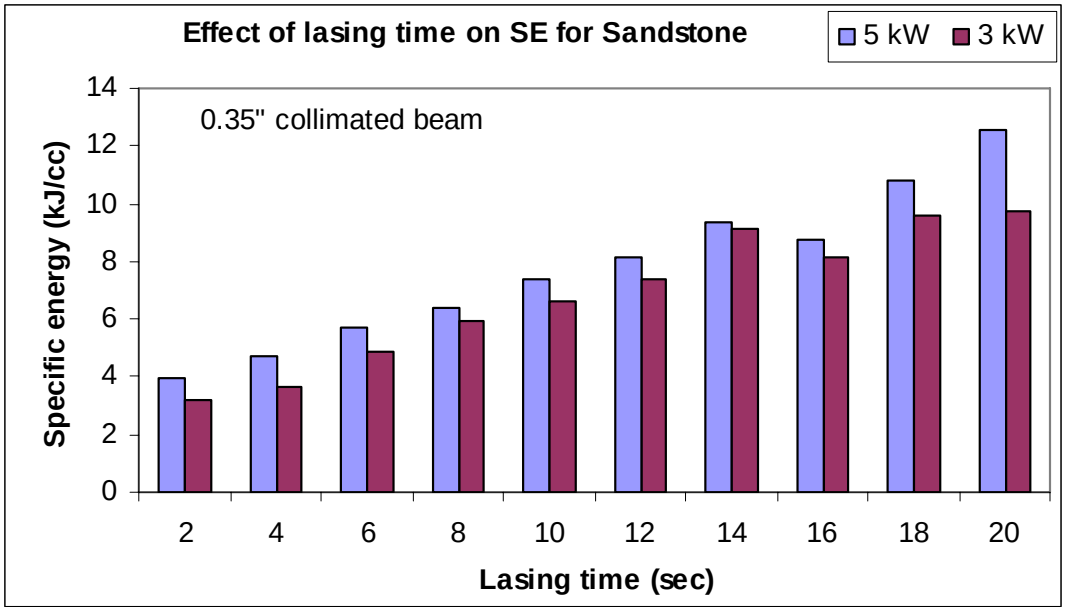

Figure 67. Collimated beam of sandstone sample lased at 3.0 and 5.0 kW using HPFL.

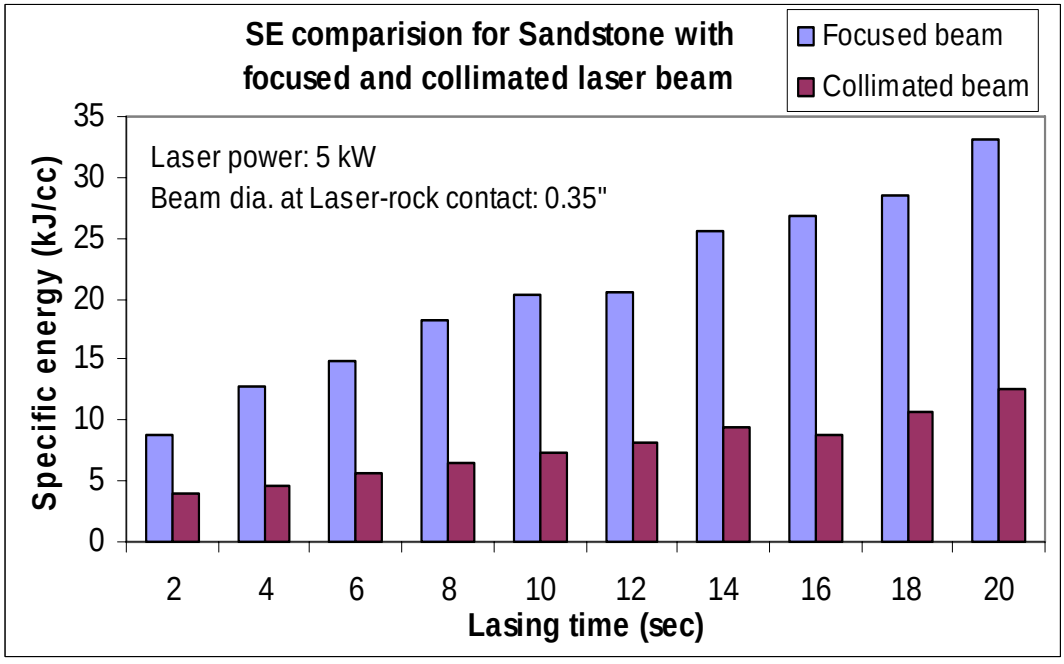

Figure 68. Comparison of focused and collimated beam exposure from 1.0 s to 20.0 s at 1.0 s increments

An increase in beam duration resulted in increasing SE values and deeper holes. The results show the same trend for sandstones, although less energy was consumed.

There is a proportional relationship between SE and power. A similar relationship also exists between SE and duration. As beam power and duration increase, temperature of exposed sandstone will first reach the spallation temperature. At this point SE values are low, as much of the absorbed energy causes material to break free. Additional increases in time and temperature further raise the temperature of rock and spalled cuttings to the melting point, where energy use is redirected and absorbed more readily for phase change.

A comparison of SE values from both collimated and focused beam shape applications is presented in Figure 68. Results show that as duration increases, SE values are lower for the collimated beam as compared to the focused beam, due in part to the shape of the beam. The conical shape of the focused beam has increasing intensity as the beam narrows to the focal point (Figure 69).

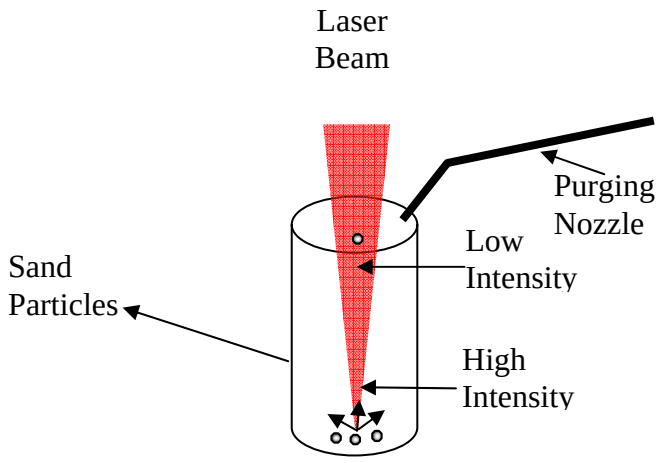

Figure 69. Focused beam has a higher intensity at the focal point.

The high intensity of the beam can more quickly raise the temperature of quartz in the exposed sandstone to its melting point than a collimated beam with the same power but lower intensity.

The experiment was repeated on a limestone sample with a 5.0 kW beam (Figure 70).

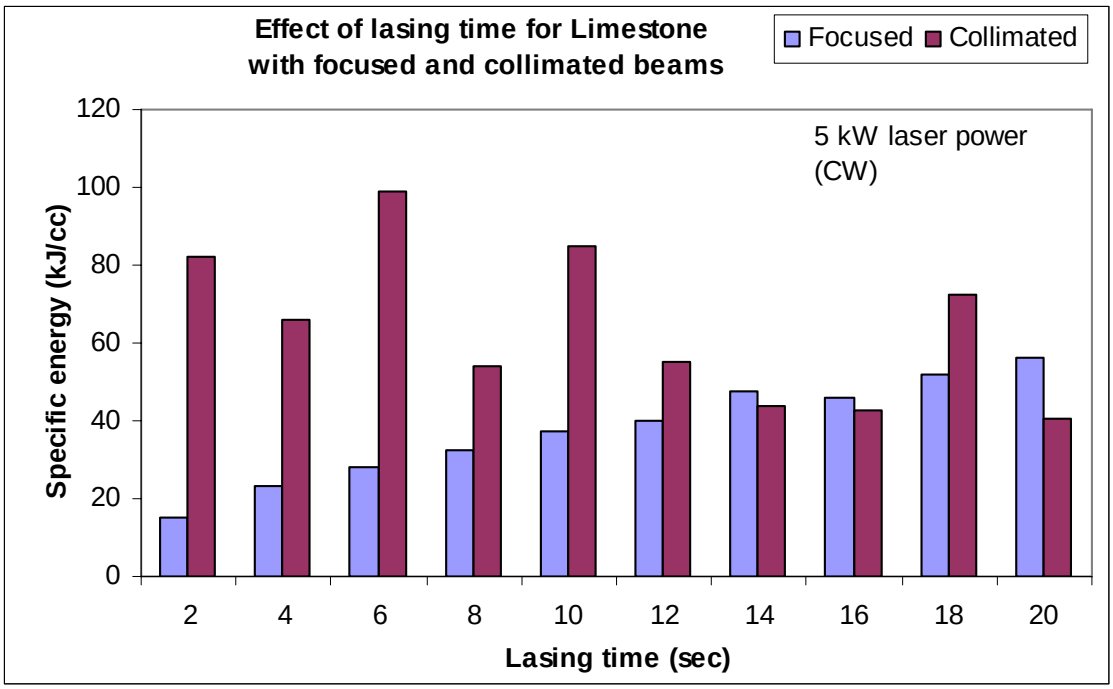

Figure 70. Comparison of focused and collimated beam when increasing duration from 1.0 s to 20.0 s at 1.0 s increments

Conclusion

The recent commercial introduction of high-power fiber lasers represented a significant step forward in realizing field-based applications of photonic energy for well construction and completion. Fiber lasers meet the multiple demands from industry regarding a field deployable system, including overall size limitations, mobile rugged on-site deployment, requisite energy delivery to target, real-time controllability and penetration of multiple materials. From an economic perspective, the order of magnitude improvement in efficiency significantly lowers input energy and waste heat dissipation requirements. They also require minimal maintenance and repair, and are commercially available.

The results from experiments performed in this report continue to support the capability of photonic energy to drill and tunnel through rock. The application of GTI's 5.34-kW fiber laser to a 1-ft cubic block of Berea sandstone was a successful demonstration of current industrial laser technology. The demonstration provided a minimal value of SE when compared with previous laser/rock interaction tests, and yet was achieved while creating the deepest tunnel to date. This was made possible, in part, by effectively removing cuttings to avoid energy losses through thermal accumulations in the matrix and the cuttings. Additionally, boundary effects were minimized by using a target with a greater mass than found in cylindrical cores, and by opening the tunnel from both sides to meet in the center.

Evaluation of changes to rock properties proved that low power applications will create a narrower thermal deformation zone than megawatt military lasers. The deformation zone extends from the tunnel face radially into the rock; however the resulting impact on fluid flow enhancement is undetermined. The importance of removing rock cuttings was again demonstrated, by means of creating tunnel diameters larger than beam diameters, and continually pushing gas purge lines into the deepening hole.

Photonic energy applications have proven themselves as a concept under lab conditions and are developing a promising outlook for niche applications in drilling and completion. Additional research remains to be performed to further accelerate this revolutionary drilling application to prototype development and field experiments. Industry partners are showing continued enthusiasm that high power lasers may become tools of choice in the near future to provide an improvement in penetration rates, reduced damage to the formation, and enhanced directional control.

References

1. DeGolyer and MacNaughton, One Energy Square, Dallas, Texas, 2000.
2. Andersen, et al, “Deep Drilling Basic Research: Volume 2 - Deep Drilling, ” GRI 90/0265.2, June 1990, 78p.
3. W.C. Maurer, Novel Drilling Techniques, Pergamon Press, 1968.
4. W.C. Maurer, Advanced Drilling Techniques, Petroleum Publishing, 1980.
5. W.T. Silfvast, Laser Fundamentals, Cambridge, 1996.
6. W.H. Somerton, Thermal Properties and Temperature-related Behavior of Rock/Fluid System. University of California, Development in Petroleum Science. Elsevier, Amsterdam-London-New York-Tokyo, 1992.
7. R.M. Graves and D.G. O'Brien, "Star Wars Laser Technology Applied to Drilling and Completing Gas wells," SPE 49259, 1998.
8. Walters, W.P. & Zukas, J.A. Fundamentals of Shaped Charges, John Wiley and Sons, 407pp., 1998.
9. Reed, C.B., Xu, Z., Parker, R.A., Gahan, B.C., Batarseh, S.I., Graves, R.M., Figueroa, H., & Deeg, W. Application of high powered lasers to drilling and completing deep wells, U. S Department of Energy Topical Report ANL/TD/TM03-02, 2003.
10. Gahan, B.C., Batarseh, S., Sharma, B., Gowelly, S. 2004. “Analysis of Efficient High-Power Fiber Lasers for Well Perforation,” SPE Paper 90661, SPE Annual Technical Conference and Exhibition, Houston, TX.

Publications

Publications by GTI staff from October 2003 to September 2004

1. Gahan, B.C., Batarseh, S., Sharma, B., Gowelly, S. 2004. "Analysis of Efficient High-Power Fiber Lasers for Well Perforation," SPE Paper 90661, SPE Annual Technical Conference and Exhibition, Houston, TX.

2. Batarseh, S., Gahan, B.C. 2004. "Deep Hole Penetration of Rock for Oil Production Using Ytterbium Fiber Laser," SPIE Poster 5448-98, SPIE High-Power Laser Ablation V, Taos, NM.

3. Gahan, B.C., Shiner, B. 2004. "New High-Power Fiber Laser Enables Cutting-Edge Research" GTI Document No. GTI-03/0207, GasTIPS 10(2004): 29-31.

4. Gahan, B.C., Batarseh, S., Parker, R.A. 2003. "Lasers May Offer Alternative to Conventional Wellbore Perforation Techniques" GTI Document No. GTI-03/0153, GasTIPS 9(2003): 25-29.

5. Batarseh, S., Gahan, B.C., Parker, R., Graves, R. 2003. "Rock Phase Control by Using High Power Laser for Production Enhancements," Paper 505, 22nd Int'l Congress on Applications of Lasers and Electronics, Jacksonville, FL.

6. Parker, R., Xu, Z., Reed, C., Graves, S., Gahan, B.C., Batarseh, S. 2003. "Drilling Large Diameter Holes in Rocks Using Multiple Laser Beams," Paper 504, 22nd Int'l Congress on Applications of Lasers and Electronics, Jacksonville, FL.

7. Reed, C., Xu, Z., Parker, R., Graves, S., Gahan, B.C., Batarseh, S., Deeg, W. 2003 "Laser Rock Drilling for Oil and Gas Wells," 2003 AAPG Mid-Continent Section Meeting, Tulsa, OK.

8. Batarseh, S.; Gahan, B.C.; Graves, R.M.; Parker, R.A. 2003. "Well Perforation Using High-Power Lasers," SPE Paper 84418, SPE Annual Technical Conference and Exhibition, Denver, CO.

9. Parker, R.A.; Gahan, B.C.; Graves, R.M.; Batarseh, S.; Xu, Z.; Reed, C.B. 2003. "Laser Drilling: Effects of Beam Application Methods on Improving Rock Removal," SPE Paper 84353, SPE Annual Technical Conference and Exhibition, Denver, CO.

Presentations

Presentations delivered from October 2003 to September 2004

Analysis of Efficient High-Power Fiber Lasers for Well Perforation
Society of Petroleum Engineers (SPE), Annual Technical Conference and Exhibition
Houston, TX, September 2004.

Improving Gas Well Drilling and Completion with High Energy Lasers
American Petroleum Institute, San Joaquin Valley Chapter
Bakersfield, CA, April 2004 (invitation)

Deep Hole Penetration for Oil Production Using Ytterbium Fiber Laser
SPIE High Power Laser Ablation V
Taos, NM, April 2004

Advances in Improving Gas Well Drilling and Completion with High Energy Lasers
Natural Gas Technologies Conference II (DOE Project Review)
Phoenix, AZ, February 2004

Rock Phase Control by Using High Power Laser for Production Enhancements
22nd Int'l Congress on Applications of Lasers and Electronics
Jacksonville, FL, October 2003

Drilling Large Diameter Holes in Rocks Using Multiple Laser Beams
22nd Int'l Congress on Applications of Lasers and Electronics
Jacksonville, FL, October 2003

Well Perforation Using High-Power Lasers
Society of Petroleum Engineers (SPE), Annual Technical Conference and Exhibition
Denver, CO, October 2003

Laser Drilling: Effects of Beam Application Methods on Improving Rock Removal
Society of Petroleum Engineers (SPE), Annual Technical Conference and Exhibition
Denver, CO, October 2003

List of Acronyms and Abbreviations

af	= after focal point
bf	= before focal point
BG, BGSS	= Berea gray sandstone
C	= Celsius/centigrade
cc	= cubic centimeter
CO_2	= carbon dioxide
COIL	= chemical oxygen iodine laser
CW	= continuous wave
DP	= diode-pumped
DTA	= differential thermal analysis
E_{abs}	= absorbed energy
E_{Decomp}	= decomposition energy
E_{dehy}	= dehydration energy
$E_{GrainExp}$	= grain expansion energy
E_{inc}	= incident electromagnetic wave
E_{melt}	= melting energy
E_{other}	= other energy
$E_{PoreExp}$	= pore expansion energy
E_{ref}	= reflected energy
E_{sc}	= scattered energy
E_{vap}	= vaporization energy
EDS	= energy dispersive system
E/O	= electrical to optical
F	= Fahrenheit
SEM	= scanning electron microscope
FP	= focal point
ft	= foot
g	= gram
J	= joule
HPFL	= high power fiber laser

Hz	= hertz
ID	= inside diameter
LP	= lamp-pumped
Ls, LS	= limestone
m	= mass
m	= meter
md	= millidarcy (Permeability Unit)
mi	= mile
MIRACL	= Mid-Infrared Advanced Chemical Laser
Nd:YAG	= neodymium-doped yttrium aluminum garnet ($Nd:Y_3Al_5O_{12}$)
oz	= ounce
Pa	= Pascal
PDPK	= pressure decay profile permeameter
psig	= pounds per square inch gauge
s	= seconds
SE	= specific energy
t	= time
TGA	= thermogravimetric analysis
V	= volume
W	= watt
x ,X	= times
XRD	= x-ray diffraction
λ	= wavelength
ρ	= density
v	= viscosity

Appendix A: Experimental Data

Experiment: Methods of Calculating Specific energy

Sample Name	Core dia. (cm)	Core length (cm)	Weight before lasing (gm)	Weight after lasing (gm)	Weight removed by lasing (gm)	Calculated spot size (inch)	Laser power (kW)	Beam duration (sec)	Density (gm/cc)	Volume removed (cc)	Specific Energy based on weight removed (kJ/cc)	hole dia (cm)	depth of penetration (cm)	Specific Energy based on hole dimensions (kJ/cc)
BG-SC2	5.005	5.298	217.9	212.8	5.1	0.3585	5.34	8	2.1	2.4	17.5	1.621	3.03	20.5
BG-SC3	5.004	5.422	222.1	216.7	5.4	0.3585	5.34	8	2.1	2.6	16.5	1.764	2.95	17.8
BG-SC4	5.004	5.342	221.8	216.9	4.9	0.3585	5.34	8	2.1	2.3	18.4	1.71	2.974	18.8
BG-SC5	5.008	5.361	221.9	217	4.9	0.3585	5.34	8	2.1	2.3	18.3	1.671	3.004	19.5
BG-SC6	5.009	5.354	221.1	216.8	4.3	0.3585	5.34	8	2.1	2.1	20.8	1.69	3.048	18.7
BG-SC7	5.004	5.419	223.2	219	4.2	0.3585	5.34	8	2.1	2.0	21.3	1.697	2.95	19.2
BG-SC8	5.003	5.313	219.9	215.9	4	0.3585	5.34	8	2.1	1.9	22.5	1.748	3.026	17.6
BG-SC9	5.004	5.403	223	218.8	4.2	0.3585	5.34	8	2.1	2.0	21.3	1.617	2.958	21.1
BG-SC10	5.004	5.398	222.7	218	4.7	0.3585	5.34	8	2.1	2.2	19.1	1.76	2.938	17.9
Average											**19.5**			**19.0**

Experiment: Effect of orientation (of structure of formation to laser) on specific energy
Material: Limestone

Face Side	Calculated spot size (inch)	Inside hole diameter (cm)	Outside hole diameter (cm)	Hole depth (cm)	Laser power (kW)	Beam duration (sec)	Specific Energy (kJ/cc)
A	0.3585	1.1	1.5	3.24	5.34	8	41.6
B	0.3585	1.1	1.4	3.49	5.34	8	38.9
C	0.3585	1.1	1.3	3.63	5.34	8	35.2
D	0.3585	1.2	1.4	3.73	5.34	8	31.8
E	0.3585	1.2	1.4	3.65	5.34	8	33.3
F	0.3585	1.1	1.5	3.54	5.34	8	36.5

Material: Sandstone

Face Side	Calculated spot size (inch)	Hole diameter (cm)	Hole depth (cm)	Laser power (kW)	Beam duration (sec)	Specific Energy (kJ/cc)
A	0.3585	1.6	3.2	5.34	8	20.4
B	0.3585	1.6	3.5	5.34	8	18.9
C	0.3585	1.6	3.6	5.34	8	18.2
D	0.3585	1.6	3.7	5.34	8	17.7
E	0.3585	1.6	3.6	5.34	8	18.1
F	0.3585	1.6	3.5	5.34	8	18.6

Experiment: Effect of boundary (heat flow) on specific energy
Material: Sandstone Spot size: 0.35”

Sample Name	Core dia. (cm)	Core length (cm)	Weight before lasing (gm)	Weight after lasing (gm)	Weight removed by lasing (gm)	Calculated spot size (inch)	Laser power (kW)	Beam duration (sec)	Density (gm /cc)	Volume removed (cc)	Specific Energy based on weight removed (kJ/cc)	Avg. Specific Energy based on weight removed (kJ/cc)
BGSS-C-B1	10.1	5.4	919.7	908.6	11.1	0.3585	5.34	4	2.10	5.27	4.05	
BBSS-C-B2	10.1	5.3	881.3	872.6	8.7	0.3585	5.34	4	2.07	4.21	5.08	
BGSS-C-B3	10.1	5.6	934.3	924	10.3	0.3585	5.34	4	2.10	4.91	4.35	4.49
BBSS-C-B4	7.5	5.4	499.6	495.3	4.3	0.3585	5.34	4	2.09	2.06	10.37	
BGSS-C-B5	7.5	5.4	504	500	4	0.3585	5.34	4	2.09	1.92	11.14	
BBSS-C-B6	7.6	5.4	501.4	498	3.4	0.3585	5.34	4	2.07	1.64	13.03	11.51
BGSS-C-B7	6.9	5.3	415.3	412.5	2.8	0.3585	5.34	4	2.10	1.33	16.01	
BBSS-C-B8	6.9	5.4	421.4	418.4	3	0.3585	5.34	4	2.09	1.43	14.91	
BGSS-C-B9	6.9	5.3	417.5	414.1	3.4	0.3585	5.34	4	2.07	1.64	13.02	14.65
BBSS-C-B10	5.1	5.4	222.7	221.4	1.3	0.3585	5.34	4	2.07	0.63	33.94	
BGSS-C-B11	5.0	5.3	219.8	218.4	1.4	0.3585	5.34	4	2.09	0.67	31.82	
BBSS-C-B12	5.0	4.5	188.8	186.4	2.4	0.3585	5.34	4	2.08	1.15	18.54	32.88
BGSS-C-B13	2.5	5.3	53.1	52.3	0.8	0.3585	5.34	4	2.08	0.39	55.44	
BBSS-C-B14	2.5	5.3	52.7	51.9	0.8	0.3585	5.34	4	2.07	0.39	55.24	
BGSS-C-B15	2.5	5.3	52.1	51.5	0.6	0.3585	5.34	4	2.06	0.29	73.19	55.34
BBSS-C-B16	1.9	5.3	30.9	30.2	0.7	0.3585	5.34	4	2.03	0.35	61.83	
BGSS-C-B17	1.9	5.3	31.9	31.2	0.7	0.3585	5.34	4	2.07	0.34	63.20	
BBSS-C-B18	1.9	5.3	31.4	31	0.4	0.3585	5.34	4	2.08	0.19	111.06	62.51

Experiment: Effect of boundary (heat flow) on specific energy
Material: Limestone Spot size: 0.35”

Sample Name	Core dia. (cm)	Core length (cm)	Weight before lasing (gm)	Weight after lasing (gm)	Weight removed by lasing (gm)	Calculated spot size (inch)	Laser power (kW)	Beam duration (sec)	Density (gm /cc)	Volume removed (cc)	Specific Energy based on weight removed (kJ/cc)	Avg. Specific Energy based on weight removed (kJ/cc)
LS-C-B1	10.1	5.4	981.3	970.5	10.8	0.3585	5.34	4	2.27	4.76	4.48	
LS-C-B2	10.1	5.4	967.6	956.9	10.7	0.3585	5.34	4	2.26	4.74	4.50	
LS-C-B3	10.1	5.2	963.2	953.4	9.8	0.3585	5.34	4	2.31	4.24	5.04	4.67
LS-C-B4	7.5	5.3	533.7	530.8	2.9	0.3585	5.34	4	2.23	1.30	16.42	
LS-C-B5	7.6	5.6	559.6	555	4.6	0.3585	5.34	4	2.23	2.06	10.37	
LS-C-B6	7.5	5.2	532.1	528	4.1	0.3585	5.34	4	2.27	1.81	11.82	12.87
LS-C-B8	6.9	5.4	455.5	451.6	3.9	0.3585	5.34	4	2.26	1.73	12.35	
LS-C-B9	6.9	5.4	462.3	459.2	3.1	0.3585	5.34	4	2.27	1.37	15.64	14.00
LS-C-B10	5.0	5.3	236.3	234.1	2.2	0.3585	5.34	4	2.25	0.98	21.82	
LS-C-B11	5.0	5.3	235.7	233.3	2.4	0.3585	5.34	4	2.24	1.07	19.97	
LS-C-B12	5.0	5.3	238	236.1	1.9	0.3585	5.34	4	2.25	0.84	25.34	22.38
LS-C-B13	2.4	5.4	52.4	51.1	1.3	0.3585	5.34	4	2.20	0.59	36.15	
LS-C-B14	2.5	5.3	56.5	55	1.5	0.3585	5.34	4	2.24	0.67	31.85	
LS-C-B15	2.5	5.3	55.1	53.4	1.7	0.3585	5.34	4	2.20	0.77	27.68	31.90

Experiment: Effect of beam density on specific energy (spot size before and after focal point)

Distance between Lens and sample: 641.5 mm for before FL exp
1358 mm for before FL exp

	Sample name	Avg. Laser power (kW)	Exposure time (sec)	Spot size (inch)	Measured horizontal dia. (cm)	Measured vertical dia. (cm)	Average Dia. (cm)	Depth of penetration (cm)	SE based on dimensions kJ/cc (cone)	Average specific energy (kJ/cc)
Sample before focal point	BF1	5.34	4	0.35	1.667	1.777	1.722	1.804	15.25211	
	BF2	5.34	4	0.35	1.651	1.739	1.695	1.761	16.12627	
	BF3	5.34	4	0.35	1.721	1.722	1.7215	1.752	15.71392	**15.51723**
	BF4	5.34	4	0.35	1.621	1.784	1.7025	1.809	15.56037	
	BF5	5.34	4	0.35	1.711	1.726	1.7185	1.85	14.93351	
Sample after focal point	AF1	5.34	4	0.35	1.329	1.371	1.35	2.202	20.33049	
	AF2	5.34	4	0.35	1.37	1.371	1.3705	2.205	19.69999	
	AF3	5.34	4	0.35	1.458	1.333	1.3955	2.287	18.31921	**19.19076**
	AF4	5.34	4	0.35	1.307	1.495	1.401	2.297	18.09653	
	AF5	5.34	4	0.35	1.339	1.4	1.3695	2.23	19.50759	

Experiment: Effect of laser power on specific energy
Material: Limestone Spot size: 0.35”

Percentage laser power (%)	Percentage laser power (kW)	beam duration (sec)	Inside hole diameter (cm)	Outside hole diameter (cm)	Hole depth (cm)	Specific energy (kJ/cc)
10	0.53	8	0.00	0.00	0.00	-
20	1.07	8	1.03	1.49	0.10	310.03
30	1.60	8	1.14	1.49	0.10	375.36
40	2.14	8	0.97	1.49	0.49	143.63
50	2.67	8	0.96	1.48	0.77	116.21
60	3.20	8	1.00	1.66	1.21	80.65
70	3.74	8	1.03	1.66	1.58	68.36
80	4.27	8	1.03	1.66	2.15	57.15
90	4.81	8	1.03	1.66	2.56	53.99
100	5.34	8	1.03	1.66	2.94	52.26

Experiment: Effect of laser power on specific energy
Material: Sandstone Spot size: 0.35”

Percentage laser power (%)	Percentage laser power (kW)	beam duration (sec)	Vertical hole diameter (cm)	Horizontal hole diameter (cm)	Hole depth (cm)	Specific energy (kJ/cc)
20	1.07	4	0.91	1.17	0.30	64.39
30	1.60	4	1.05	1.35	0.56	39.34
40	2.14	4	1.09	1.39	1.03	26.60
50	2.67	4	1.19	1.39	1.15	24.99
60	3.20	4	1.11	1.40	1.25	31.91
70	3.74	4	1.16	1.37	1.41	30.08
80	4.27	4	1.18	1.57	1.40	33.39
90	4.81	4	1.17	1.43	1.47	36.39
100	5.34	4	1.16	1.29	1.31	46.14

Experiment: Effect of beam duration on specific energy (Samples 1-20)
Material: Limestone Spot size: 0.35”

Sample name	Avg. Laser power (kW)	Exposure time (sec)	Spot size (inch)	Measured horizontal dia. (cm)	Depth of penetration (cm)	SE based on dimensions kJ/cc (cone)	Average SE based on dimensions kJ/cc (cone)
1	5.34	1	0.3585	1.29	0.86	14.38	
2	5.34	1	0.3585	1.29	0.86	14.26	14.32
3	5.34	2	0.3585	1.27	1.68	15.05	
4	5.34	2	0.3585	1.27	1.68	15.08	15.06
5	5.34	3	0.3585	1.26	2.28	16.85	
6	5.34	3	0.3585	1.26	2.29	16.89	16.87
7	5.34	4	0.3585	1.26	2.22	23.24	
8	5.34	4	0.3585	1.26	2.22	23.22	23.23
9	5.34	5	0.3585	1.26	2.27	28.36	
10	5.34	5	0.3585	1.26	2.25	28.59	28.48
11	5.34	6	0.3585	1.26	2.75	28.17	
12	5.34	6	0.3585	1.26	2.77	27.91	28.04
13	5.34	7	0.3585	1.26	2.91	30.96	
14	5.34	7	0.3585	1.26	2.88	31.35	31.15
15	5.34	8	0.3585	1.26	3.34	30.86	
16	5.34	8	0.3585	1.26	3.01	34.29	32.58
17	5.34	9	0.3585	1.26	3.37	34.38	
18	5.34	9	0.3585	1.26	3.35	34.59	34.48
19	5.34	10	0.3585	1.26	3.47	37.12	
20	5.34	10	0.3585	1.26	3.46	37.27	37.20

Experiment: Effect of beam duration on specific energy (Samples 21-40)
Material: Limestone Spot size: 0.35”

Sample name	Avg. Laser power (kW)	Exposure time (sec)	Spot size (inch)	Measured horizontal dia. (cm)	Depth of penetration (cm)	SE based on dimensions kJ/cc (cone)	Average SE based on dimensions kJ/cc (cone)
22	5.34	11	0.3585	1.26	3.60	39.40	39.30
23	**5.34**	**12**	**0.3585**	1.26	**3.64**	42.49	
24	5.34	12	0.3585	1.26	4.07	38.03	40.26
25	5.34	13	0.3585	1.26	4.15	40.37	
26	5.34	13	0.3585	1.26	3.97	42.24	41.31
27	5.34	14	0.3585	1.26	3.77	47.81	
28	5.34	14	0.3585	1.26	3.84	46.97	47.39
29	5.34	15	0.3585	1.26	4.41	43.82	
30	**5.34**	**15**	**0.3585**	1.26	**3.79**	50.96	47.39
31	5.34	16	0.3585	1.26	4.58	45.07	
32	5.34	16	0.3585	1.26	4.40	46.87	45.97
33	5.34	17	0.3585	1.26	4.30	50.96	
34	5.34	17	0.3585	1.26	4.92	44.57	47.76
35	5.34	18	0.3585	1.26	4.49	51.68	
36	5.34	18	0.3585	1.26	4.45	52.10	51.89
37	**5.34**	**19**	**0.3585**	1.26	**4.18**	58.60	
38	5.34	19	0.3585	1.26	4.95	49.44	54.02
39	5.34	20	0.3585	1.26	4.70	54.83	
40	5.34	20	0.3585	1.26	4.46	57.77	56.30

Experiment: Effect of beam duration on specific energy (Samples 1-20)
Material: Sandstone Spot size: 0.35”

Sample name	Avg. Laser power (kW)	Exposure time (sec)	Spot size (inch)	Measured horizontal dia. (cm)	Measured vertical dia. (cm)	Average Dia. (cm)	Depth of penetration (cm)	SE based on dimensions kJ/cc (cone)	Average SE based on dimensions kJ/cc (cone)
1	5.34	1	0.3585	1.66	1.66	1.66	0.86	8.64	
2	5.34	1	0.3585	1.66	1.66	1.66	0.86	8.58	8.61
3	5.34	2	0.3585	1.66	1.66	1.66	1.68	8.75	
4	5.34	2	0.3585	1.66	1.66	1.66	1.68	8.75	8.75
5	5.34	3	0.3585	1.68	1.72	1.70	2.28	9.26	
6	5.34	3	0.3585	1.68	1.72	1.70	2.29	9.24	9.25
7	5.34	4	0.3585	1.65	1.72	1.69	2.22	12.97	
8	5.34	4	0.3585	1.68	1.72	1.70	2.22	12.72	12.84
9	5.34	5	0.3585	1.63	1.71	1.67	2.27	16.15	
10	5.34	5	0.3585	1.64	1.73	1.68	2.25	15.99	16.07
11	5.34	6	0.3585	1.69	1.76	1.72	2.75	15.04	
12	5.34	6	0.3585	1.69	1.76	1.72	2.77	14.88	14.96
13	5.34	7	0.3585	1.62	1.74	1.68	2.91	17.38	
14	5.34	7	0.3585	1.60	1.75	1.67	2.88	17.78	17.58
15	5.34	8	0.3585	1.70	1.70	1.70	3.34	17.00	
16	5.34	8	0.3585	1.71	1.63	1.67	3.01	19.48	18.24
17	5.34	9	0.3585	1.59	1.71	1.65	3.37	19.95	
18	5.34	9	0.3585	1.59	1.69	1.64	3.35	20.30	19.95
19	5.34	10	0.3585	1.68	1.74	1.71	3.47	20.09	
20	5.34	10	0.3585	1.64	1.74	1.69	3.46	20.62	20.35

Experiment: Effect of beam duration on specific energy (Samples 21-40)
Material: Sandstone Spot size: 0.35”

Sample name	Avg. Laser power (kW)	Exposure time (sec)	Spot size (inch)	Measured horizontal dia. (cm)	Measured vertical dia. (cm)	Average Dia. (cm)	Depth of penetration (cm)	SE based on dimensions kJ/cc (cone)	Average SE based on dimensions kJ/cc (cone)
21	5.34	11	0.3585	1.66	1.77	1.72	3.62	21.08	
22	5.34	11	0.3585	1.60	1.77	1.69	3.60	21.96	21.52
23	5.34	12	0.3585	1.61	1.44	1.53	3.64	28.91	
24	5.34	12	0.3585	1.64	1.79	1.71	4.07	20.52	20.52
25	5.34	13	0.3585	1.62	1.79	1.70	4.15	22.02	
26	5.34	13	0.3585	1.67	1.78	1.72	3.97	22.55	22.29
27	5.34	14	0.3585	1.65	1.75	1.70	3.77	26.21	
28	5.34	14	0.3585	1.68	1.77	1.73	3.84	24.95	25.58
29	5.34	15	0.3585	1.67	1.79	1.73	4.41	23.16	
30	5.34	15	0.3585	1.54	1.54	1.54	3.79	34.18	23.16
31	5.34	16	0.3585	1.64	1.79	1.72	4.58	24.22	
32	5.34	16	0.3585	1.59	1.59	1.59	4.40	29.34	26.78
33	5.34	17	0.3585	1.57	1.75	1.66	4.30	29.26	
34	5.34	17	0.3585	1.61	1.80	1.70	4.92	24.31	26.79
35	5.34	18	0.3585	1.61	1.80	1.70	4.49	28.17	
36	5.34	18	0.3585	1.60	1.78	1.69	4.45	28.94	28.55
37	5.34	19	0.3585	1.40	1.68	1.54	4.18	39.00	
38	5.34	19	0.3585	1.57	1.77	1.67	4.95	28.04	28.04
39	5.34	20	0.3585	1.59	1.80	1.70	4.70	30.20	
40	5.34	20	0.3585	1.52	1.67	1.60	4.46	35.89	33.05

Experiment: Effect of pulsation on specific energy
Material: Limestone **Spot size: 0.35”**
Duty cycle: 99 %

Experiment Name	Frequency (hz)	Inside hole diameter (cm)	Outside hole diameter (cm)	Hole depth (cm)	Laser power (kW)	Beam duration (sec)	Specific energy (kJ/cc)	Average specific energy (kJ/cc)
A10	10	1.06	1.66	0.94	5.34	4	76.27	
B10	10	0.99	1.60	1.10	5.34	4	75.26	75.77
A50	50	0.99	1.64	0.96	5.34	4	84.80	
B50	50	1.05	1.65	1.03	5.34	4	71.33	78.07
A100	100	1.04	1.63	1.00	5.34	4	74.48	
B100	100	1.04	1.64	0.81	5.34	4	91.92	83.20
A150	150	1.02	1.62	0.96	5.34	4	81.67	
B150	150	1.04	1.60	0.97	5.34	4	76.39	79.03
A200	200	1.00	1.65	1.03	5.34	4	78.03	
B200	200	1.03	1.63	1.04	5.34	4	74.07	76.05
A300	300	1.09	1.65	0.97	5.34	4	70.06	
B300	300	1.01	1.66	0.98	5.34	4	80.55	75.30
A350	350	0.99	1.65	1.02	5.34	4	80.23	
B350	350	1.03	1.62	1.04	5.34	4	72.36	76.30

Experiment: Effect of pulsation on specific energy (continued)
Material: Limestone **Spot size: 0.35”**
Duty cycle: 99 %

Experiment Name	Frequency (hz)	Inside hole diameter (cm)	Outside hole diameter (cm)	Hole depth (cm)	Laser power (kW)	Beam duration (sec)	Specific energy (kJ/cc)	Average specific energy (kJ/cc)
A400	400	1.01	1.65	1.00	5.34	4	79.89	
B400	400	1.02	1.62	1.02	5.34	4	76.34	78.12
A500	500	1.05	1.67	1.03	5.34	4	71.27	
B500	500	1.03	1.70	1.04	5.34	4	73.21	72.24
A600	600	1.01	1.66	1.03	5.34	4	76.64	
B600	600	0.97	1.66	1.15	5.34	4	74.10	75.37
A700	700	0.96	1.64	1.00	5.34	4	87.11	
B700	700	1.08	1.66	0.99	5.34	4	69.62	78.36
A800	800	1.02	1.68	0.99	5.34	4	78.12	
B800	800	1.09	1.69	0.95	5.34	4	71.34	74.73
A900	900	1.03	1.67	0.93	5.34	4	81.96	
B900	900	1.02	1.66	1.10	5.34	4	70.85	76.40

Experiment: Effect of pulsation on specific energy
Material: Limestone **Spot size: 0.35”**
Duty cycle: 50 %

Frequency (hz)	Inside hole diameter (cm)	Outside hole diameter (cm)	Hole depth (cm)	Laser power (kW)	Beam duration (sec)	Specific energy (kJ/cc)
10	1.25	-	0.30	5.34	4	86.45
50	1.28	-	0.29	5.34	4	86.76
100	1.3	-	0.29	5.34	4	84.40
200	0.98	-	0.16	5.34	4	265.48
300	0.398	-	0.14	5.34	4	1839.54
400	1.05	-	0.01	5.34	4	7400.38
500	no hole	-		5.34	4	
600	no hole	-		5.34	4	
700	no hole	-		5.34	4	
800	no hole	-		5.34	4	
900	no hole	-		5.34	4	
cw	1.253	1.42	1.00	5.34	4	51.97

Experiment: Effect of pulsation on specific energy
Material: Limestone **Spot size: 0.35”**
Duty cycle: 50 %

Frequency (hz)	Inside hole diameter (cm)	Outside hole diameter (cm)	Hole depth (cm)	Laser power (kW)	Beam duration (sec)	Specific energy (kJ/cc)
1	1.09	1.40	1.03	5.34	8	67.00
2	1.09	1.40	0.97	5.34	8	70.80
3	1.09	1.40	0.93	5.34	8	73.84
4	1.09	1.40	0.87	5.34	8	78.93
5	1.09	1.40	0.69	5.34	8	99.52
6	1.09	1.40	0.64	5.34	8	107.30
7	1.09	1.40	0.68	5.34	8	100.99
8	1.09	1.40	0.68	5.34	8	100.99
9	1.09	1.40	0.68	5.34	8	100.99
10	1.09	1.40	0.71	5.34	8	96.72

Experiment: Effect of pulsation on specific energy
Material: Sandstone **Spot size: 0.35”**
Duty cycle: 99 %

Experiment Name	Frequency (hz)	Hole diameter (horizontal)(cm)	Hole diameter (vertical)(cm)	Average hole diameter (cm)	Hole depth (cm)	Laser power (kW)	Beam duration (sec)	Specific energy (kJ/cc)	Average specific energy (kJ/cc)
A10	10	1.42	1.60	1.51	1.69	5.34	4	20.99	
B10	10	1.42	1.61	1.51	2.12	5.34	4	16.65	18.82
A50	50	1.42	1.56	1.49	2.20	5.34	4	16.54	
B50	50	1.42	1.56	1.49	2.23	5.34	4	16.34	16.44
A100	100	1.42	1.56	1.49	2.24	5.34	4	16.26	
B100	100	1.42	1.56	1.49	1.78	5.34	4	20.49	18.37
A150	150	1.42	1.56	1.49	2.24	5.34	4	16.26	
B150	150	1.42	1.56	1.49	2.28	5.34	4	15.99	16.12
A200	200	1.42	1.56	1.49	2.29	5.34	4	15.89	
B200	200	1.42	1.56	1.49	2.34	5.34	4	15.57	15.73
A300	300	1.42	1.56	1.49	1.87	5.34	4	19.45	
B300	300	1.42	1.56	1.49	2.24	5.34	4	16.28	17.86
A350	250	1.42	1.56	1.49	2.23	5.34	4	16.29	
B350	350	1.42	1.56	1.49	2.29	5.34	4	15.92	16.10

Experiment: Effect of pulsation on specific energy (continued)
Material: Sandstone **Spot size: 0.35”**
Duty cycle: 99 %

Experiment Name	Frequency (hz)	Hole diameter (horizontal)(cm)	Hole diameter (vertical)(cm)	Average hole diameter (cm)	Hole depth (cm)	Laser power (kW)	Beam duration (sec)	Specific energy (kJ/cc)	Average specific energy (kJ/cc)
B400	400	1.42	1.56	1.49	1.70	5.34	4	21.38	18.50
A500	500	1.42	1.56	1.49	2.20	5.34	4	16.52	
B500	500	1.42	1.56	1.49	2.25	5.34	4	16.16	16.34
A600	600	1.42	1.56	1.49	2.25	5.34	4	16.17	
B600	600	1.42	1.56	1.49	2.26	5.34	4	16.13	16.15
A700	700	1.42	1.56	1.49	1.66	5.34	4	21.92	
B700	700	1.42	1.56	1.49	2.19	5.34	4	16.64	19.28
A800	800	1.42	1.56	1.49	2.23	5.34	4	16.34	
B800	800	1.42	1.56	1.49	2.22	5.34	4	16.37	16.35
A900	900	1.42	1.56	1.49	2.22	5.34	4	16.41	
B900	900	1.42	1.56	1.49	1.65	5.34	4	22.12	19.26
A999	999	1.42	1.56	1.49	2.12	5.34	4	17.18	
B999	999	1.42	1.56	1.49	2.08	5.34	4	17.47	17.33

Experiment: Effect of pulsation on specific energy
Material: Sandstone **Spot size: 0.35”**
Duty cycle: 50 %

Frequency (hz)	Horizontal hole diameter (cm)	Vertical hole diameter (cm)	Average hole diameter (cm)	Hole depth (cm)	Laser power (kW)	Beam duration (sec)	Specific energy (kJ/cc)
1	1.42	1.60	1.51	2.21	5.34	8	16.29
2	1.41	1.54	1.47	2.19	5.34	8	17.20
3	1.39	1.57	1.48	2.13	5.34	8	17.53
4	1.40	1.59	1.50	1.96	5.34	8	18.60
5	1.32	1.40	1.36	1.51	5.34	8	29.31
6	1.39	1.49	1.44	1.86	5.34	8	21.15
7	1.37	1.44	1.40	2.07	5.34	8	19.99
8	1.41	1.45	1.43	1.56	5.34	8	25.58
9	1.27	1.22	1.24	1.47	5.34	8	35.84
10	1.02	1.02	1.02	1.32	5.34	8	59.55
50	1.07	1.07	1.07	1.30	5.34	8	54.72
100	1.43	1.43	1.43	2.09	5.34	8	19.12
200	1.26	1.22	1.24	1.25	5.34	8	42.35
300	1.38	1.38	1.38	1.86	5.34	8	22.94
400	1.47	1.39	1.43	1.39	5.34	8	28.78
500	1.28	1.28	1.28	1.15	5.34	8	43.36
600	1.29	1.29	1.29	1.15	5.34	8	43.08
700	1.41	1.41	1.41	1.22	5.34	8	33.62
800	1.35	1.35	1.35	1.22	5.34	8	36.83
900	1.37	1.35	1.36	0.90	5.34	8	49.23
999	1.30	1.30	1.30	0.69	5.34	8	69.76

Experiment: Effect of purge gas and saturation on specific energy
Material: Sandstone Spot size: 0.35”

Sample Name	Core dia. (mm)	Core length (mm)	Weight (dry) before lasing (gm)	Weight (wet) before lasing (gm)	Weight after lasing (gm)	Weight removed (gm)	Specific density (gm/cc)	Volume removed (cc)	SE (kJ/cc)	Average SE (kJ/cc)
BG-P-AR-SW1	50.48	51.68	221.9	240.4	235.8	4.6	2.15	2.18	18.37	
BG-P-AR-SW2	50.48	51.62	220.7	239.3	234.7	4.6	2.14	2.18	18.37	
BG-P-AR-SW3	50.48	51.49	220.4	238.8	234.3	4.5	2.14	2.13	18.77	18.50
BG-P-AR-SB1	50.53	52.2	221.6	240.1	235.3	4.8	2.12	2.27	17.60	
BG-P-AR-SB2	50.5	51.46	220.9	239.4	234.3	5.1	2.14	2.41	16.56	
BG-P-AR-SB3	50.46	51.5	220.6	238.9	234	4.9	2.14	2.32	17.24	17.14
BG-P-AR-SO1	50.71	51.89	221.7	237.9	234.7	3.2	2.12	1.52	26.40	
BG-P-AR-SO2	50.54	52.1	221.8	237.9	234.6	3.3	2.12	1.56	25.60	
BG-P-AR-SO3	50.42	52	221.4	237.8	234.5	3.3	2.13	1.56	25.60	25.87
BG-P-N-SB1	50.62	52.4	221.5	240.5	236.6	3.9	2.10	1.85	21.66	
BG-P-N-SB2	50.49	52.38	221.4	240.8	236.7	4.1	2.11	1.94	20.60	
BG-P-N-SB3	50.49	52.11	220.4	240	235.3	4.7	2.11	2.23	17.97	20.08
BG-P-N-SW1	50.48	52.5	221.1	240.6	**236**	4.6	2.10	2.18	18.37	
BG-P-N-SW2	50.48	52.28	220.7	240.1	**235.7**	4.4	2.11	2.08	19.20	
BG-P-N-SW3	50.48	52.19	220.6	239.6	234.7	4.9	2.11	2.32	17.24	18.27
BG-P-N-SO1	50.48	51.98	219.9	238.1	234.8	3.3	2.11	1.56	25.60	
BG-P-N-SO2	50.51	52.67	220.9	239.1	236	3.1	2.09	1.47	27.25	
BG-P-N-SO3	50.44	51.79	221.5	236.8	233.8	3	2.14	1.42	28.16	27.00

Nomenclature
BG: Burea sandstone B: Brine N: Nitrogen Ar: Argon P: Purge gas O: Oil A: Air S: Saturation W: water H: Helium

Experiment: Effect of purge gas and saturation on specific energy
Material: Sandstone Spot size: 0.35”

Sample Name	Core dia. (mm)	Core length (mm)	Weight (dry) before lasing (gm)	Weight (wet) before lasing (gm)	Weight after lasing (gm)	Weight removed (gm)	Specific density (gm/cc)	Volume removed (cc)	SE (kJ/cc)	Average SE (kJ/cc)
BG-P-A-SB1	50.44	53.66	220.5	240.2	235.9	4.3	2.06	2.04	19.65	
BG-P-A-SB2	50.48	51.96	220.9	240.6	236.5	4.1	2.12	1.94	20.60	
BG-P-A-SB3	50.42	51.88	214.3	235.3	230.3	5	2.07	2.37	16.90	19.05
BG-P-A-SW1	50.49	51.96	220.6	240.1	236.3	3.8	2.12	1.80	22.23	
BG-P-A-SW2	50.4	51.96	213.8	234.9	230.3	4.6	2.06	2.18	18.37	
BG-P-A-SW3	50.51	51.91	220.7	240.5	236.1	4.4	2.12	2.08	19.20	19.93
BG-P-A-SO1	50.46	52	221.1	236.4	233.4	3	2.13	1.42	28.16	
BG-P-A-SO2	50.43	51.95	223	237.6	234.6	3	2.15	1.42	28.16	
BG-P-A-SO3	50.51	52.66	220	237.3	234.2	3.1	2.08	1.47	27.25	27.86
BG-P-H-SB1	50.5	51.82	219.7	239.2	235.2	4	2.12	1.89	21.12	
BG-P-H-SB2	50.48	52.15	222.9	241.6	238.2	3.4	2.14	1.61	24.85	
BG-P-H-SB3	50.48	51.86	222.4	240	237.4	2.6	2.14	1.23	32.49	26.15
BG-P-H-SW1	50.47	52.47	222.1	240	236.8	3.2	2.12	1.52	26.40	
BG-P-H-SW2	50.48	51.78	219.9	238.9	235.4	3.5	2.12	1.66	24.14	
BG-P-H-SW3	50.55	51.35	221	238.9	235.3	3.6	2.14	1.70	23.47	24.67
BG-P-H-SO1	50.48	52.14	223	238.6	236	2.6	2.14	1.23	32.49	
BG-P-H-SO2	50.53	52.06	222.9	238.5	236	2.5	2.14	1.18	33.79	
BG-P-H-SO3	50.51	52.5	223.1	238.5	236.1	2.4	2.12	1.14	35.20	33.83

Nomenclature:
BG: Burea sandstone B: Brine N: Nitrogen Ar: Argon P: Purge gas O: Oil A: Air S: Saturation W: water H: Helium

Experiment: Effect of purge gas and saturation on specific energy
Material: Sandstone Spot size: 0.35”

Sample Name	Core dia. (mm)	Core length (mm)	Weight (dry) before lasing (gm)	Weight (wet) before lasing (gm)	Weight after lasing (gm)	Weight removed (gm)	Specific density (gm/cc)	Volume removed (cc)	SE (kJ/cc)	Average SE (kJ/cc)
BG-P-Ar1	50.47	49.91	209	209	204.2	4.8	2.09	2.27	17.60	
BG-P-Ar2	50.48	49.86	209.8	209.8	205.7	4.1	2.10	1.94	20.60	
BG-P-Ar3	50.49	50	209.9	209.9	205.9	4	2.10	1.89	21.12	19.77
BG-P-H1	50.45	49.41	207.9	207.9	204.2	3.7	2.10	1.75	22.83	
BG-P-H2	50.52	49.86	210.9	210.9	206.1	4.8	2.11	2.27	17.60	
BG-P-H3	50.49	49.14	209.4	209.4	203.8	5.6	2.13	2.65	15.09	18.51
BG-P-N1	50.47	49.98	209	209	205.6	3.4	2.09	1.61	24.85	
BG-P-N2	50.5	49.85	211.8	211.8	206.5	5.3	2.12	2.51	15.94	
BG-P-N3	50.47	50.13	209.6	209.6	205.7	3.9	2.09	1.85	21.66	20.82
BG-P-A1	50.49	49.95	209.8	209.8	206.7	3.1	2.10	1.47	27.25	
BG-P-A2	50.49	49.76	207.3	207.3	204.3	3	2.08	1.42	28.16	
BG-P-A3	50.43	51.49	219.1	219.1	216	3.1	2.13	1.47	27.25	27.55

Nomenclature:
BG: Burea sandstone B: Brine N: Nitrogen Ar: Argon P: Purge gas O: Oil A: Air S: Saturation W: water H: Helium

Experiment: Effect of purge gas and saturation on specific energy
Material: Limestone Spot size: 0.35”

Sample Name	Core dia. (mm)	Core length (mm)	Weight (dry) before lasing (gm)	Weight (wet) before lasing (gm)	Weight after lasing (gm)	Weight Difference (gm)	Specific gravity (gm/cc)	Volume removed (cc)	Specific energy (kJ/cc)	Average SE (kJ/cc)
LS-P-AR-SW1	50.46	51.84	236.3	251.3	246	5.3	2.28	2.33	18.37	
LS-P-AR-SW2	50.45	51.56	233	248.3	245.3	3	2.26	1.33	32.19	
LS-P-AR-SW3	50.48	51.35	234	249.1	246.1	3	2.28	1.32	32.42	27.66
LS-P-AR-SB1	50.46	51.81	234.1	250	247	3	2.26	1.33	32.17	
LS-P-AR-SB2	50.45	51.82	235.7	250.8	247.8	3	2.28	1.32	32.40	
LS-P-AR-SB3	50.47	51.74	233.6	249.2	246.2	3	2.26	1.33	32.14	32.24
LS-P-AR-SO1	50.45	51.28	232.4	242.4	240.6	1.8	2.27	0.79	53.81	
LS-P-AR-SO2	50.49	52.06	234.9	246.3	244.6	1.7	2.25	0.75	56.63	
LS-P-AR-SO3	50.43	51.45	233.7	243.8	242.1	1.7	2.27	0.75	57.15	55.86
LS-P-N-SB1	50.48	51.66	233.5	249.1	246.4	2.7	2.26	1.20	35.73	
LS-P-N-SB2	50.47	51.67	233.9	249.1	246.4	2.7	2.26	1.19	35.80	
LS-P-N-SB3	50.44	50.45	228.7	243.9	241.3	2.6	2.27	1.15	37.28	36.27
LS-P-N-SW1	50.49	51.45	233.3	248.6	245.4	3.2	2.26	1.41	30.24	
LS-P-N-SW2	50.44	51.6	232.5	247.9	244.5	3.4	2.25	1.51	28.33	
LS-P-N-SW3	50.47	51.75	235.1	250	246.6	3.4	2.27	1.50	28.53	29.03
LS-P-N-SO1	50.46	51.62	234.1	244.3	242.7	1.6	2.27	0.71	60.55	
LS-P-N-SO2	50.43	51.87	234.5	246.2	244.6	1.6	2.26	0.71	60.43	
LS-P-N-SO3	50.44	51.58	232.9	244.6	243	1.6	2.26	0.71	60.33	60.44

Nomenclature:
BG: Burea sandstone B: Brine N: Nitrogen Ar: Argon P: Purge gas O: Oil A: Air S: Saturation W: water H: Helium

Experiment: Effect of purge gas and saturation on specific energy
Material: Limestone Spot size: 0.35”

Sample Name	Core dia. (mm)	Core length (mm)	Weight (dry) before lasing (gm)	Weight (wet) before lasing (gm)	Weight after lasing (gm)	Weight Difference (gm)	Specific gravity (gm/cc)	Volume removed (cc)	Specific energy (kJ/cc)	Average SE (kJ/cc)
LS-P-A-SB1	50.44	51.76	233.9	248.2	245.6	2.6	2.26	1.15	37.16	
LS-P-A-SB2	50.45	51.32	233.2	248.3	245.8	2.5	2.27	1.10	38.84	
LS-P-A-SB3	50.47	49.85	228.4	243.1	240.3	2.8	2.29	1.22	34.94	36.98
LS-P-A-SW1	50.48	51.62	231.3	246.9	243.3	3.6	2.24	1.61	26.57	
LS-P-A-SW2	50.43	51.71	236.3	250.4	246.8	3.6	2.29	1.57	27.15	
LS-P-A-SW3	50.43	51.53	236.7	251.2	247.9	3.3	2.30	1.43	29.77	27.83
LS-P-A-SO1	50.48	51.81	235.8	247	245.1	1.9	2.27	0.84	51.13	
LS-P-A-SO2	50.42	51.59	232.6	244.7	242.7	2	2.26	0.89	48.23	
LS-P-A-SO3	50.44	51.39	233.2	244.1	242.2	1.9	2.27	0.84	51.06	50.14
LS-P-H-SB1	50.42	51.4	234.7	249.4	247.2	2.2	2.29	0.96	44.41	
LS-P-H-SB2	50.44	49.8	225.1	240	237.7	2.3	2.26	1.02	42.02	
LS-P-H-SB3	50.42	49.65	227.7	242.8	240.2	2.6	2.30	1.13	37.74	41.39
LS-P-H-SW1	50.43	51.69	231.5	247.1	244.6	2.5	2.24	1.11	38.31	
LS-P-H-SW2	50.45	51.26	232.3	247.6	245.2	2.4	2.27	1.06	40.35	
LS-P-H-SW3	50.42	51.03	229.4	244.9	242.4	2.5	2.25	1.11	38.47	39.05
LS-P-H-SO1	50.43	51.87	233.7	245.6	244.1	1.5	2.26	0.66	64.24	
LS-P-H-SO2	50.43	51.28	230.7	243.6	242	1.6	2.25	0.71	60.14	
LS-P-H-SO3	50.43	51.62	232.4	244.8	243.6	1.2	2.25	0.53	80.24	68.21

Nomenclature:
BG: Burea sandstone B: Brine N: Nitrogen Ar: Argon P: Purge gas O: Oil A: Air S: Saturation W: water H: Helium

Experiment: Effect of purge gas and saturation on specific energy
Material: Limestone Spot size: 0.35”

Sample Name	Core dia. (mm)	Core length (mm)	Weight (dry) before lasing (gm)	Weight (wet) before lasing (gm)	Weight after lasing (gm)	Weight Difference (gm)	Specific gravity (gm/cc)	Volume removed (cc)	Specific energy (kJ/cc)	Average SE (kJ/cc)
LS-P-Ar1	50.39	49.44	228.1	225.6	224.1	1.5	2.31	0.65	65.89	
LS-P-Ar2	50.44	49.66	228	225.5	223.9	1.6	2.30	0.70	61.35	
LS-P-Ar3	50.36	49.77	223.9	223.9	221.9	2	2.26	0.89	48.24	58.49
LS-P-H1	50.44	49.34	227.6	227.6	226.1	1.5	2.31	0.65	65.75	
LS-P-H2	50.42	49.81	224	224	222.5	1.5	2.25	0.67	64.15	
LS-P-H3	50.46	49.64	229.9	229.9	228.4	1.5	2.32	0.65	65.96	65.28
LS-P-N1	50.35	49.87	227.6	227.6	225	2.6	2.29	1.13	37.66	
LS-P-N2	50.48	49.88	223.8	223.8	221.3	2.5	2.24	1.12	38.31	
LS-P-N3	50.43	49.49	224.3	224.3	221.7	2.6	2.27	1.15	37.28	37.75
LS-P-A1	50.37	47.83	213.5	213.5	211.6	1.9	2.24	0.85	50.37	
LS-P-A2	50.45	49.27	222.3	222.3	219.9	2.4	2.26	1.06	40.18	
LS-P-A3	50.41	49.77	223.3	223.3	221.2	2.1	2.25	0.93	45.73	45.42

Nomenclature:
BG: Burea sandstone B: Brine N: Nitrogen Ar: Argon P: Purge gas O: Oil A: Air S: Saturation W: water H: Helium

Experiment: Time of penetration for casing material
Material: steel Spot size: 0.35”

Plate thickness (inch)	Laser power (kW)	Time of penetration Air-purge (sec)	Time of penetration N2-purge (sec)
0.25	5.34	2.45	3.81
0.35	5.34	3	4.72
0.4	5.34	3.59	5.53
0.5	5.34	4.91	7.1
0.6	5.34	6.43	9.69
0.75	5.34	10.27	15.01
1	5.34	20.21	28.46

Experiment: Time of penetration for casing material
Material: Cement (Class A) **Spot size: 0.35”**

Plate thickness (inch)	Laser power (kW)	Time of penetration (sec)
0.25	5.34	1.86
0.35	5.34	2.37
0.4	5.34	2.69
0.5	5.34	2.5
0.7	5.34	4.43
0.8	5.34	4.73
0.9	5.34	6
1	5.34	7.03

Experiment: Time of penetration for casing material
Material: Cement (50-50) **Spot size: 0.35”**

Plate thickness (inch)	Laser power (kW)	Time of penetration (sec)
0.25	5.34	1.09
0.35	5.34	1.3
0.4	5.34	1.35
0.5	5.34	1.6
0.6	5.34	2.52
0.7	5.34	2.98
0.8	5.34	3.3
0.9	5.34	3.65
1	5.34	4.46
2	5.34	9.49

Experiment: Time of penetration for casing material
Material: Cement (SY 250) **Spot size: 0.35”**

Plate thickness (inch)	Laser power (kW)	Time of penetration (sec)
0.25	5.34	0.96
0.35	5.34	1.23
0.4	5.34	1.39
0.5	5.34	1.88
0.6	5.34	1.98
0.7	5.34	2.49
0.8	5.34	2.72
0.9	5.34	3.36
1	5.34	3.77
2	5.34	7.84

Experiment: Time of penetration for casing material
Material: Composite: 0.25" thick steel plate + varying cement layer + 2" thick sandstone core
Spot size: 0.35”

Sample name	cement layer thickness	Laser power (kW)	Time of penetration (sec)	Average time of penetration (sec)
BG-C-S-0.25-1	0.25	5.34	27.04	27.04
BG-C-S-0.35-1	0.35	5.34	29.2	
BG-C-S-0.35-2	0.35	5.34	27.01	28.11
BG-C-S-0.4-1	0.4	5.34	28.8	
BG-C-S-0.4-2	0.4	5.34	30.11	29.46
BG-C-S-0.5-1	0.5	5.34	26.86	
BG-C-S-0.5-2	0.5	5.34	29.95	28.41
BG-C-S-0.6-1	0.6	5.34	35.78	
BG-C-S-0.6-2	0.6	5.34	37.38	36.58
BG-C-S-0.7-1	0.7	5.34	36.06	
BG-C-S-0.7-2	0.7	5.34	47.76	41.91
BG-C-S-0.8-1	0.8	5.34	35.63	
BG-C-S-0.8-2	0.8	5.34	35.26	35.45
BG-C-S-0.9-1	0.9	5.34	40.08	
BG-C-S-0.9-2	0.9	5.34	30.13	35.11
BG-C-S-1-1	1	5.34	46.15	
BG-C-S-1-2	1	5.34	39.05	42.60

Experiment: Time of penetration for casing material
Material: Composite: 0.25" thick steel plate + varying cement layer + 2" thick limestone core
Spot size: 0.35”

Sample name	cement layer thickness (inch)	Laser power (kW)	Time of penetration (sec)	Average time of penetration (sec)
LS-C-S-0.25-1	0.25	5.34	17.11	
LS-C-S-0.25-2	0.25	5.34	17.04	17.08
LS-C-S-0.35-1	0.35	5.34	16.45	
LS-C-S-0.35-2	0.35	5.34	-	16.45
LS-C-S-0.4-1	0.4	5.34	17.75	
LS-C-S-0.4-2	0.4	5.34	17.8	17.78
LS-C-S-0.5-1	0.5	5.34	18.18	
LS-C-S-0.5-2	0.5	5.34	19.51	18.85
LS-C-S-0.6-1	0.6	5.34	20.65	
LS-C-S-0.6-2	0.6	5.34	19.9	20.28
LS-C-S-0.7-1	0.7	5.34	21.03	
LS-C-S-0.7-2	0.7	5.34	20.34	20.69
LS-C-S-0.8-1	0.8	5.34	20.53	
LS-C-S-0.8-2	0.8	5.34	21.59	21.06
LS-C-S-0.9-1	0.9	5.34	22.29	
LS-C-S-0.9-2	0.9	5.34	21.4	21.85
LS-C-S-1-1	1	5.34	23.8	
LS-C-S-1-2	1	5.34	23.98	23.89

Experiment: Effect of laser power on specific energy (0.35” collimated beam)
Material: Sandstone

Percentage laser power (%)	laser power (kW)	beam duration (sec)	Vertical hole diameter (cm)	Horizontal hole diameter (cm)	Hole depth (cm)	Specific energy (kJ/cc)
20	1.07	4	1.24	1.14	0.51	20.81
30	1.60	4	1.33	1.22	0.62	22.32
40	2.14	4	1.36	1.32	1.06	16.65
50	2.67	4	1.41	1.33	1.34	15.31
60	3.20	4	1.44	1.37	1.67	14.14
70	3.74	4	1.51	1.39	1.8	13.92
80	4.27	4	1.53	1.47	1.96	14.23
90	4.81	4	1.54	1.46	2.14	14.47
100 10	5.34 0.53	4 8	1.53 0.8	1.53 0.86	2.34 0.12	14.89
20	1.07	8	1.19	1.03	0.37	62.29
30	1.60	8	1.28	1.27	0.8	37.35
40	2.14	8	1.38	1.29	1.56	21.97
50	2.67	8	1.36	1.33	2.66	16.58
60	3.20	8	1.41	1.34	2.8	17.59
70	3.74	8	1.47	1.47	2.1	25.17
80	4.27	8	1.52	1.41	2.68	21.08
90	4.81	8	1.43	1.5	3.34	21.50
100	5.34	8	1.49	1.59	3.57	20.59

Experiment: Effect of laser power on specific energy (0.35” collimated beam)
Material: Limestone

Percentage laser power (%)	laser power (kW)	beam duration (sec)	Inside hole diameter (cm)	Outside hole diameter (cm)	Hole depth (cm)	Specific energy (kJ/cc)
10	0.53	4	0	0	0	-
20	1.07	4	0	0	0	-
30	1.60	4	0	0	0	-
40	2.14	4	0	0	0	-
50	2.67	4	1.05	1.44	0.20	185.94
60	3.20	4	1.05	1.55	0.35	127.23
70	3.74	4	1.05	1.55	0.38	134.90
80	4.27	4	1.12	1.70	0.54	95.83
90	4.81	4	1.13	1.69	0.68	85.50
100	5.34	4	1.13	1.75	0.79	81.37
10	0.53	8	0	0	0	-
20	1.07	8	0	0	0	-
30	1.60	8	0	0	0	-
40	2.14	8	0	0	0	-
50	2.67	8	0.68	1.43	0.34	529.80
60	3.20	8	0.86	1.59	0.89	147.39
70	3.74	8	0.99	1.69	1.24	94.41
80	4.27	8	1.06	1.74	1.68	69.19
90	4.81	8	1.05	1.76	2.06	64.78
100	5.34	8	1.09	1.78	2.42	57.17

Experiment: Effect of beam duration on specific energy (0.35” collimated beam)
Material: Sandstone

Sample name	Avg. Laser power (kW)	Exposure time (sec)	Spot size (inch)	Measured horizontal dia. (cm)	Measured vertical dia. (cm)	Average dia. (cm)	Depth of penetration (cm)	SE based on dimensions kJ/cc (cone)
1	5.34	2	0.35	1.47	1.56	1.52	1.40	4.23
2	5.34	4	0.35	1.53	1.5	1.52	2.36	5.02
3	5.34	6	0.35	1.48	1.51	1.50	3.00	6.08
4	5.34	8	0.35	1.5	1.5	1.50	3.54	6.83
5	5.34	10	0.35	1.53	1.5	1.52	3.77	7.86
6	5.34	12	0.35	1.5	1.49	1.50	4.21	8.67
7	5.34	14	0.35	1.52	1.53	1.53	4.08	10.03
8	5.34	16	0.35	1.49	1.67	1.58	4.68	9.31
9	5.34	18	0.35	1.53	1.69	1.61	4.10	11.52
10	5.34	20	0.35	1.5	1.6	1.55	4.21	13.44

Experiment: Effect of beam duration on specific energy (0.35” collimated beam)
Material: Sandstone

Sample name	Avg. Laser power (kW)	Exposure time (sec)	Spot size (inch)	Measured horizontal dia. (cm)	Measured vertical dia. (cm)	Average dia. (cm)	Depth of penetration (cm)	SE based on dimensions kJ/cc (cone)
1	3.20	2	0.35	1.6	1.27	1.44	1.17	3.39
2	3.20	4	0.35	1.55	1.28	1.42	2.07	3.94
3	3.20	6	0.35	1.42	1.17	1.30	2.81	5.19
4	3.20	8	0.35	1.32	1.22	1.27	3.18	6.36
5	3.20	10	0.35	1.37	1.25	1.31	3.35	7.10
6	3.20	12	0.35	1.34	1.35	1.35	3.43	7.89
7	3.20	14	0.35	1.37	1.25	1.31	3.41	9.76
8	3.20	16	0.35	1.46	1.43	1.45	3.60	8.68
9	3.20	18	0.35	1.49	1.63	1.56	2.94	10.26
10	3.20	20	0.35	1.37	1.44	1.41	3.98	10.38

Experiment: Effect of beam duration on specific energy (0.35” collimated beam)
Material: Limestone

Sample name	Laser power (kW)	Exposure time (sec)	Spot size (inch)	Measured inside dia. (cm)	Measured outside dia. (cm)	Depth of penetration (cm)	SE based on dimensions kJ/cc (cone)
1	5.34	2	0.35	0.92	1.38	0.55	87.63
2	5.34	4	0.35	0.88	1.49	1.5	70.24
3	5.34	6	0.35	0.91	1.61	1.4	105.56
4	5.34	8	0.35	0.94	1.63	3.21	57.53
5	5.34	10	0.35	0.69	1.86	4.74	90.38
6	5.34	12	0.35	0.98	1.83	4.34	58.72
7	5.34	14	0.35	1.08	1.83	5.23	46.81
8	5.34	16	0.35	1.1	1.82	5.91	45.64
9	5.34	18	0.35	0.97	1.84	5.05	77.27
10	5.34	20	0.35	1.2	1.9	6.58	43.05

Appendix B: DOE Project Review Presentation

February 9, 2004
Phoenix, AZ

Slide 1

Advances in Improving Gas Well Drilling and Completion with High Energy Lasers

Natural Gas Technologies II

Phoenix, AZ

Brian C. Gahan
Samih Batarseh
Gas Technology Institute

February 9, 2004

Slide 2

Presentation Outline

> GTI Laser Applications Background
> Laser/Rock Interaction Research
> Laser Applications
> Fiber Laser
> Summary

Slide 3

GTI LASER APPLICATIONS BACKGROUND

GRI-Funded Feasibility Study

> Laser Drilling Experiments – 11/97
  – Reduce D&C Costs/Increase Reserves
  – Unconventional Resources
> Three High-Powered Military Lasers
  – **COIL** - Chemical Oxygen Iodine Laser
  – **MIRACL** - Mid Infra-Red Advanced Chemical Laser
  – **CO_2** Laser
> Various Rock Types Studied
  – Sandstone, Limestone, Shale
  – Granite, Concrete, Salt

Slide 4

GTI LASER APPLICATIONS BACKGROUND

Specific Energy Defined

$$SE = \frac{\text{Energy Input}}{\text{Volume Removed}} = \frac{P}{dV/dt}$$

$$= \frac{kW}{cm^3/sec} = \frac{kJ}{cm^3}$$

gti

Slide 5

GTI LASER APPLICATIONS BACKGROUND

GRI-Funded Study Conclusions

- Previous Literature **Overestimated** SE
- Existing Lasers Able to Penetrate All Rock
- Laser/Rock Interactions Are a Function of Rock and Laser (Spall, Melt or Vaporize)
- Secondary Effects Reduce Destruction
- Melt Sheaths Similar to Ceramic

Study Conclusions Indicate Additional Research is Warranted

gti

Slide 6

LASER/ROCK INTERACTION RESEARCH

GTI/DOE Laser Drilling Project

First Phase Objectives

1. Laser Cutting Energy Assessment
2. Variable Pulse Laser Effects (Nd:YAG)
3. Lasing Through Liquids

gti

NETL Halliburton Company PDVSA

Slide 7

LASER/ROCK INTERACTION RESEARCH

Nd:YAG Laser (ANL)

Neodymium Yttrium Aluminum Garnet

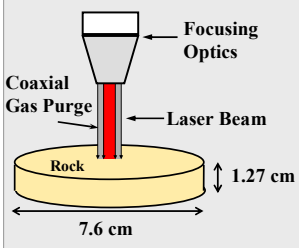

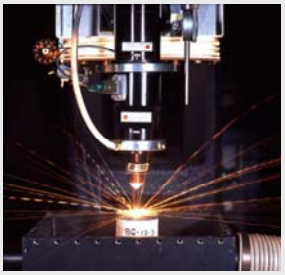

gti

Slide 8

LASER/ROCK INTERACTION RESEARCH

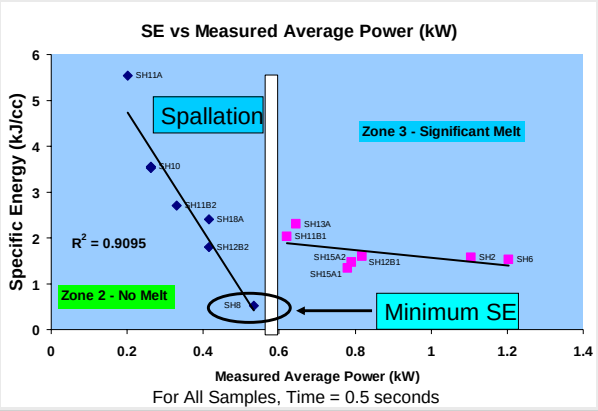

For All Samples, Time = 0.5 seconds

gti

Slide 9

LASER/ROCK INTERACTION RESEARCH

Water Saturated Easier to Break

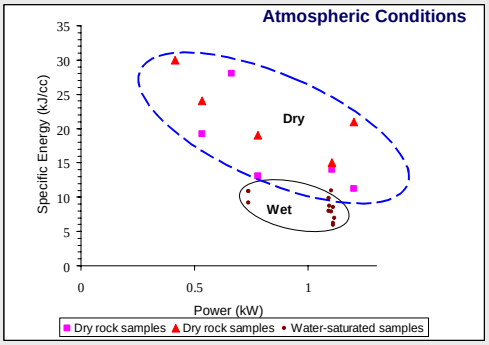

gti

Slide 10

LASER/ROCK INTERACTION RESEARCH

Conclusions: GTI/DOE Phase I

- Optimal Laser Parameters Observed to Minimize SE for Each Rock Type
- Shorter Total Duration Pulses Reduce Secondary Effects from Heat Accumulation
- SE for Shale 10x Less Than SS or LS
- Pulsed Lasers Cut Faster & With Less Energy Than Continuous Wave Lasers.
- Fluid Saturated Rocks Cut Faster Than Dry Rocks.

gti

Slide 11

LASER/ROCK INTERACTION RESEARCH

Paradigm Shift Results

- Change in Application Theory – Rate of Application: Blasting vs Chipping
- Unlimited Downhole Applications due to Precision and Control (i.e., direction, power, etc.)
- Off-Ramp Approach to Commercialization and Technology Integration
  - Completions Less Complex Than Drilling
  - Allows Technology Leveraging
  - Rolling Integration Into Industry

gti

Slide 12

LASER/ROCK INTERACTION RESEARCH

Multiple-Hole Test Series

- Performed July 2002
- Test Effects of Laser Application Techniques on Specific Energy
  - Avoid Melt
  - Minimize SE Values
- Apply Multiple Beam Bursts in Varied Geometric Patterns
  - Mimics Results of Rock Cutters
  - Cumulative Effects of Multiple Bursts
    - Not Continuous Blast

gti

Slide 13

LASER/ROCK INTERACTION RESEARCH

Multiple-Hole Test Series

> Key Design Considerations
- Geometric Pattern Applications
- Beam Overlap and Spacing
- Focal Distance Changes While Lasing
- Beam Intercept Angles
- Purging Systems
- Thermal Relaxation Time Between Shots

Hexagonal Closest Packing Arrangement

Slide 14

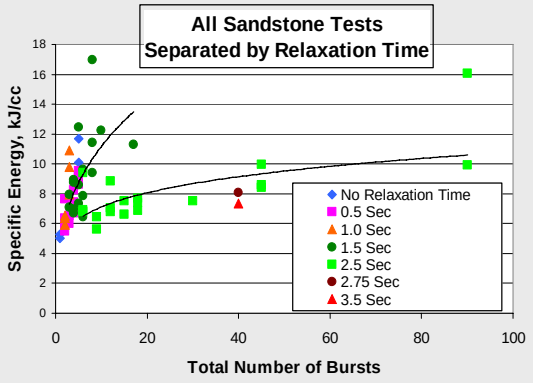

All sandstone samples (one, two, three and four-spot), highlighting the major trend differences in observed SE values between 1.5 and 2.5 seconds relaxation time between successive laser beam bursts.

Slide 15

LASER/ROCK INTERACTION RESEARCH

Multiple-Hole Test Series

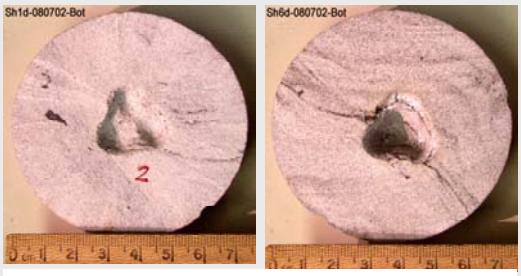

Photos of the lowest SE result (SH1D-2, left), and highest SE (SH6D, right). Sample SH6D exhibits a small amount of melt inside the hole.

Slide 16

LASER/ROCK INTERACTION RESEARCH

DOE/GTI Continuation of Work

> DOE NETL (2002-05)

Task 2.0: Continuation of Fundamental Research and Development – In-Situ Conditions

Task 3.0: Systems Development Issues in Laser Well Construction

Task 4.0: High Energy Laser Perforation and Completion Techniques

gti

Slide 17

LASER APPLICATIONS

Downhole Laser Applications

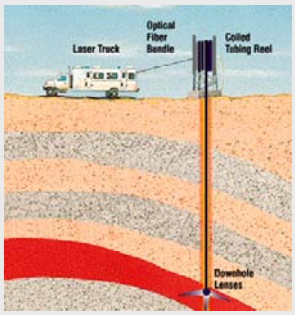

gti

Slide 18

LASER APPLICATIONS

Laser Application in Oil and Gas

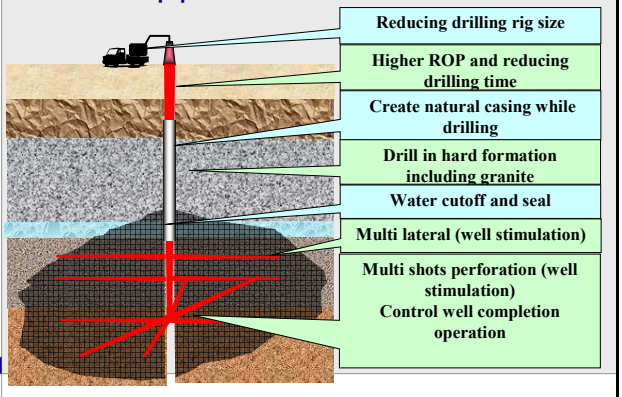

gti

Slide 19

LASER APPLICATIONS

Downhole Laser Perforation

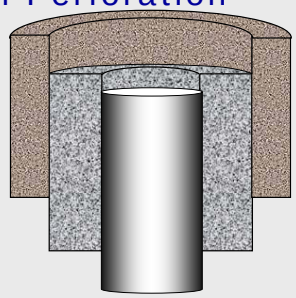

gti

Slide 20

LASER APPLICATIONS

Downhole Laser Perforation

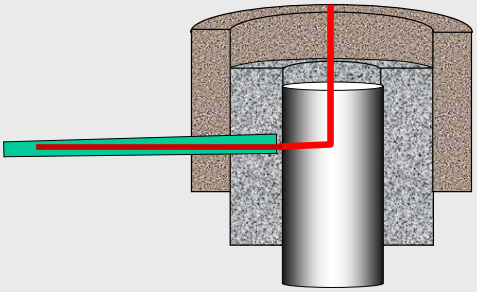

gti

Slide 21

LASER APPLICATIONS

Benefits of Laser Perforation

- Non-Explosive Technology
- Real-Time Control: Input vs. Output
- Potential for "Extended Perforation" and Other Completion Methods
- Stimulate While Creating Perforations

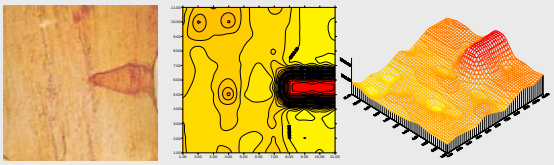

gti

Slide 22

FIBER LASER

GTI High Power Fiber Laser

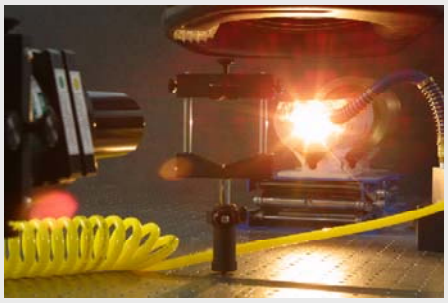

gti

Slide 23

FIBER LASER

GTI High Power Fiber Laser

- Largest Research Fiber Laser in US
  - 5 kW Multiclad Ytterbium-doped active fiber
  - 1.07 micron wavelength (near IR)
- Most Efficient Commercial High-Power Laser
  - 10X Improvement Over Current Lasers (20+%)
- Meets Field Application Requirements
  - Portable, Durable, Reliable
  - Fiber Delivery to Downhole Targets
- Multiple Applications Considered Beyond E&P
  - Utilities (Pavement Cutting)
  - Military (Concrete Ablation & Destruction)
  - Extraterrestrial (Mars Drilling Project)

gti

Slide 24

FIBER LASER

HPFL Advantages

More Power, Easily Scalable	5 - 7x, up to 30KW
Better Beam Quality	2 - 3x
Higher Efficiency	3 -10x
Greater Reliability	20 - 50x
Lower Operation Cost	3 -10x
Lower Maintenance Cost	5 -10x
Smaller Size	10 - 20x
Longer Fiber Delivery	3 - 5x
Lower Potential Cost	1.5 - 2x

gti

Slide 25

FIBER LASER

HPFL Perforation: Limestone

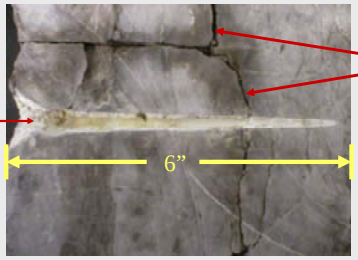

HPFL Perforation in Reservoir Limestone
Length: 6 inches Power: 5.34 kW Beam: CW

gti

Slide 26

FIBER LASER

HPFL Perforation: Limestone

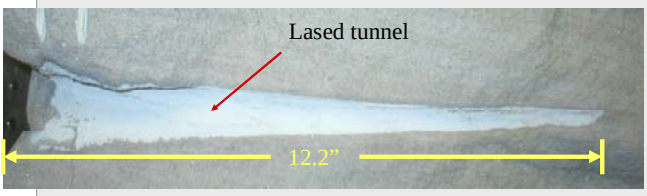

HPFL Perforation in Quarry Limestone
Length: 12.2 inches Power: 5.34 kW Beam: CW

gti

Slide 27

FIBER LASER

HPFL Perforation: Sandstone

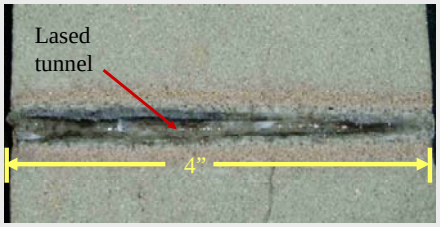

HPFL Perforation in Berea Sandstone
Length: 4 inches Power: 5.34 kW Beam: CW

gti

Slide 28

FIBER LASER

HPFL Perforation: Composite

HPFL Perforation through steel, cement, and sandstone
Power: 4.4 kW Beam: CW

gti

Slide 29

FIBER LASER

HPFL System Components

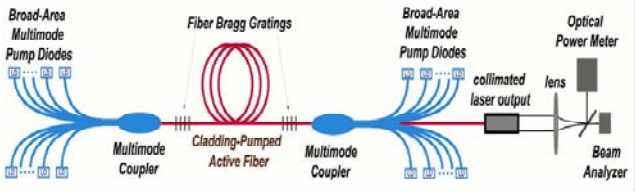

Active Fiber :	**Pump Diodes :**
Multi-Clad, Circular Cladding	Multimode
~20m Total Length	100mm stripe
High Yb^{3+} Concentration	Up to 5.0W Output Power

gti

Slide 30

FIBER LASER

EM Spectrum

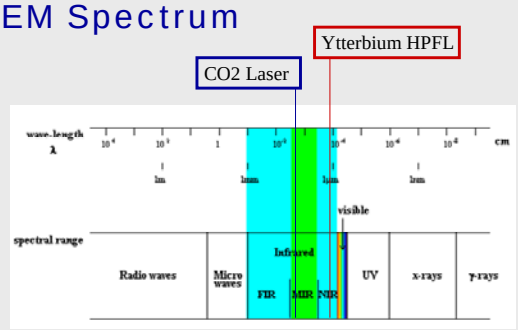

gti

Slide 31

FIBER LASER

HPFL – Main Features

- >150W CW Output Power
- TEM_{00} operation ($M^2 < 1.05$)
- Single Mode Fiber Delivery Line
- Focusable up to 20mm Spot Size
- 110V AC operation
- Compact & Air Cooled
- > 20% Wall-Plug Efficiency
- >50,000 Hours @ 24/7 Lifetime
- No Service Operation
- Operation in wide range of ambient conditions

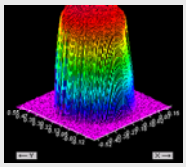

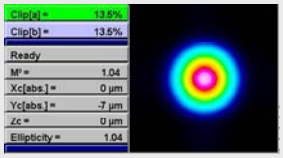

Slide 32

SUMMARY

GTI Leading Laser Apps R&D

> Unique Capabilities, Expertise, Network
> Successful R&D Results
> Advanced HPFL Lab
> Performing R&D With Industry Partners
> Exclusive Laser Industry Partner (IPG)
> Near and Long Term Project Portfolio

Slide 33

www.gastechnology.org